Investigating the Role of Cerebral Cortex in Consciousness

By

Rong Mao

A dissertation submitted in partial fulfillment of

the requirements for the degree of

Doctor of Philosophy

(Neuroscience)

at the

UNIVERSITY OF WISCONSIN-MADISON

2023

Date of final oral examination: 06/01/2023

The dissertation is approved by the following members of the Final Oral Committee:

Chiara Cirelli, Professor, Psychiatry
Giulio Tononi, Professor, Psychiatry
Matthew I. Banks, Professor, Anesthesiology
Xin Huang, Associate Professor, Neuroscience
Yuri Saalmann, Associate Professor, Psychology

Acknowledgements

These years in Madison, on the other side of the planet from my hometown, have been years that I spent with my family of choice out of the world.

My sincere gratitude to Chiara Cirelli, for all her invaluable guidance and patient hands-on teaching throughout the years. Heartfelt appreciation to Chiara and Giulio Tononi for serving as my ideals for true scientists and scholars, and for their tireless mentoring. I constantly admired their sharp minds in every conversation, the pure joy they find in every discovery big or small, their walking library-like knowledge, as well as their unwavering commitment and focus amidst the many demands of work and life. I am also honored to have and grateful to my advisory committee professors, Matthew I. Banks, Xin Huang, Yuri Saalmann, for their deep insights and indispensable support throughout my journey. And my gratefulness to Jess A. Cardin, Quentin Perrenoud and the lab, for their pivotal enlightenment and training as an undergraduate.

My thanks especially to Matias Lorenzo Cavelli as my incredible teacher. I had the great fortune to work with him and will always cherish his Uruguayan vibe. It has also been a true pleasure to work with and being inspired by my brilliant teammates and friends Graham Findlay, and Kort Driessen, Tom Bugnon, William Marshall. And to each and every one of my precious friends in the lab—their genuine companionship has lifted me up from life's dramas many times, and I am indebted to them in ways that are difficult to express in a few words. I am also thankful to my cherished friends outside of the lab who have kept me grounded and supported me through thick and thin in this New World. And to my old friends, who have always believed in me and had me rooted.

Finally, my deepest gratitude goes to my family in China, who sent me off overseas at the pandemic outburst. They provided me with unconditional love and support, asking for nothing in return. My grandma and parents, thank you for waiting.

Table of Contents

Abstract

Consciousness is the subjective, phenomenal experience of anything. The assessment of consciousness level is critical in basic science for ethical considerations, as well as in clinical settings for patient care. The Perturbational Complexity Index (PCI) and the related measure PCI^{st} (st, state transitions) reliably evaluate the level of consciousness in humans by computing the spatiotemporal complexity of responses in the cerebral cortex. However, little is known about the cellular and network mechanisms that underlie these indices' capacity to measure consciousness. In the first part of my thesis, I aim to fully validate the use of PCI^{st} in rodents, explore its underlying mechanisms, and examine how different cortical areas and layers contribute to the ability of PCI^{st} to assess consciousness levels.

Indices like PCI^{st} operate on the assumption that the cerebral cortex plays a critical role in supporting consciousness, as evidenced by clinical and experimental studies. Despite this, the question of whether the direct activation of cortex alone is sufficient to produce consciousness has yet to be answered. Furthermore, there is currently a contentious debate whether the posterior parietal cortex and/or the frontal cortex are essential for consciousness. To address these gaps in knowledge, the second part of my thesis aims to investigate the sufficiency of the cerebral cortex in supporting consciousness and to examine the distinct roles played by the anterior and posterior cortical regions, using a comatose mouse model.

By utilizing optogenetic manipulations combined with intracortical and EEG recordings in rodents, my results uncover that 1) the PCI^{st} index is a viable means of assessing the level of consciousness in mice and rats; 2) the direct activation of cortical neurons is sufficient to elicit behavioral arousal and/or cortical activation from sleep, brainstem coma, and anesthesia; 3)

posterior cortical regions play a key role in supporting consciousness in rodents, while the contribution of anterior regions is possibly less significant; and 4) superficial and deep cortical layers both contribute to the ability of PCI^{st} to track consciousness level across behavioral states, suggesting that both superficial and deep cortical layers may be important for the manifestation and content of consciousness.

Chapter I:

Introduction

Consciousness is subjective, phenomenal experience of anything—for example, entertaining a thought, perceiving a scene, or enduring pain (Tononi, 2012; Oizumi et al., 2014; Tononi et al., 2016). Evaluating the level of consciousness is crucial for ethical considerations in general as well as the wellbeing of patients at the bedside, making it a key focus of basic and clinical research (Sarasso et al. 2021).

In humans, the level of consciousness is reliably assessed by quantifying the spatiotemporal complexity of cortical responses using Perturbational Complexity Index (PCI) and related PCI^{st} (st, state transitions) (Casali et al. 2013; Casarotto et al. 2016; Comolatti et al. 2019). These measures are high in wake and rapid eye movement (REM) sleep, when subjects retrospectively report vivid experiences, and low in non-rapid eye movement (NREM) sleep and slow wave anesthesia (Casali et al. 2013; Comolatti et al. 2019). Nevertheless, the cellular and network mechanisms responsible for the ability of these measures to reflect the level of consciousness are poorly understood. In NREM sleep and slow wave anesthesia, when PCI/PCI^{st} values are low, cortical neurons fire more or less synchronously (Steriade, Nuñez, and Amzica 1993). A long-standing hypothesis has been that in those states, the stimulation used to measure PCI/PCI^{st} is more likely to trigger a large OFF period, silencing the cortical network, impairing the communication among areas (Massimini et al. 2005), and thus resulting in a simple evoked response (Sarasso et al. 2021; Pigorini et al. 2015). However, studies in humans (Pigorini et al. 2015) and rodents (Arena, Comolatti, et al. 2021) so far could not provide direct evidence for the cessation of cortical unit firing. This leads to my first project **(Chapter II)**, which seeks to fully validate the use of PCI^{st} in rodents, investigate its mechanisms underlying consciousness, and characterize the roles of different layers and cortical areas.

Measures like PCI and PCIst are based on the notion that the cerebral cortex is essential for consciousness, which is supported by clinical and experimental evidence (Dehaene and Changeux 2011; Koch et al. 2016). For example, the peripheral nervous system, cerebellum and hippocampus, seem to be neither necessary nor sufficient for consciousness (Posner and Plum, 2007; Selimbeyoglu and Parvizi, 2010; Scoville and Milner, 1957; Lemon and Edgley, 2010). Brainstem lesions can result in immediate coma in patients (Parvizi and Damasio, 2003), but in the presence of wide cortical damage, a functional brainstem reticular formation is unable to sustain the consciousness of patients (Laureys et al., 2004; Boly et al., 2008). In experimental setup, the perception of visual stimuli is correlated with an enhanced fMRI activation in the cortical networks (Dehaene et al., 2001). However, despite strong evidence indicating the significance of the cortex, whether the direct activation of cortex alone is sufficient to produce consciousness remains to be determined. Moreover, within the cortex, whether its posterior parietal (Boly et al., 2017a) or frontal (Odegaard et al., 2017) part is essential for consciousness is under hot debate (Suzuki and Larkum, 2020; Dembski et al., 2021). To address these gaps, my second project **(Chapter III)** aims to investigate the sufficiency of the cerebral cortex in supporting consciousness and elucidate the roles of anterior and posterior cortical areas.

PCIst in humans

We infer that people around are conscious because we are conscious ourselves and that they are behaviorally and physically alike us (Descartes 1996). However, there are clinical conditions when the patients are unable to communicate with doctors and family and therefore the level of consciousness is difficult to assess (Sanders et al. 2012; Alkire, Hudetz, and Tononi 2008;

Laureys, Owen, and Schiff 2004). Given this quandary, the availability of an objective measure of consciousness that is independent of the sensory processing, verbal/motor outputs and the subject participation would be of immense value. PCI^{st} has been demonstrated to be highly effective in achieving this objective and has been shown to produce reliable results in human subjects (Comolatti et al. 2019).

PCI^{st} discriminated between consciousness and unconsciousness in healthy humans, by having higher values in wake state with immediate subjective reports, and lower values in NREM sleep, midazolam/xenon/propofol slow wave anesthesia, where the subjects were unresponsive with no report upon awakening (Comolatti et al. 2019). PCI^{st} was also able to detect consciousness in brain-injured patients (Comolatti et al. 2019): patients with locked-in syndrome (where the patient remains conscious although unable to communicate with the external world) and individuals who emerged from minimally conscious state all had high PCI^{st} values; the majority of patients in minimally conscious state (MCS, with signs of nonreflexive behaviors) yielded high values; whereas most of the patients with unresponsive wakefulness syndrome (UWS; i.e. vegetative state, VS; only reflexive behavior) resulted in low PCI^{st} values. Subsequently, PCI^{st} has been tested and implemented in a number of studies, demonstrating promising and fruitful outcomes (Sinitsyn et al. 2020; Sarasso et al. 2020; Zelmann et al. 2023; Yong Wang et al. 2022; Huntley et al. 2022; Hönigsperger, Storm, and Arena 2022; Arena et al. 2022; Arena, Juel, et al. 2021). For instance, in human subjects, it exhibited high diagnostic accuracy in differentiating between UWS and MCS patients, as well as provided valuable prognostic information regarding the likelihood of their behavioral improvements over a one-year period (Yong Wang et al. 2022). In people with severe Alzheimer's disease, PCI^{st} values

were around or below the threshold for consciousness, indicating a diminished capacity for conscious awareness and especially for some individuals (Huntley et al. 2022). This finding is highly pertinent for the healthcare of severe Alzheimer's disease patients, who often experience cognitive and verbal impairments that make it difficult to ascertain their experience.

The precursor to PCIst, PCI (Casali et al. 2013), has also been demonstrated to reliably track changes in conscious level across various physiological states, anesthesia and clinical conditions. Notably, in states of REM sleep or ketamine anesthesia, where individuals were unresponsive but exhibited delayed reports of conscious experience upon awakening, PCI was shown to produce high values (Sarasso et al. 2015; Casarotto et al. 2016). This provided evidence that PCI accurately reflects the level of conscious awareness rather than the degree of connection to the external environment. Recently, it was reported that up to three months prior to the reemergence of behavioral responsiveness in UWS patients, high PCI values were detected, indicating a recovery capacity for consciousness (Rosanova et al. 2023).

PCIst and PCI have been shown to reliably assess the level of consciousness on an individual level across a range of conditions. For example, the study by Casarotto et al. (2016b) analyzed PCI data from a group of 150 healthy individuals and established an empirical cutoff value that achieved 100% sensitivity and specificity when distinguishing between conscious and unconscious states. This cutoff value also demonstrated a sensitivity of 94.7% when detecting patients with minimal consciousness and identified nine of 43 unresponsive VS patients with high PCI values, which overlapped with the distribution of the benchmark conscious condition. In a recent study, PCI outperformed the spectral analysis of spontaneous electroencephalographic (EEG) within the same cohort of 40 MCS patients (Casarotto et al. 2023). Researchers observed

a significant amount of variability in the spontaneous EEG among MCS patients, with a non-negligible number of patients exhibiting predominant slow wave activity (SWA; 0.5-4Hz) and highly reduced alpha power, a pattern which was proposed to be associated with unconsciousness (Colombo et al. 2019; Sokoliuk and Cruse 2018). In contrast, PCI values consistently indicated a capacity for consciousness in all MCS patients, which is in line with the presence of discernible behavioral signs of awareness. In another investigation, it was discovered that the spatial and spectral gradients of spontaneous EEG were unable to stratify un/consciousness like PCI could, for patients with UWS/MCS caused by anoxia (Colombo et al. 2023). Moreover, when subjects were conscious albeit under an altered state produced by sub-anesthetic ketamine (Farnes et al. 2020) or psilocybin (Ort et al. 2023), PCI remained high even though the spontaneous EEG activities showed increased diversity. This suggests that while the spontaneous complexity may reflect the ongoing content of experience, PCI serves as a better measurement of the level of consciousness / capacity to sustain consciousness. Given the superior performance of PCI/ PCIst over other advanced methods to assess consciousness level, it was recently advocated that the use of these methods be expanded to a wider range of clinical settings, including intensive care units (Edlow et al. 2023). Doing so would greatly aid in predicting patient recovery and prevent premature withdrawal of life-sustaining therapy.

The underlying rationale of PCIst

The outstanding performance of PCIst /PCI in assessing the level of consciousness is attributed to its theoretical foundation, as it was intentionally developed to measure the capacity of a system for integration and information according to the integrated information theory (IIT) (Casali et al.

2013; Comolatti et al. 2019; Massimini et al. 2022). As stated by this theory, a system must be both integrated and differentiated to be conscious, and the greater the degree of integration and differentiation, the more conscious the system is (Tononi 2004; Albantakis et al. 2022). PCI^{st} /PCI captures the joint presence of integration and differentiation by firstly perturbing the system at one site, and then measuring the spatiotemporal complexity of the responses at other sites (Casali et al. 2013). The output value is high if a distributed set of spatial locations of the system responds to stimulation with differing, long-lasting latencies, suggesting a high level of consciousness. In contrast, if the responses are localized and short-lasting, or global but stereotypical across sites and time, the value is low, suggesting a low consciousness level (Casali et al. 2013).

This "perturb and measure" approach assesses the causal structure of a system, as opposed to other measures of consciousness that focus on the spontaneous or resting-state brain activities and examine the correlational network properties (Engemann et al. 2018; Colombo et al. 2019; Curley et al. 2022; Casarotto et al. 2023; Colombo et al. 2023). PCI^{st} /PCI quantifies neuronal interactions from a causal perspective, thus resulting in a more reliable and comprehensive assessment of brain complexity with a higher signal-to-noise ratio (Sarasso et al. 2021). In comparison to measures that use peripheral stimuli (Engemann et al. 2018), PCI^{st} /PCI's direct cortical stimulation does not depend on the integrity of sensory inputs and is a more reliable approach for indexing the capacity of consciousness. The methods that rely on peripheral stimuli, nevertheless, still bypass the output stage and are useful for evaluating the perception of certain sensory modalities (Binder, Górska, and Griskova-Bulanova 2017).

In practice, PCI^{st} /PCI is calculated by analyzing the scalp/intracranial EEG responses to transcranial magnetic stimulation (TMS) or intracranial single-pulse electrical stimulation (Casali et al. 2013; Comolatti et al. 2019; Sarasso et al. 2021). Since the cerebral cortex has been shown to be crucial for consciousness (see section '**Identifying full NCC'**), PCI^{st} /PCI repeatedly stimulates and records from the cortex, obtaining trial-averaged cortical event related potentials (ERPs) within each state. The complexity of the ERPs is subsequently measured using strategies of principal component decomposition and recurrence quantification analysis for PCI^{st} (Comolatti et al. 2019), or nonparametric statistical analysis and algorithmic complexity for PCI (Casali et al. 2013). These computations result in a final value, namely PCI^{st} or PCI, which captures both the spatial and temporal complexity of the cortical evoked responses and reflects the capacity of consciousness.

PCI^{st}, as compared to PCI, applies strategies that compute the complexity using the direct recording at EEG sensors, instead of the derived responses at the level of cortical sources estimated from the inverse solution (Casali et al. 2013; Comolatti et al. 2019). This offers a crucial advantage of enabling faster analysis, ideally in real-time. Moreover, alternative and cost-effective setups can be utilized, eliminating the need to implement high-density EEG combined with TMS guided by individualized MRI scans (Comolatti et al. 2019).

Although PCI^{st} demonstrates a strong theoretical foundation and effectively tracks the level of consciousness in humans, the cellular and network mechanisms that underlie its performance was, until recently, largely unknown. To address these questions, I used rodent models in which I could perform intracortical / cell-type specific perturbations, as well as recordings of local field potentials (LFPs) and unit activity across multiple cortical areas and

layers. If we assume that the theoretical foundation of PCI^{st} is correct, and that the method of obtaining PCI^{st} values applies to conscious experience in general, we would predict that this approach would also be effective in other mammalian species, such as rodents. **Chapter II** first validates the use of PCI^{st} in rodents, then further investigates its neural mechanisms, and finally examines whether it exhibits any cortical regionality or layer specificity.

The study of the neural correlates of consciousness

The search of what is essential for conscious experience is also known as the study of the neural correlates of consciousness (NCC). For every conscious percept, there will be a neural correlate. Inducing the NCC will induce the perception; inactivating the NCC will eliminate it (Crick and Koch, 1990, 1995b; Chalmers, 2000). To understand why certain systems are conscious but not others, and why some are conscious of a higher level or possess experiences of specific kinds, it is imperative to delineate NCC (Crick and Koch, 1990). NCC are defined as the minimum neural mechanisms jointly sufficient for any one specific conscious experience. They are further distinguished as content-specific NCC, and full NCC. Content-specific NCC are understood as the neural substrates that give rise to experience of particular content, like a face; while full NCC are the neural correlates common to all experiences irrespective of the content, that is, the ensemble of all content-specific NCC (Koch et al., 2016)

To study content-specific NCC, recent advances implemented no-report paradigms. In one exemplary case, during binocular rivalry, the method contrasts the brain activities of when the participant perceived one image or the other, as indicated by eye movement tracking the perceived motion or by pupil size adapted to the perceived luminance (Frässle et al., 2014). To

identify the full NCC, researchers can in principle approximate it by sampling a wide range of content-specific NCC, or alternatively, by contrasting conditions in which conscious experiences in their entirety is present versus absent. These two approaches make progress hand in hand in practical term (Boly et al., 2013). The latter approach can be particularly fruitful when employed with within-state, no-task paradigms: contrasting brain activities within a certain state with or without conscious experience, for instance NREM sleep as indexed by a subsequent dream report (Siclari et al., 2017).

Moreover, it is important to distinguish the full NCC from background conditions, which enable consciousness, yet do not contribute directly to its contents (Koch et al., 2016). Background conditions include, for instance, global enabling factors such as blood flow, oxygen and other nutrients; as well as the proposed neural activating systems, such as the brainstem reticular formation (Schiff, 2010). These factors or neural mechanisms enable or modulate the activity of the whole NCC or of large parts of it, and thus enable or modulate the general level of consciousness (de Graaf and Sack, 2014). Furthermore, in a broader term, background conditions also include those that modulate the activity of only some content-specific NCC, concerning particular kinds of experience (Boly et al., 2017b). For example, processing loops involving attention or working memory (Aru et al., 2012), sensory pathways activating primary sensory cortices, and verbal or motor outputs involved in task-related reports on conscious experience (Tsuchiya et al., 2015). In this way, background conditions can be understood as the ‘prerequisites’ and ‘consequences’ of the experience, without specifying its contents directly (Aru et al., 2012).

Identifying full NCC

Human clinical and experimental evidence, together with animal studies have established that the full NCC does not incorporate the peripheral nervous system. Clinically, patient subjected to complete spinal cord injury with dissociation between head and spine would suffer a complete motor and sensory quadriplegia, but remain fully conscious (McDonald et al., 2002); almost every patient with a limb amputated will experience phantom limb—the vivid feeling that the limb is still present, and likely painful (Ramachandran and Hirstein, 1998). In fact, stimulation applied directly to the brain demonstrates that perception can be elicited in the central nervous system without involvement of the periphery (Selimbeyoglu and Parvizi, 2010). While in contrast, lesions in various brain regions of patients cause coma, a dramatic loss of consciousness state (Posner and Plum, 2007). Altogether, evidence demonstrates that the full NCC locates within the central, but not the peripheral nervous system.

Furthermore, there is strong evidence that the full NCC is not the whole brain either. The adult human cerebellum contains 80% of all brain neurons, and four times more than the cerebral cortex (~16 billion in cortex vs 69 billion in cerebellum) (Herculano-Houzel, 2012), has a highly intricate anatomy and with heavy afferent and efferent projections (Baumann et al., 2015). However, lesion cases in cerebellum showed little effect on conscious contents (Lemon and Edgley, 2010). In a recent example, a young mother was admitted to hospital with the complaint of dizziness related symptoms, and the consistent inability of walking steadily. When examined, it was found that she had a complete absence of cerebellum (Yu et al., 2015). Despite mild mental retardation and medium motor ataxia, her comprehensive normal manifestation of

consciousness provides strong evidence that the cerebellum is not necessary for being conscious per se.

There is strong evidence that the hippocampus is not required for consciousness. For instance, bilateral hippocampal lesions in the well-known patient H.M., did not cause unconsciousness (Scoville and Milner, 1957). After surgical ablations of medial temporal lobe structures including the anterior two thirds of his hippocampi and nearly all entorhinal cortices (Corkin et al., 1997; Annese et al., 2014), H.M. was conscious indistinguishably from normal people, well-mannered, intelligent above average with superior performances on many perceptual tasks (Milner, 1968). Nonetheless, there is evidence that selective bilateral hippocampal damage may cause deficit in visual imagery and mental time travel, as well as facilitate a shift in the main content of minder-wondering from visual scenario to semantic thoughts regarding the present time (McCormick et al., 2018).

Early studies showed that the electrical stimulation of the brainstem reticular formation in the anesthetized cat produces a wake-like EEG pattern with low voltage, high frequency activity (Moruzzi and Magoun, 1949). On the other hand, lesions in dorsolateral pontine tegmentum or the paramedian midbrain usually result in immediate coma clinically in human patients (Parvizi and Damasio, 2003; Posner and Plum, 2007). However, preserved brainstem reticular formation function is not sufficient to sustain the consciousness of patients with wide frontal-parietal cortical network dysfunction, who typically remain unresponsive in VS (Laureys et al., 2004; Boly et al., 2008). Moreover, when waken up from NREM sleep, people report to have conscious dreaming experience two thirds of the time (Siclari et al., 2013), even if the activity in most activating systems is minimal compared to wake (Nir and Tononi, 2010; Brown et al.,

2012). Furthermore, a recent rat study infused noradrenergic agonists into prefrontal or posterior parietal cortex respectively, which produced wake-like frontal and parietal EEGs in both cases (Pal et al., 2018). Therefore, it is likely that brainstem structures are in fact representatives of background conditions; such neural activating systems are essential for physiological arousal and enabling consciousness, but do not serve as part of the NCC per se (Boly et al., 2017b).

Akinetic mutism, associated with impairment in decision making and self-initiated actions, is the major behavioral consequence resulting from unilateral or bilateral lesions in (Bhatia and Marsden, 1994) or dysfunction of the network encompassing the basal ganglia (Darby et al., 2019). The inability to move and speak in these patients represents a particular challenge to assess consciousness experimentally. The extent of the atrophy in the basal ganglia in these patients was found to be negatively correlated with the total score of clinical measures of consciousness (Lutkenhoff et al., 2015). However, it was also found that children with severe bilateral basal ganglia atrophy and degeneration, bedridden and unable to perform voluntary movements, are still responsive to sensory stimuli. They may possess no verbal skills, but could communicate nonverbally with their parents (Straussberg et al., 2002). These lesion studies do not provide strong evidence for altered conscious levels in these subjects, leaving open the question whether the basal ganglia can directly contribute to consciousness.

The claustrum, connected reciprocally with most cortical regions (Torgerson et al., 2015); (Yun Wang et al. 2019), was hypothesized to play a critical role in information integration leading to consciousness, like a ‘conductor’ of various cortical regions (Crick and Koch, 2005). In one patient, unilateral electrical stimulation of white matter underneath the claustrum was reported to cause unconsciousness in ten out of ten trials, during which the patient stared blankly

with arrest of volitional behavior and was unresponsive, and there was no subsequent recollection of any experience. Such unconscious state was initiated and terminated immediately after the stimulation onset and offset, respectively, without inducing seizure (Koubeissi et al., 2014). However, complete or severe bilateral claustrum lesions or degeneration do not cause unconsciousness in patients (Straussberg et al., 2002; Damasio et al., 2013). In mice, bilateral stimulation or ablation of a subpopulation of excitatory claustrum neurons was found to coordinate widespread cortical SWA, but did not change the behavior (Narikiyo et al., 2020). In fact, the claustrum was recently found to be an ancient structure present also in reptiles like pogona, where it is involved in the generation of sharp waves during slow-wave sleep (Norimoto et al., 2020). Overall, the current evidence does not support a direct role of the claustrum in regulating consciousness per se.

Coma and VS are both characterized by unresponsiveness. In coma, there is an absence of arousal with eyes closed during resting state as well as under stimulation. The VS instead, is characterized by the recovery of crude arousal states cycling, including periods with eyes open. Both conditions can be observed after bilateral thalamic lesions, but these lesions usually also involve neighboring white matter tracts connecting to the brainstem arousal centers (Posner and Plum, 2007). Chronic bilateral thalamic electrical stimulation, for instance of the central midline thalamic nuclei including central lateral nuclei, may promote behavioral improvements in some patients with disorders of consciousness (Schiff et al., 2007). Acute stimulations in animals under general anesthesia, for example electrical stimulations of the central lateral thalamus in macaque under isoflurane or propofol (Redinbaugh et al., 2020), of the intralaminar and mediodorsal thalamic nuclei under propofol (Bastos et al., 2021), or optogenetic stimulations of

the ventromedial thalamus in mouse under sevoflurane (sevo) and dexmedetomidine (dex) (Honjoh et al., 2017), may increase the behavioral arousal level and lead to wake-like electrophysiologic patterns of activity. However, thalamic cell-body-specific lesions in animals do not cause coma or VS. For example, one week after surgical near complete bilateral thalamic lesions, rats monitored for at least five continuous days evidenced minimal changes during wakefulness, in terms of behavior, EEGs and cortical expression of Fos, an immediate early gene whose induction is used as a proxy for strong neuronal activation (Fuller et al., 2011). These results are consistent with an early study with behavior and EEGs recording, although in that study the lesion was less extensive and fewer experimental details were reported (Buzsaki et al., 1988). Furthermore, during human REM sleep, intracortical pulvinar recording exhibits low-frequency, high amplitude activity, while the cortical arousal is preserved (Magnin et al., 2004). All in all, it seems that under normal wake condition, the thalamus is involved in and shapes cortical activation, but whether it is part of NCC remains unclear.

Fronto-parietal cortical networks were suggested as the candidate full NCC (Dehaene and Changeux, 2011). An early fMRI experiment, for example, asked participants to name the word whenever they saw it briefly presented on the screen (Dehaene et al., 2001). Researchers then contrasted the fMRI activations evoked by word presentations that were either readable or made invisible by masking, and found a significantly higher activation in prefrontal and parietal cortical areas in the visible trials. Although such experiments highlight content-specific NCCs, for instance the neural correlates of ‘seeing a word’, they also identify brain regions that are involved in task-related processes, like working memory and decision making (Boly et al., 2013).

On the other hand, large frontal lesions in human (Brickner, 1952), and complete prefrontal cortex resection in monkey (Jacobsen, 1931; Wade, 1952) do not produce unconsciousness. In contrast, large posterior brain lesions predict permanent coma or VS in patients (Kampfl et al., 1998b; Kampfl et al., 1998a), and clinical imaging studies highlight the medial posterior cortex, encompassing the precuneus and adjacent posterior cingulate cortex, as the brain region whose activity positively correlates with conscious level most tightly (Laureys et al., 2004). Measured by metabolic activity, such posterior zone is the most active brain region in healthy conscious control subjects, and this remains true, albeit to a less degree, in locked-in syndrome patients. This posterior zone shows instead decreased activity in minimally conscious state individuals, and is the most silent brain region in unconscious VS patients. In experimental setup, in order to avoid the confounds of state-dependent brain mechanisms and task related neural processes, a within-state, no-task paradigm on human participants recently identified the brain activity associated with dream versus no-dream experiences during NREM sleep and REM sleep, and in both cases found the posterior cortical regions as a candidate for the full NCC during dreaming sleep (Siclari et al., 2017). Nevertheless, there is also evidence stressing the importance of frontal, especially prefrontal cortex (PFC), in conscious experience. For example, in a task combined with multiunit recordings (Mante et al., 2013), macaques make saccades to report either the color or the direction of the majority of moving dots on the screen, depending on the cue of a given trial. Researchers are able to decode the task-irrelevant or, say, unattended information from the activity in an area of PFC named frontal eye field, indicating that this region could be essential for specific perceptual content, besides being involved in task-related

processes. In summary, the role of frontal versus parietal cortices in NCC currently remains under hot debate (Boly et al., 2017b; Odegaard et al., 2017).

While most of the current debate is about the contribution to consciousness of different cortical areas, there is still very little direct, causal, evidence that the cortex is part of the core mechanism required for consciousness. As mentioned, perhaps the strongest evidence includes cases of patients with preserved function of the brainstem reticular formation but with wide frontal-parietal cortical network dysfunction, who typically remain unresponsive in vegetative state (Laureys et al., 2004; Boly et al., 2008). In **Chapter III,** I address this gap by performing direct optogenetic stimulation of cortical neurons in mice during three behavioral states characterized by progressively deeper unresponsiveness, including sleep, a coma-like state caused by muscimol injection in the midbrain, and deep sevoflurane-dexmedetomidine anesthesia.

References

Albantakis, Larissa, Leonardo Barbosa, Graham Findlay, Matteo Grasso, Andrew M. Haun, William Marshall, William GP Mayner, et al. 2022. “Integrated Information Theory (IIT) 4.0: Formulating the Properties of Phenomenal Existence in Physical Terms.” arXiv. http://arxiv.org/abs/2212.14787.

Alkire, Michael T., Anthony G. Hudetz, and Giulio Tononi. 2008. “Consciousness and Anesthesia.” *Science* 322 (5903): 876–80. https://doi.org/10.1126/science.1149213.

Arena, A., R. Comolatti, S. Thon, A. G. Casali, and J. F. Storm. 2021. “General Anesthesia Disrupts Complex Cortical Dynamics in Response to Intracranial Electrical Stimulation in Rats.” *ENeuro* 8 (4). https://doi.org/10.1523/ENEURO.0343-20.2021.

Arena, A., B. E. Juel, R. Comolatti, S. Thon, and J. F. Storm. 2021. “Does the Posteromedial Cortex Play a Primary Role for the Capacity for Consciousness in Rats?” bioRxiv. https://doi.org/10.1101/2021.01.22.427747.

Arena, A, B E Juel, R Comolatti, S Thon, and J F Storm. 2022. “Capacity for Consciousness under Ketamine Anaesthesia Is Selectively Associated with Activity in Posteromedial Cortex in Rats.” *Neuroscience of Consciousness* 2022 (1): niac004. https://doi.org/10.1093/nc/niac004.

Binder, Marek, Urszula Górska, and Inga Griskova-Bulanova. 2017. “40Hz Auditory Steady-State Responses in Patients with Disorders of Consciousness: Correlation between Phase-Locking Index and Coma Recovery Scale-Revised Score.” *Clinical Neurophysiology* 128 (5): 799–806. https://doi.org/10.1016/j.clinph.2017.02.012.

Casali, Adenauer G., Olivia Gosseries, Mario Rosanova, Mélanie Boly, Simone Sarasso, Karina R. Casali, Silvia Casarotto, et al. 2013. “A Theoretically Based Index of Consciousness Independent of Sensory Processing and Behavior.” *Science Translational Medicine* 5 (198): 198ra105-198ra105. https://doi.org/10.1126/scitranslmed.3006294.

Casarotto, Silvia, Angela Comanducci, Mario Rosanova, Simone Sarasso, Matteo Fecchio, Martino Napolitani, Andrea Pigorini, et al. 2016. “Stratification of Unresponsive Patients by an Independently Validated Index of Brain Complexity.” *Annals of Neurology* 80 (5): 718–29. https://doi.org/10.1002/ana.24779.

Casarotto, Silvia, Gabriel Hassan, Mario Rosanova, Simone Sarasso, Chiara-Camilla Derchi, Pietro Trimarchi, Alessandro Viganò, et al. 2023. “Dissociations between Spontaneous EEG Features and the Perturbational Complexity Index in the Minimally Conscious State.” Preprint. Preprints. https://doi.org/10.22541/au.167957646.66325236/v1.

Colombo, Michele Angelo, Angela Comanducci, Silvia Casarotto, Chiara-Camilla Derchi, Jitka Annen, Alessandro Viganò, Alice Mazza, et al. 2023. “Beyond Alpha Power: EEG Spatial and Spectral Gradients Robustly Stratify Disorders of Consciousness.” *Cerebral Cortex*, March, bhad031. https://doi.org/10.1093/cercor/bhad031.

Colombo, Michele Angelo, Martino Napolitani, Melanie Boly, Olivia Gosseries, Silvia Casarotto, Mario Rosanova, Jean-Francois Brichant, et al. 2019. “The Spectral Exponent of the Resting EEG Indexes the Presence of Consciousness during Unresponsiveness Induced by Propofol, Xenon, and Ketamine.” *NeuroImage* 189 (April): 631–44. https://doi.org/10.1016/j.neuroimage.2019.01.024.

Comolatti, Renzo, Andrea Pigorini, Silvia Casarotto, Matteo Fecchio, Guilherme Faria, Simone Sarasso, Mario Rosanova, et al. 2019. "A Fast and General Method to Empirically Estimate the Complexity of Brain Responses to Transcranial and Intracranial Stimulations." *Brain Stimulation* 12 (5): 1280–89. https://doi.org/10.1016/j.brs.2019.05.013.

Curley, William H., Yelena G. Bodien, David W. Zhou, Mary M. Conte, Andrea S. Foulkes, Joseph T. Giacino, Jonathan D. Victor, Nicholas D. Schiff, and Brian L. Edlow. 2022. "Electrophysiological Correlates of Thalamocortical Function in Acute Severe Traumatic Brain Injury." *Cortex; a Journal Devoted to the Study of the Nervous System and Behavior* 152 (July): 136–52. https://doi.org/10.1016/j.cortex.2022.04.007.

Dehaene, Stanislas, and Jean-Pierre Changeux. 2011. "Experimental and Theoretical Approaches to Conscious Processing." *Neuron* 70 (2): 200–227. https://doi.org/10.1016/j.neuron.2011.03.018.

Dembski, Cole, Christof Koch, and Michael Pitts. 2021. "Perceptual Awareness Negativity: A Physiological Correlate of Sensory Consciousness." *Trends in Cognitive Sciences*, June, S1364661321001467. https://doi.org/10.1016/j.tics.2021.05.009.

Descartes, René. 1996. *Discourse on the Method: And, Meditations on First Philosophy*. Yale University Press.

Edlow, Brian L., Matteo Fecchio, Yelena G. Bodien, Angela Comanducci, Mario Rosanova, Silvia Casarotto, Michael J. Young, et al. 2023. "Measuring Consciousness in the Intensive Care Unit." *Neurocritical Care*, April. https://doi.org/10.1007/s12028-023-01706-4.

Engemann, Denis A, Federico Raimondo, Jean-Rémi King, Benjamin Rohaut, Gilles Louppe, Frédéric Faugeras, Jitka Annen, et al. 2018. "Robust EEG-Based Cross-Site and Cross-Protocol Classification of States of Consciousness." *Brain* 141 (11): 3179–92. https://doi.org/10.1093/brain/awy251.

Farnes, Nadine, Bjørn E. Juel, André S. Nilsen, Luis G. Romundstad, and Johan F. Storm. 2020. "Increased Signal Diversity/Complexity of Spontaneous EEG, but Not Evoked EEG Responses, in Ketamine-Induced Psychedelic State in Humans." *PLOS ONE* 15 (11): e0242056. https://doi.org/10.1371/journal.pone.0242056.

Hönigsperger, Christoph, Johan F. Storm, and Alessandro Arena. 2022. "The Activity of Deep Cortical Layers Characterizes the Complexity of Brain Responses during Wakefulness Following Electrical Stimulation." bioRxiv. https://doi.org/10.1101/2022.07.13.499946.

Huntley, Jonathan, Daniel Bor, Feng Deng, Marco Mancuso, Pedro A. M. Mediano, Lorina Naci, Adrian M. Owen, Lorenzo Rocchi, Avital Sternin, and Robert Howard. 2022. "Assessing Awareness in Severe Alzheimer's Disease." *Frontiers in Human Neuroscience* 16: 1035195. https://doi.org/10.3389/fnhum.2022.1035195.

Koch, Christof, Marcello Massimini, Melanie Boly, and Giulio Tononi. 2016. "Neural Correlates of Consciousness: Progress and Problems." *Nature Reviews Neuroscience* 17 (5): 307–21. https://doi.org/10.1038/nrn.2016.22.

Laureys, Steven, Adrian M Owen, and Nicholas D Schiff. 2004. "Brain Function in Coma, Vegetative State, and Related Disorders." *The Lancet Neurology* 3 (9): 537–46. https://doi.org/10.1016/S1474-4422(04)00852-X.

Massimini, Marcello, Fabio Ferrarelli, Reto Huber, Steve K. Esser, Harpreet Singh, and Giulio Tononi. 2005. “Breakdown of Cortical Effective Connectivity During Sleep.” *Science* 309 (5744): 2228–32. https://doi.org/10.1126/science.1117256.

Massimini, Marcello, Simone Sarasso, Silvia Casarotto, and Mario Rosanova. 2022. “Measures of Differentiation and Integration: One Step Closer to Consciousness.” *Behavioral and Brain Sciences* 45. https://doi.org/10.1017/S0140525X21002016.

Ort, Andres, John W. Smallridge, Simone Sarasso, Silvia Casarotto, Robin von Rotz, Andrea Casanova, Erich Seifritz, Katrin H. Preller, Giulio Tononi, and Franz X. Vollenweider. 2023. “TMS-EEG and Resting-State EEG Applied to Altered States of Consciousness: Oscillations, Complexity, and Phenomenology.” *IScience*, April, 106589. https://doi.org/10.1016/j.isci.2023.106589.

Pigorini, Andrea, Simone Sarasso, Paola Proserpio, Caroline Szymanski, Gabriele Arnulfo, Silvia Casarotto, Matteo Fecchio, et al. 2015. “Bistability Breaks-off Deterministic Responses to Intracortical Stimulation during Non-REM Sleep.” *NeuroImage* 112 (May): 105–13. https://doi.org/10.1016/j.neuroimage.2015.02.056.

Rosanova, Mario, Silvia Casarotto, Camilla Derchi, Gabriel Hassan, Simone Russo, Simone Sarasso, Alessandro Viganò, Marcello Massimini, and Angela Comanducci. 2023. “The Perturbational Complexity Index Detects Capacity for Consciousness Earlier than the Recovery of Behavioral Responsiveness in Subacute Brain-Injured Patients.” *Brain Stimulation: Basic, Translational, and Clinical Research in Neuromodulation* 16 (1): 371. https://doi.org/10.1016/j.brs.2023.01.731.

Sanders, Robert D., Giulio Tononi, Steven Laureys, Jamie W. Sleigh, and David S. Warner. 2012. “Unresponsiveness ≠ Unconsciousness.” *Anesthesiology* 116 (4): 946–59. https://doi.org/10.1097/ALN.0b013e318249d0a7.

Sarasso, Simone, Melanie Boly, Martino Napolitani, Olivia Gosseries, Vanessa Charland-Verville, Silvia Casarotto, Mario Rosanova, et al. 2015. “Consciousness and Complexity during Unresponsiveness Induced by Propofol, Xenon, and Ketamine.” *Current Biology* 25 (23): 3099–3105. https://doi.org/10.1016/j.cub.2015.10.014.

Sarasso, Simone, Adenauer Girardi Casali, Silvia Casarotto, Mario Rosanova, Corrado Sinigaglia, and Marcello Massimini. 2021. “Consciousness and Complexity: A Consilience of Evidence.” *Neuroscience of Consciousness*, August, niab023. https://doi.org/10.1093/nc/niab023.

Sarasso, Simone, Sasha D’Ambrosio, Matteo Fecchio, Silvia Casarotto, Alessandro Viganò, Cristina Landi, Giulia Mattavelli, et al. 2020. “Local Sleep-like Cortical Reactivity in the Awake Brain after Focal Injury.” *Brain* 143 (12): 3672–84. https://doi.org/10.1093/brain/awaa338.

Sinitsyn, Dmitry O., Alexandra G. Poydasheva, Ilya S. Bakulin, Liudmila A. Legostaeva, Elizaveta G. Iazeva, Dmitry V. Sergeev, Anastasia N. Sergeeva, et al. 2020. “Detecting the Potential for Consciousness in Unresponsive Patients Using the Perturbational Complexity Index.” *Brain Sciences* 10 (12): 917. https://doi.org/10.3390/brainsci10120917.

Sokoliuk, Rodika, and Damian Cruse. 2018. “Listening for the Rhythm of a Conscious Brain.” *Brain* 141 (11): 3095–97. https://doi.org/10.1093/brain/awy267.

Steriade, M., A. Nuñez, and F. Amzica. 1993. “A Novel Slow (< 1 Hz) Oscillation of Neocortical Neurons in Vivo: Depolarizing and Hyperpolarizing Components.” *The Journal of Neuroscience: The Official Journal of the Society for Neuroscience* 13 (8): 3252–65. https://doi.org/10.1523/JNEUROSCI.13-08-03252.1993.

Tononi, Giulio. 2004. “An Information Integration Theory of Consciousness.” *BMC Neuroscience* 5 (1): 42. https://doi.org/10.1186/1471-2202-5-42.

Wang, Yong, Zikang Niu, Xiaoyu Xia, Yang Bai, Zhenhu Liang, Jianghong He, and Xiaoli Li. 2022. “Application of Fast Perturbational Complexity Index to the Diagnosis and Prognosis for Disorders of Consciousness.” *IEEE Transactions on Neural Systems and Rehabilitation Engineering* 30: 509–18. https://doi.org/10.1109/TNSRE.2022.3154772.

Wang, Yun, Peng Xie, Hui Gong, Zhi Zhou, Xiuli Kuang, Yimin Wang, An-an Li, et al. 2019. “Complete Single Neuron Reconstruction Reveals Morphological Diversity in Molecularly Defined Claustral and Cortical Neuron Types,” 49.

Zelmann, Rina, Angelique Paulk, Fangyun Tian, Gustavo Balanza, Jaquelin Dezha Peralta, Britni Crocker, G Rees Cosgrove, et al. 2023. “Differential Cortical Network Engagement During States of Un/Consciousness in Humans.” Preprint. In Review. https://doi.org/10.21203/rs.3.rs-2006868/v3.

Annese J, Schenker-Ahmed NM, Bartsch H, Maechler P, Sheh C, Thomas N, Kayano J, Ghatan A, Bresler N, Frosch MP, Klaming R, Corkin S (2014) Postmortem examination of patient H.M.'s brain based on histological sectioning and digital 3D reconstruction. Nature communications 5:3122.

Aru J, Bachmann T, Singer W, Melloni L (2012) Distilling the neural correlates of consciousness. Neuroscience and biobehavioral reviews 36:737-746.

Bastos AM, Donoghue JA, Brincat SL, Mahnke M, Yanar J, Correa J, Waite AS, Lundqvist M, Roy J, Brown EN, Miller EK (2021) Neural effects of propofol-induced unconsciousness and its reversal using thalamic stimulation. Elife 10.

Baumann O, Borra RJ, Bower JM, Cullen KE, Habas C, Ivry RB, Leggio M, Mattingley JB, Molinari M, Moulton EA, Paulin MG, Pavlova MA, Schmahmann JD, Sokolov AA (2015) Consensus paper: the role of the cerebellum in perceptual processes. Cerebellum 14:197-220.

Bhatia KP, Marsden CD (1994) The behavioural and motor consequences of focal lesions of the basal ganglia in man. Brain 117 (Pt 4):859-876.

Boly M, Massimini M, Tsuchiya N, Postle BR, Koch C, Tononi G (2017a) Are the Neural Correlates of Consciousness in the Front or in the Back of the Cerebral Cortex? Clinical and Neuroimaging Evidence. The Journal of Neuroscience 37:in press.

Boly M, Massimini M, Tsuchiya N, Postle BR, Koch C, Tononi G (2017b) Are the Neural Correlates of Consciousness in the Front or in the Back of the Cerebral Cortex? Clinical and Neuroimaging Evidence. The Journal of neuroscience : the official journal of the Society for Neuroscience 37:9603-9613.

Boly M, Baars B, Seth AK, Wilke M, Ingmundson P, Laureys S, Edelman D, Tsuchiya N (2013) Consciousness in humans and non-human animals: recent advances and future directions. Front Psychol 4:625.

Boly M, Phillips C, Tshibanda L, Vanhaudenhuyse A, Schabus M, Dang-Vu TT, Moonen G, Hustinx R, Maquet P, Laureys S (2008) Intrinsic brain activity in altered states of consciousness: how conscious is the default mode of brain function? Annals of the New York Academy of Sciences 1129:119-129.

Brickner RM (1952) Brain of patient A. after bilateral frontal lobectomy; status of frontal-lobe problem. AMA archives of neurology and psychiatry 68:293-313.

Brown RE, Basheer R, McKenna JT, Strecker RE, McCarley RW (2012) Control of sleep and wakefulness. Physiol Rev 92:1087-1187.

Buzsaki G, Bickford RG, Ponomareff G, Thal LJ, Mandel R, Gage FH (1988) Nucleus basalis and thalamic control of neocortical activity in the freely moving rat. Journal of Neuroscience 8:4007-4026.

Chalmers DJ (2000) What is a neural correlate of consciousness. In: Neural correlates of consciousness: Empirical and ….

Corkin S, Amaral DG, Gonzalez RG, Johnson KA, Hyman BT (1997) H. M.'s medial temporal lobe lesion: findings from magnetic resonance imaging. The Journal of neuroscience : the official journal of the Society for Neuroscience 17:3964-3979.

Crick F, Koch C (1990) Towards a neurobiological theory of consciousness. Seminars in the Neurosciences 2:263-275.

Crick F, Koch C (1995b) Are we aware of neural activity in primary visual cortex? Nature 375:121-123.

Crick FC, Koch C (2005) What is the function of the claustrum? Philos Trans R Soc Lond B Biol Sci 360:1271-1279.

Damasio A, Damasio H, Tranel D (2013) Persistence of Feelings and Sentience after Bilateral Damage of the Insula. Cerebral cortex 23:833-846.

Darby RR, Joutsa J, Fox MD (2019) Network localization of heterogeneous neuroimaging findings. Brain 142:70-79.

de Graaf TA, Sack AT (2014) Using brain stimulation to disentangle neural correlates of conscious vision. Front Psychol 5:1019.

Dehaene S, Changeux J-P (2011) Experimental and theoretical approaches to conscious processing. Neuron 70:200-227.

Dehaene S, Naccache L, Cohen L, Bihan DL, Mangin JF, Poline JB, Riviere D (2001) Cerebral mechanisms of word masking and unconscious repetition priming. Nature neuroscience 4:752-758.

Frässle S, Sommer J, Jansen A, Naber M, Einhäuser W (2014) Binocular rivalry: frontal activity relates to introspection and action but not to perception. J Neurosci 34:1738-1747.

Fuller PM, Sherman D, Pedersen NP, Saper CB, Lu J (2011) Reassessment of the structural basis of the ascending arousal system. J Comp Neurol 519:933-956.

Herculano-Houzel S (2012) The remarkable, yet not extraordinary, human brain as a scaled-up primate brain and its associated cost. Proceedings of the National Academy of Sciences of the United States of America 109 Suppl 1:10661-10668.

Honjoh S, Sasai S, Schiereck SS, Tononi G, Cirelli C (2017) Regulation of cortical activity and arousal by the matrix cells of the ventromedial thalamic nucleus Nature communications:In revision.

Jacobsen CF (1931) A study of cerebral functions in learning; the frontal lobes. J Comp Neurol 52.

Kampfl A, Schmutzhard E, Franz G, Pfausler B, Haring HP, Ulmer H, Felber S, Golaszewski S, Aichner F (1998a) Prediction of recovery from post-traumatic vegetative state with cerebral magnetic-resonance imaging. Lancet 351:1763-1767.

Kampfl A, Franz G, Aichner F, Pfausler B, Haring HP, Felber S, Luz G, Schocke M, Schmutzhard E (1998b) The persistent vegetative state after closed head injury: clinical and magnetic resonance imaging findings in 42 patients. J Neurosurg 88:809-816.

Koubeissi MZ, Bartolomei F, Beltagy A, Picard F (2014) Electrical stimulation of a small brain area reversibly disrupts consciousness. Epilepsy Behav 37:32-35.

Lemon RN, Edgley SA (2010) Life without a cerebellum. Brain 133:652-654.

Lutkenhoff ES, Chiang J, Tshibanda L, Kamau E, Kirsch M, Pickard JD, Laureys S, Owen AM, Monti MM (2015) Thalamic and extrathalamic mechanisms of consciousness after severe brain injury. Ann Neurol 78:68-76.

Magnin M, Bastuji H, Garcia-Larrea L, Mauguiere F (2004) Human thalamic medial pulvinar nucleus is not activated during paradoxical sleep. Cerebral cortex 14:858-862.

Mante V, Sussillo D, Shenoy KV, Newsome WT (2013) Context-dependent computation by recurrent dynamics in prefrontal cortex. Nature 503:78-84.

McCormick C, Rosenthal CR, Miller TD, Maguire EA (2018) Mind-Wandering in People with Hippocampal Damage. The Journal of neuroscience : the official journal of the Society for Neuroscience 38:2745-2754.

McDonald JW, Becker D, Sadowsky CL, Jane JA, Sr., Conturo TE, Schultz LM (2002) Late recovery following spinal cord injury. Case report and review of the literature. J Neurosurg 97:252-265.

Milner B (1968) Visual recognition and recall after right temporal-lobe excision in man. Neuropsychologia 6:191-210.

Moruzzi G, Magoun HW (1949) Brain stem reticular formation and activation of the EEG. Electroencephalogr Clin Neurophysiol 1:455-473.

Narikiyo K, Mizuguchi R, Ajima A, Shiozaki M, Hamanaka H, Johansen JP, Mori K, Yoshihara Y (2020) The claustrum coordinates cortical slow-wave activity. Nature neuroscience 23:741-753.

Nir Y, Tononi G (2010) Dreaming and the brain: from phenomenology to neurophysiology. Trends in cognitive sciences 14:88-100.

Norimoto H, Fenk LA, Li HH, Tosches MA, Gallego-Flores T, Hain D, Reiter S, Kobayashi R, Macias A, Arends A, Klinkmann M, Laurent G (2020) A claustrum in reptiles and its role in slow-wave sleep. Nature 578:413-418.

Odegaard B, Knight RT, Lau H (2017) Should a Few Null Findings Falsify Prefrontal Theories of Conscious Perception? The Journal of neuroscience : the official journal of the Society for Neuroscience 37:9593-9602.

Oizumi M, Albantakis L, Tononi G (2014) From the phenomenology to the mechanisms of consciousness: integrated information theory 3.0. PLoS Comput Biol 10:e1003588.

Pal D, Dean JG, Liu T, Li D, Watson CJ, Hudetz AG, Mashour GA (2018) Differential Role of Prefrontal and Parietal Cortices in Controlling Level of Consciousness. Curr Biol 28:2145-2152 e2145.

Parvizi J, Damasio AR (2003) Neuroanatomical correlates of brainstem coma. Brain 126:1524-1536.

Posner JB, Plum F (2007) Plum and Posner's diagnosis of stupor and coma, 4th Edition. Oxford ; New York: Oxford University Press.

Ramachandran VS, Hirstein W (1998) The perception of phantom limbs. The D. O. Hebb lecture. Brain 121 (Pt 9):1603-1630.

Redinbaugh MJ, Phillips JM, Kambi NA, Mohanta S, Andryk S, Dooley GL, Afrasiabi M, Raz A, Saalmann YB (2020) Thalamus Modulates Consciousness via Layer-Specific Control of Cortex. Neuron 106:66-75 e12.

Roth BL (2016) DREADDs for Neuroscientists. Neuron 89:683-694.

Schiff ND, Giacino JT, Kalmar K, Victor JD, Baker K, Gerber M, Fritz B, Eisenberg B, Biondi T, O'Connor J, Kobylarz EJ, Farris S, Machado A, McCagg C, Plum F, Fins JJ, Rezai AR (2007) Behavioural improvements with thalamic stimulation after severe traumatic brain injury. Nature 448:600-603.

Scoville WB, Milner B (1957) Loss of recent memory after bilateral hippocampal lesions. Journal of Neurology, Neurosurgery, and Psychiatry 20:11-21.

Selimbeyoglu A, Parvizi J (2010) Electrical stimulation of the human brain: perceptual and behavioral phenomena reported in the old and new literature. Front Hum Neurosci 4:46.

Siclari F, Larocque JJ, Postle BR, Tononi G (2013) Assessing sleep consciousness within subjects using a serial awakening paradigm. Front Psychol 4:542.

Siclari F, Baird B, Perogamvros L, Bernardi G, LaRocque JJ, Riedner B, Boly M, Postle BR, Tononi G (2017) The neural correlates of dreaming. Nature neuroscience 20:872-878.

Straussberg R, Shorer Z, Weitz R, Basel L, Kornreich L, Corie CI, Harel L, Djaldetti R, Amir J (2002) Familial infantile bilateral striatal necrosis: clinical features and response to biotin treatment. Neurology 59:983-989.

Suzuki M, Larkum ME (2020) General Anesthesia Decouples Cortical Pyramidal Neurons. Cell 180:666-676 e613.

Tononi G (2012) The Integrated Information Theory of Consciousness: An Updated Account (vol 150, pg 56, 2012). Archives Italiennes De Biologie 150:56-90.

Tononi G, Boly M, Massimini M, Koch C (2016) Integrated information theory: from consciousness to its physical substrate. Nat Rev Neurosci.

Torgerson CM, Irimia A, Goh SY, Van Horn JD (2015) The DTI connectivity of the human claustrum. Hum Brain Mapp 36:827-838.

Tsuchiya N, Wilke M, Frassle S, Lamme VA (2015) No-Report Paradigms: Extracting the True Neural Correlates of Consciousness. Trends in cognitive sciences 19:757-770.

Wang, Y., Xie, P., Gong, H., Zhou, Z., Kuang, X., Wang, Y., Li, A., Li, Y., Liu, L., Veldman, M. B., Daigle, T. L., Hirokawa, K. E., Lesnar, P., Jiang, S., Yu, Y., Wakeman, W., Zeng, S., Yuan, J., Nguyen, T. N., … Zeng, H. (2019). Complete single neuron reconstruction reveals morphological diversity in molecularly defined claustral and cortical neuron types. 49.

Chapter II:

Sleep/wake changes in perturbational complexity in rats and mice

Matias Lorenzo Cavelli*, Rong Mao*, Graham Findlay, Kort Driessen, Tom Bugnon, Giulio Tononi, Chiara Cirelli

* Indicates co-first authors; Published in *iScience* (2023). 26:106186

Summary

In humans, the level of consciousness is assessed by quantifying the spatiotemporal complexity of cortical responses using Perturbational Complexity Index (PCI) and related PCI^{st} (st, state transitions). Here we validate PCI^{st} in freely moving rats and mice by showing that it is lower in NREM sleep and slow wave anesthesia than in wake or REM sleep, as in humans. We then show that 1) low PCI^{st} is associated with the occurrence of an OFF period of neuronal silence; 2) stimulation of deep, but not superficial, cortical layers leads to reliable PCI^{st} changes across sleep/wake and anesthesia; 3) consistent PCI^{st} changes are independent of which single area is being stimulated or recorded, except for recordings in mouse prefrontal cortex. These experiments show that PCI^{st} can reliably measure vigilance states in unresponsive animals and support the hypothesis that it is low when an OFF period disrupts causal interactions in cortical networks.

Introduction

The Perturbational Complexity Index – PCI – was developed in humans as a tool to quantify the complexity of the cortical event related potentials (ERPs) triggered by transcranial magnetic stimulation (TMS) [1]. The underlying rationale was provided by the integrated information theory of consciousness, according to which high complexity, resulting from the combined presence of high integration and high information in corticothalamic networks, is a prerequisite for being conscious [2-4]. In agreement with the theory, during wake, REM sleep, and ketamine anesthesia, when subjects retrospectively report vivid experiences, PCI is high because the stimulation triggers complex responses that are long-lasting and spread across many cortical regions. By contrast, during slow wave sleep and deep slow wave anesthesia, when subjects retrospectively report that they were not conscious, PCI is low because the response to stimulation either remains local, indicative of low integration, or is global but stereotyped, reflecting low differentiation [1]. The analysis of PCI data from a benchmark population of 150 subjects in whom the presence or loss of consciousness could be established unequivocally led to the identification of an empirical PCI cutoff that, in healthy subjects, could discriminate between conscious and unconscious conditions with nearly 100% sensitivity and specificity [1]. These results prompted the use of PCI to gauge the level of consciousness in patients in vegetative state (unresponsive wakefulness syndrome) and other difficult clinical situations where patients are either unresponsive or minimally responsive [5]. Recently, another method to determine the complexity of the ERP was introduced, called PCIst, which calculates the overall number of non-redundant "state transitions" (st) caused by the stimulation [6]. PCIst has been validated using TMS and then extended to cases in which the cortical response was measured after deep intracranial electrical

stimulation. It was found that PCI^{st} is nearly as accurate as PCI but easier and faster to compute, hence more suitable in clinical settings [6].

Although PCI and PCI^{st} are recognized as sensitive and specific measures to assess consciousness [7], the underlying cellular and network mechanisms are largely unexplored. In NREM sleep and slow wave anesthesia, when PCI/PCI^{st} values are low, cortical neurons are not tonically active but alternate more or less synchronously between ON periods of firing and OFF periods of silence [8]. It has been hypothesized that, under such conditions, cortical networks may be "bistable," that is, they may not be able to support sustained causal interactions but, after brief periods of activity, necessarily fall into periods of silence. Under a bistable regime, strong stimuli are likely to silence the cortical network by triggering a large OFF period, thereby impairing causal interactions among cortical areas and resulting in a simple evoked response and low values of PCI/PCI^{st} [7,9]. So far, however, studies in humans [9] and a recent study in anesthetized rats [10] could not provide direct evidence for the cessation of cortical unit firing underlying bistability.

In this study, we investigate PCI^{st} responses in freely-moving rodents—both rats and mice—using electrical and optogenetic stimulation accompanied by unit recording probes with multiple contacts (Neuropixels and NeuroNexus probes). We first demonstrate that PCI^{st} reveal changes in the complexity of neuronal responses with behavioral state—wake, NREM sleep, REM sleep, as well as anesthesia - that are similar to those observed in humans. Thus, PCI^{st} can serve as a reliable indicator of consciousness in laboratory animals, one that is highly validated in humans and that, unlike the standard righting reflex, can be employed in unresponsive states. We show that PCI^{st} changes can be recorded from a single site of penetration across multiple contacts,

without the need to record from separate areas. We also show that the reduction of PCI^{st} is associated with the triggering of neuronal OFF periods. We further investigate how different cortical areas and layers are involved in triggering and expressing complex neural responses and how, within each behavioral state, baseline activity can modulate the evoked response.

Results

Analysis of PCI^{st} in rats using electrical stimulation. PCI^{st} measurements started only after the sleep/waking pattern had normalized, usually at least one week after surgery. As expected since rats are nocturnal, animals spent most of the light period asleep and were mainly awake at night (Fig. 1A). Electrical stimuli were delivered only during the light period and trials occurred across several days to limit the number of stimuli delivered each day (Fig. 1A; ~100 in each of the behavioral states: waking, NREM sleep, REM sleep). PCI^{st} was measured after electrical stimulation delivered by a laminar probe implanted perpendicular to the cortical surface, and recording was performed using one high-density Neuropixels probe (Fig. 1B). As in humans [6], PCI^{st} was derived from the averaged (across all trials) ERP for each of the cortical channels (~ 80 to 100 channels in each rat), first by identifying the principal components that accounted for at least 99% of the response strength to the stimulation and then by calculating, for each component, the number of state transitions in the evoked response relative to the pre-stimulus baseline (Fig. 1C). Unlike in humans, however, all channels came from the same area (e.g. parietal association cortex, PtA). In almost all cases the electrodes spanned all layers of a given area, with the exception of the prefrontal cortex in which recordings came mainly from the deep layers.

In the first set of experiments electrical stimuli were always delivered to the deep layers, and the cortical areas targeted for stimulation and recording varied across animals (Fig. 2A). In most cases, independent of the location of the stimulating and recording electrodes, rats (n = 8) showed more complex responses in wake and in REM sleep than in NREM sleep (Fig. 2B), leading to high PCI^{st} values in wake, low in NREM sleep, and intermediate or high in REM sleep in one or more of the recorded areas (Fig. 2A). In a few cases in which the recording electrode was contralateral and distant from the stimulating electrode (e.g. left M2 and right V2; left PtA and right M2) the evoked response was minimal or absent in one or more vigilance states, precluding PCI^{st} analysis or resulting in inconsistent changes across states (Fig. 2A). The number of principal components of the ERPs ranged from 1 to 4; most often there were 2 and the number did not change across behavioral states. Thus, changes in PCI^{st} were driven mostly by changes in the number of state transitions (Fig. 2B-C). PCI^{st} values in NREM sleep decreased on average by 50 ± 20% relative to wake and by 51 ± 27% compared to REM sleep, resulting in significant changes at the group level (paired ANOVA; $F_{(1.69,\ 23.7)} = 33.4$; $p < 0.0001$; $\eta^2 = 0.70$; Fig. 2D; Tukey correction for multiple comparison on Fig. 2D). The Phase Locking Factor (PLF), which measures for how long the evoked response remains phased locked to the original stimulus, was calculated for each recording site in wake and sleep. PLF was measured in the 8-40 Hz range because higher frequencies (40-200 Hz) did not discriminate across behavioral states (Fig. 2B), consistent with the results in humans [9]. We found long PLF in wake and REM sleep and short PLF in NREM sleep ($F_{(1.80,\ 25.2)} = 13.05$; $p = 0.0002$; $\eta^2 = 0.48$) and PCI^{st} and PLF values were positively correlated (Fig. 2E). Grouping the recording sites in more anterior (M2, mPFC, Of) and more posterior (M1, PtA, V2) sites did not reveal any major difference, that is, significant sleep/wake differences in

PCI^{st} could be detected in all areas (Fig. 2F; Frontal: $F_{(1.48, 10.4)} = 14.84$; $p = 0.0015$; $\eta^2 = 0.67$; Posterior: $F_{(1.38, 8.32)} = 23.11$; $p = 0.0007$; $\eta^2 = 0.79$). To assess the contribution of superficial and deep layers, for each recording site PCI^{st} was also calculated separately for the channels in the upper and lower half of the laminar probe. In general, both superficial and deep channels contributed to the sleep/wake changes (Fig. 2G; superficial: $F_{(1.58, 17.4)} = 17.02$; $p = 0.0001$; $\eta^2 = 0.62$; deep: $F_{(1.24, 13.6)} = 6.47$; $p = 0.019$; $\eta^2 = 0.37$).

In 8 rats PCI^{st} was also compared between wake and deep anesthesia, with loss of righting reflex, induced using sevoflurane (2%; 14 areas) or dexmedetomidine (100ug/kg; 6 areas) (Fig. 3A). In all cases, independent of the location of stimulating and recording electrodes, PCI^{st} was lower under anesthesia compared to waking and the difference was mainly driven by changes in the number of state transitions (Fig. 3B,C). In most cases PLF values were lower under anesthesia and were positively correlated with PCI^{st} values (Fig. 3D). PCI^{st} values in anesthesia did not differ significantly from those during NREM sleep (W, NREM, A; $F_{(1.74, 27.9)} = 66.7$; $p < 0.0001$; $\eta^2 = 0.81$; NREM vs A, $p = 0.1267$).

In 4 rats the stimulation was delivered at different depths spanning superficial and deep layers, and the response was measured across all layers (Fig. 4A,B). ERPs in both ipsilateral and contralateral cortex were large when deep layers were stimulated and small or undetectable when the stimulation was restricted to the most superficial layers (Fig. 4C,D). As a result, in both ipsilateral and contralateral cortex the sleep/wake changes in PCI^{st} were robust for stimulation of deep and middle layers, but inconsistent when only the most superficial layers were stimulated (Fig. 4E,F).

To test whether electrical stimulation triggers an OFF period, Neuropixels recordings were spike-sorted using the Kilosort2.5 algorithm [11], followed by manual curation (see Methods). We focused on 6 rats that had a good yield of cortical units (67 ± 42 single units, 38 ± 31 MUA per cortical area, mean ± std dev) and in which electrical stimulation produced robust ERPs in all 3 states, resulting in reliable changes in PCI^{st}. For each rat and each area separately, we first analyzed sleep in baseline and after 6 hours of sleep deprivation, without electrical stimulation, to define the range in the duration of the OFF periods. From the peri-slow-wave time histograms corresponding to all areas (Fig. 5A) we obtained an average duration of OFF periods of 48 ± 14 ms (mean ± std dev; range 35-68 ms) during baseline sleep and of 97 ± 37 ms (range 48-152 ms) during the first 2 hours of recovery sleep after sleep deprivation. We then tested whether the electrical stimulation triggered a bona fide OFF period, as defined based on the analysis in sleep, and calculated its average duration for each experimental condition (wake, NREM sleep, REM sleep). In 5 out of 6 rats periods of neuronal silence (62 ± 27 msec, mean ± std dev) were induced during NREM sleep (Fig. 5A) and their amplitude and laminar distribution were very similar to those of the spontaneous OFF periods (Fig. 5B). This pattern applied to all areas examined (M1, M2, Of, PtA). OFF periods were induced less frequently in wake and REM sleep as compared to NREM sleep. Specifically, "effectiveness", defined as the percentage of trials per animal with evoked OFF periods of at least 30 ms, was 48 ± 45 % in wake, 81 ± 21 % in NREM sleep, and 48 ± 42 % in REM sleep ($F_{(1.06, 8.49)} = 9.87$, $p = 0.012$; $\eta^2 = 0.55$; Wake vs REM $p > 0.05$). Even when present, the average duration of the evoked OFF periods was shorter in wake and REM sleep as compared to NREM sleep (Fig. 5A; eOFF: Wake 17 ± 25 msec, NREM 42 ± 37 msec, REM 12 ± 24 msec; $F_{(1.07, 8.57)} = 8.35$, $p = 0.017$, $\eta^2 = 0.51$; Wake vs REM

$p > 0.05$). Similar results were obtained when evoked OFF periods were measured at the single trial level (Wake 39 ± 41 msec, NREM 80 ± 37 msec, REM 37 ± 38 msec; $F_{(1.15, 9.19)} = 37.68$, $p = 0.0001$; $\eta^2 = 0.82$; Wake vs REM $p > 0.05$). Finally, when present in wake and REM sleep, the occasional OFF periods were followed by a rebound in firing that exceeded the pre-stimulation levels of spiking, which was not the case for the OFF periods evoked in NREM sleep. In two rats in which OFF periods were present in all three behavioral states (albeit longer in NREM sleep), the rebound firing was still present only in wake and REM sleep (Fig. 5A). In a few cases no clear OFF periods in NREM sleep were observed in the peri-stimulus time histogram, but the mean firing rate still showed a decline after the electrical stimulation, while no clear decrease in unit activity occurred in wake and REM sleep. In summary, OFF periods occur in most cases after stimulation during NREM sleep. OFF periods are less likely to be induced in wake and REM sleep and when they occur, they are shorter and, unlike those in NREM sleep, usually followed by a strong rebound in unit firing. Finally, in a few animals with high yield of both cortical and thalamic units the single-unit peri-stimulus time histogram showed that electrical stimulation during NREM sleep triggered a period of strongly reduced activity in both cortex and thalamus. Notably, however, the thalamic OFF period was shorter, leading to an earlier rebound of firing in thalamus than in cortex, a pattern also seen during physiological NREM sleep (Fig. 5C). In wake and REM sleep the thalamic OFF period was shorter than in NREM sleep and was not followed by a clear rebound in firing.

Analysis of PCIst in mice using optogenetic stimulation. Cortical stimuli were delivered at least 1-2 weeks after surgery to allow the sleep/wake pattern to normalize. Mice, like rats, were asleep

mainly during the day and had several hours of spontaneous wake at night, and stimuli were delivered only during the light phase (Fig. 6A). In CaMKIIα::ChR2 mice the excitatory opsin is expressed in the pyramidal neurons of the cortex and hippocampus [12]. For the stimulation of the posterior parietal association area (PtA), the optic fibers were placed on the cortical surface to avoid the stimulation of the hippocampus. For anterior stimulation, optic fibers were implanted deep in prefrontal cortex to target as much as possible all layers (Fig 6B). ERPs recorded from PtA and other areas outside the prefrontal cortex (V2, S1) showed a pattern consistent with the one seen in rats: responses were complex in wake and REM sleep and tended to be larger but more stereotyped in NREM sleep (Fig. 6C). This pattern occurred independent of the stimulated area (PtA or prefrontal cortex) and resulted in PCI^{st} values that were higher in wake than in NREM sleep, and almost always higher in REM sleep than in NREM sleep (Fig. 6D,G; $F_{(1.35, 8.14)} = 6.23$; $p = 0.0302$; $\eta^2 = 0.51$). By contrast, ERPs recorded from frontal and prefrontal cortex were either small or stereotyped across states (Fig. 6E), and led to PCI^{st} values that did not differ significantly across states but were higher in NREM sleep than in wake (Fig. 6D,G; $F_{(1.08, 3.24)} = 2.21$; $p = 0.2298$; $\eta^2 = 0.42$).

In 9 mice PCI^{st} was also measured in deep anesthesia (sevoflurane, 1-2%; dexmedetomidine 70-100μg/kg) (Fig. 7A-C). ERPs recorded from PtA and other posterior areas showed complex responses in wake and more stereotyped responses in anesthesia, while ERPs recorded from frontal and prefrontal cortex were often small or stereotyped in all cases (Fig. 7A,B). PCI^{st} values recorded in posterior areas were always lower in anesthesia than in wake, while in anterior areas they were inconsistent (Fig. 7D).

Next, we tested whether the optogenetic stimulation triggers OFF periods also in mice. Independent of whether the stimulation was anterior or posterior, OFF periods were consistently recorded from PtA during NREM sleep but were absent in wake; during REM sleep OFF periods were either absent or, when present, they were followed by a rebound firing that exceeded the pre-stimulation levels. In prefrontal cortex, by contrast, long OFF periods followed by strong rebound firing occurred in all states.

Finally, we tested whether the stimulation had differential effects depending on the background activity just before the pulse was delivered. For wake and REM sleep the analyses focused on the amount of theta activity [13-15] and were performed in rats, whose Neuropixels probes allowed the precise detection of theta activity in the dorsal hippocampus (Fig. 9A). Trials were sorted by baseline theta power 1 sec before the pulse and by the duration of the evoked OFF periods (Fig. 9B,F). In both wake and REM sleep we found a negative correlation between pre-stimulation theta activity and the duration of the evoked OFF period (Fig. 9C,G), although only in REM sleep the latter differed significantly between trials with the lowest and highest theta activity (Fig. 9D,H). The analysis in NREM sleep was performed in both rats and mice after ranking the trials based on the amount of time spent OFF during the last 0.5 sec before the stimulus was delivered (Fig. 9J). The ability to evoke an OFF period was negatively correlated with the time spent OFF pre-stimulation (Fig. 9K) and trials with longer time spent OFF resulted in significantly shorter evoked OFF periods in mice, and a similar trend in rats (Fig. 9L,N). Of note, however, within each behavioral state PCIst values did not differ between trials with the lowest and the highest theta (Fig. 9E,I), or between trials with the most and the least pre-stimulation time spent OFF (Fig. 9M,O). This is likely because the difference in the duration of

the evoked OFF periods between these groups of "low" and "high" trials was small. Moreover, the duration of the evoked OFF periods was shorter in wake and REM sleep than in NREM sleep, even when comparing the most extreme cases, i.e., wake or REM sleep trials with the longest evoked OFF periods (lowest theta; Fig. 9D,H)) with NREM sleep trials with the shortest evoked OFF periods (most time OFF in baseline; Fig. 9L).

Discussion

Measures of perturbational complexity, such as PCI and PCIst, can be used to assess the presence and absence of consciousness without relying on behavioral reports. These indices have been validated in a large number of human subjects in many different conditions [5] and have shown unrivaled sensitivity and specificity [7]. They have also proven their value in inferring the presence and absence of consciousness in unresponsive patients [5].

Our first goal was to validate the use of PCIst in animal models of spontaneous sleep and wake. We found that PCIst is high in wake and REM sleep and low in NREM sleep in both rats and mice, as it is in humans [1,5]. In humans, wakefulness is invariably conscious, and REM sleep is most often accompanied by dreaming. By contrast, consciousness frequently fades during NREM sleep, especially early in the night, when the EEG shows high amplitude slow waves, especially in posterior cortex [16]. The similarity of the results obtained in freely moving rodents suggests that PCIst may be used as a reliable readout of the effectiveness of causal interactions in corticothalamic networks that are thought to underlie the capacity for experience [3].

We also found that, as in humans, PCI^{st} is reduced in rats and mice under deep slow wave anesthesia with sevoflurane and/or dexmedetomidine. These results confirm and extend the findings of a recent study in head fixed rats [10]. In that study, propofol and sevoflurane anesthesia induced large slow waves and led to a decrease in PCI^{st} associated with decreased phase-locking, whereas ketamine anesthesia was associated with wake-like EEG activity and with PCI^{st} values intermediate between wake and propofol/sevoflurane. Thus, in both humans and rodents, conditions characterized by the presence of widespread cortical slow waves (deep NREM sleep, propofol, sevoflurane and dexmedetomidine anesthesia) are associated with low PCI^{st} values, while wake-like EEG activity is associated with intermediate or high PCI^{st} (ketamine anesthesia, REM sleep, wake).

Which cellular and network mechanisms underly the ability of measures of perturbational complexity to reflect the level of consciousness? Theoretical considerations predict that the loss of consciousness should be associated with a breakdown of causal interactions within corticothalamic networks [3]. In patients, deep intracranial stimulation during wake triggered complex and long-lasting cortical evoked responses that were deterministically linked to the initial stimulus [9]. By contrast, the same stimulation during NREM sleep (REM sleep was not studied) triggered a suppression of high frequencies (>20Hz) and an associated increase in low frequencies (<4Hz). Moreover, when cortical activity resumed, it was not phased-locked to the original stimulus, and the cessation of phase locking was correlated in time with the suppression of high frequencies [9]. However, due to the unavailability of unit recordings in humans [9] and rats [10], it could not be determined whether the drop in high frequencies and the loss of a deterministic

response during NREM sleep reflects the occurrence of a period of neuronal silence due to neuronal bistability.

The present recordings in freely moving rats show that phase locking to electrical stimulation was also long in wakefulness and REM sleep and short in NREM sleep. Moreover, unit recordings in both rats and mice demonstrate that low PCI^{st} values during NREM sleep and slow wave anesthesia are indeed associated with the early occurrence of OFF periods. This provides direct support to the hypothesis that sustained causal interactions that lead to high PCI^{st} cannot take place when cortical networks are bistable. In some cases, electrical or optogenetic stimulation during wake or REM sleep also triggered neuronal silence, but the OFF period was shorter than in NREM sleep. Intriguingly, these OFF periods were followed by a strong rebound in cortical firing that was absent in NREM sleep. A local, low-amplitude, short-lasting increase in low frequencies (< 4Hz) after deep intracranial stimulation can also occur during wakefulness in humans, while the suppression of high frequencies only occurs during NREM sleep [9]. Previous evidence indicates that OFF periods may be triggered by Martinotti cells that powerfully inhibit every other neuronal population [17]. Thus, strong local stimulation may activate Martinotti cells strongly enough to trigger local OFF periods even in wakefulness [17].

In humans, phase locking was suppressed during NREM sleep predominantly in the alpha and beta bands (8-30 Hz), while phase locking in the 30-100 Hz gamma band was short-lasting and comparable in wake and NREM sleep [9]. In our study, phase locking was suppressed in NREM sleep in the 8-40 Hz band but not in the gamma band (40-200 Hz), compared to both wake and REM sleep. Several studies in monkeys have revealed consistent patterns of neuronal dynamics across layers in both frontal and visual areas, with gamma activity being higher in superficial than

in deep layers [18-20]. Alpha/beta rhythms, on the other hand, are higher in deep layers, from where they modulate alpha/beta and gamma activity in the superficial layers [19-22]. Gamma activity in superficial layers has been associated with feedforward transmission from lower to higher areas, attention, and maintenance of working memory, while alpha oscillations have been linked to feedback oscillations [19,20,23,24]. Since PCI^{st} and phase locking values are positively correlated, it may be that the longer phase locking during wake and REM sleep relative to NREM sleep is associated with the activation of feedback loops in cortico-cortical circuits and may sustain the higher spatiotemporal complexity observed in conscious states [9].

Consistent with the presence of clear functional differences across cortical layers, we also found that the stimulation of both anterior and posterior rat cortex provided consistent PCI^{st} results when applied to the deep and middle layers but not when delivered to the most superficial layers. In the rat primary auditory cortex pyramidal neurons in layer 2/3 show more selective and sparser auditory responses compared to layer 5 pyramidal neurons, and correlated activity is strong for local and distal neuron pairs in deep layers but only for local pairs in superficial layers [25]. Large, thick-tufted pyramidal cells of L5b are involved in cortico-subcortical loops, and layer 6 pyramidal cells project to the thalamus, while pyramidal cells in L2/3 have the densest cortico-cortical anatomical connections compared to infragranular layers [26]. Thus, together with the activation of feedback loops, the stimulation of neurons in the deep and middle layers is more likely to recruit cortico-thalamic and other cortico-subcortical loops, increasing the probability that a single distant recording site detects a complex evoked response during wake.

On the other hand, at the recording site both superficial and deep channels contributed to high PCI^{st} in wake and REM sleep and low PCI^{st} in NREM sleep and anesthesia. It is currently

unknown whether supragranular or infragranular layers, all cortical layers, or only specific cellular populations are especially important to account for the presence and content of consciousness. In humans, a negative slow cortical potential likely originating from supragranular layers [27] appears between stimulus onset and behavioral response only when a near-threshold stimulus is perceived [28] and has been proposed as 'generalized awareness negativity', a physiological correlate of consciousness across sensory domains [29]. In mice, on the other hand, deep general anesthesia decouples the signaling from the apical dendrites to the cell body of layer 5 but not of layer 2/3 pyramidal neurons [30]. Thus, loss of consciousness under anesthesia was associated with the impaired activity of pyramidal neurons in deep but not in superficial layers.

In humans, PCI^{st} values are calculated based on EEG or intracranial signals coming from multiple cortical sites. The recent study in anesthetized rats also calculated PCI^{st} using a grid of 16 EEG screws covering bilaterally most of the dorsal cortex [10]. Here, we found that changes in perturbational complexity could be reliably estimated from a single recording probe, albeit one endowed with multiple contacts across its length. We hypothesize that high PCI^{st} values during wake and REM sleep may reflect the triggering of complex reverberatory activity across multiple cortico-thalamic and cortico-cortical loops that impinge on different contacts at different times. By contrast, during NREM sleep, and even more so during anesthesia, this reverberatory activity may be blocked by the widespread occurrence of OFF periods. As shown in Fig. 5B, it is sometimes possible to document the triggering of reverberatory activity, in this case a cortico-thalamic volley followed by a cortico-thalamic OFF period, which is brief in wake and REM sleep. This is followed by rebound spiking occurring first in thalamic neurons, possibly

triggering secondary cortical activity that is complex and long-lasting in wake and REM sleep, but localized and short-lasting in NREM sleep (see also [31,32]).

An intriguing observation is that in rats PCI^{st} changed across vigilance states (high in wake and REM sleep, low in NREM sleep and anesthesia), regardless of the site of stimulation and of whether the recording electrode was placed in anterior or posterior cortex. In mice results were similar, except when recording from prefrontal electrodes, which showed inconsistent PCI^{st} changes with behavioral state. This may be because neural circuits in frontal/prefrontal areas are less developed in mice than in rats [33]. However, a key methodological difference is that in rats we used high-intensity electrical stimulation (as in humans), likely recruiting a broad cortical network and fibers of passage. In mice, we used instead optogenetic stimulation to selectively target neighboring excitatory pyramidal neurons. This was adequate to trigger complex responses from posterior cortex during wake and REM sleep, but not from anterior cortex. Perhaps anterior areas may be organized in a way less suitable for sustaining causal interactions that are both integrated and differentiated, and thereby consciousness, in line with lesion, stimulation, and recording studies [34].

Overall, our experiments show that measures of perturbational complexity can be used for the reliable assessment of vigilance state in rodents. In humans, purely behavioral readouts, even refined ones such as the Glasgow Coma scale revised, administered by expert neurologists, result in a substantial proportion of false negatives in unresponsive patients. In animals, behavioral readouts such as the righting reflex are even more difficult to evaluate [35,36]. Thus, PCI^{st} may offer a promising proxy for assessing consciousness in animals, with potential benefits in terms of research ethics and well-being.

Limitations of the study

In this work, we found that changes in perturbational complexity could be estimated from a single probe recording from one cortical area, but we did not sample all areas. We also did not assess how subcortical areas might contribute to changes in perturbational complexity. Lastly, although we tried to use weak electrical or optogenetic pulses, we cannot totally rule out that nearby areas or passing fibers may have been recruited during the cortical stimulation.

Acknowledgements and Funding sources: Supported by U.S. Department of Defense grant W911NF1910280 (CC, GT), NIH grant 1R01GM116916 (GT), the Tiny Blue Dot Foundation (GT) and the Templeton World Charity Foundation (CC).

Author contributions: MLC, RM conducted the experiments, performed analysis, and wrote parts of the paper; GF, KD, TB performed analysis; GT and CC designed the experiments and wrote the paper.

Conflict of interest statement: Giulio Tononi is Chair of Board and has a financial interest in Intrinsic Powers Inc. Relevant patent: US 8,457,731 B2 (Method for assessing anesthetization; GT). All other authors declare no competing financial or non-financial interests.

Figure 1. Experimental design. A, distribution of wake, NREM sleep and REM sleep during a continuous 24-hour recording in a representative rat. The black line shows slow wave activity (SWA, a. u.). As expected, SWA (the power in the 0.5 - 4 Hz range in cortical local field potentials) is elevated during NREM sleep and peaks at the beginning of the light period, the major sleep phase. Electrical stimuli (lightning bolts) were delivered during the light phase only. **B,** schematic of the rat brain displaying the position of the electrodes and coronal sections showing the location of stimulating and recording probes in one representative rat. **C,** left, averaged (across all trials) event related potentials (ERPs) for all cortical channels, each channel re-referenced to the white matter. To calculate PCI^{st}, the ERPs for each cortical channel (81 channels in this example) are averaged across all trials (n=100 trials) and decomposed to identify the principal components (PC) of the ERPs. The "up and down" of each PC (state transitions, ST) are calculated after thresholding and compared between post- and pre-stimulation (distance matrix). PCI^{st} is the sum of the post/pre differences in ST (ΔNST) for all PCs (see Methods for details). In this and the following figures, the first (PtA in this example) and second (PtA in this example) cortical area indicate the site of stimulation and recording, respectively.

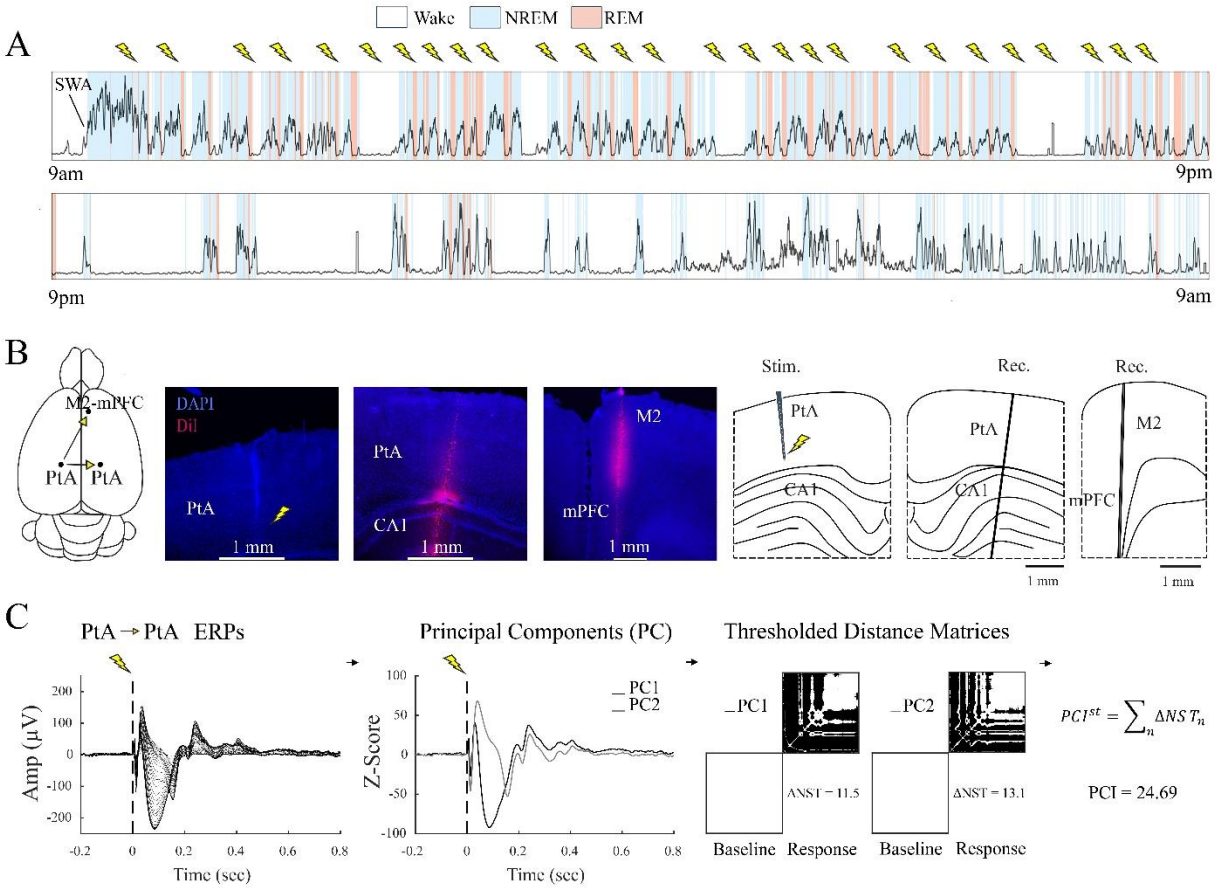
A
Wake
NREM
REM
SWA
9am
9pm
9pm
9am
B
M2-mPFC
PtA
PtA
DAPI
DiI
PtA
1 mm
PtA
CA1
1 mm
M2
mPFC
1 mm
Stim.
Rec.
Rec.
PtA
CA1
PtA
CA1
M2
mPFC
1 mm
1 mm
C
PtA → PtA ERPs
Principal Components (PC)
Thresholded Distance Matrices
Amp (μV)
Time (sec)
Z-Score
PC1
PC2
Time (sec)
PC1
PC2
ΔNST = 11.5
ΔNST = 13.1
Baseline
Response
Baseline
Response
$PCI^{st} = \sum_n \Delta NST_n$
PCI = 24.69

Figure 2. Sleep/wake changes in PCIst in rat cortex. A, histology in a representative rat and schematic location of stimulating and recording electrodes in each animal, with corresponding PCIst values in wake (W), NREM sleep (N) and REM sleep (R). Empty and filled symbols indicate more anterior and more posterior regions, respectively, where PCIst was measured. The cases (n = 5) in which ERPs were absent in wake are not included. M1, primary motor; M2, secondary motor; mPFC, medial prefrontal; Of, orbitofrontal; PtA, parietal association; V2, secondary visual. **B,** example of ERPs, their principal components (PC), and phase locking factor (PLF) for one rat (PtA, * in panel A). PLF is shown separately for the 8-40 Hz range and the 40-200 Hz range. The latter was not used in the main analysis because it does not discriminate across behavioral states. **C,** number of PC (left) and changes in the number state transitions ((ΔNST, right) for all experiments. Note that in most experiments PC = 2, independent of sleep and wake. **D,** group level changes in PCIst across waking and sleep. **E,** group level changes in max PLF across waking and sleep and correlation with PCIst. **F,G** group level changes in PCIst across wake and sleep shown separately for recording in anterior and posterior cortical regions, and for superficial and deep channels.

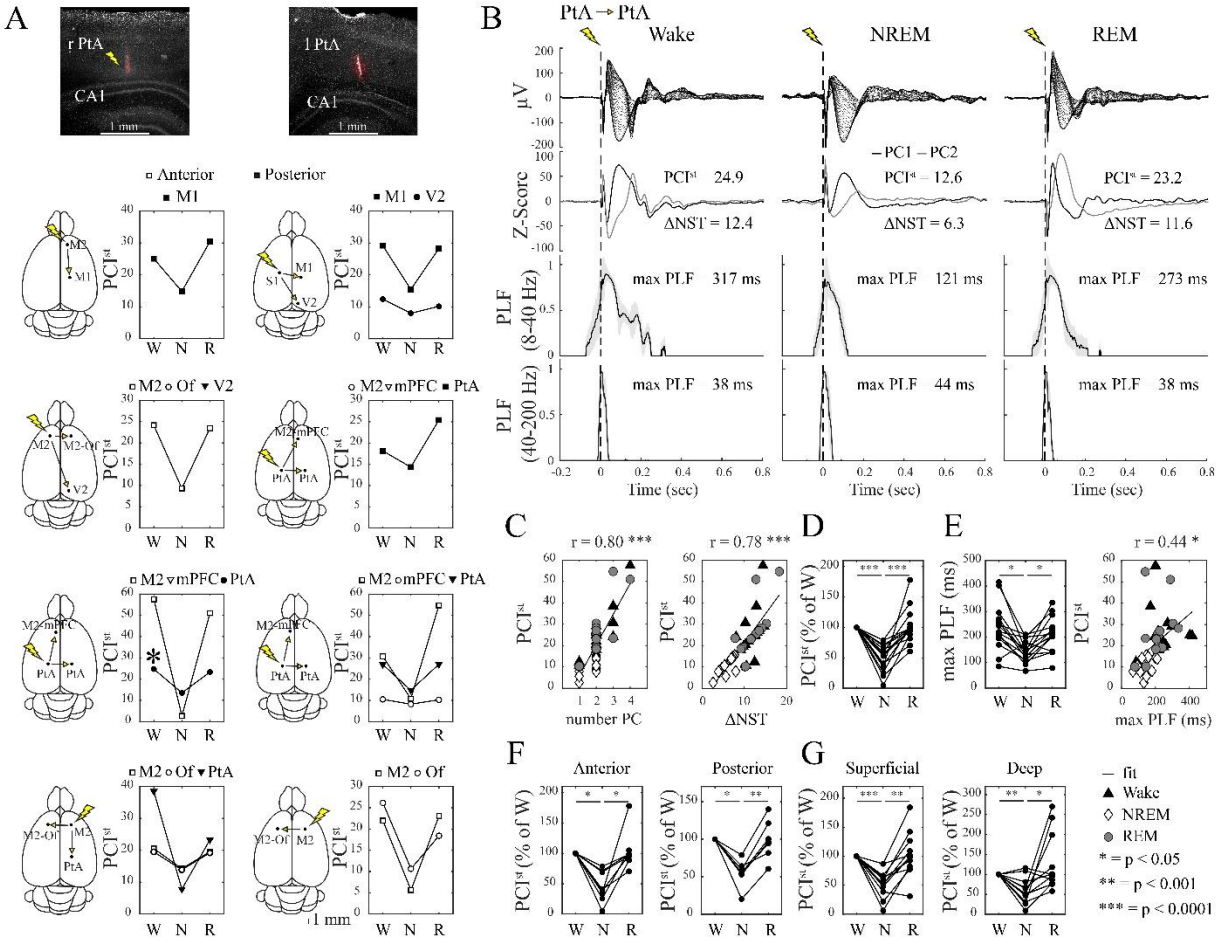
A
r PtA
CA1
1 mm
l PtA
CA1
1 mm
Anterior
Posterior
M1
M1 V2
M2 Of V2
M2 mPFC PtA
M2 mPFC PtA
M2 mPFC PtA
M2 Of PtA
M2 Of
1 mm
W N R
B
PtA→PtA
Wake
NREM
REM
μV
Z-Score
PCI^M 24.9
PCI^M 12.6
PCI^M 23.2
PC1 – PC2
ΔNST = 12.4
ΔNST = 6.3
ΔNST = 11.6
PLF (8-40 Hz)
max PLF 317 ms
max PLF 121 ms
max PLF 273 ms
PLF (40-200 Hz)
max PLF 38 ms
max PLF 44 ms
max PLF 38 ms
Time (sec)
C
r = 0.80 ***
r = 0.78 ***
r = 0.44 *
number PC
ΔNST
max PLF (ms)
D
E
F
Anterior
Posterior
G
Superficial
Deep
PCI^st (% of W)
fit
Wake
NREM
REM
* = p < 0.05
** = p < 0.001
*** = p < 0.0001

Figure 3. Anesthesia-induced changes in PCIst in rat cortex. A, example of ERPs (top), their principal components (PC, middle), and phase locking factor (PLF, bottom) for one representative rat. **B,** number of PC (left) and changes in the number of state transitions ((ΔNST, right) for all experiments. **C,** group level changes in PCIst between wake and anesthesia. Cases in which ERPs were absent in wake are not included (n = 5). **D,** group level changes in max PLF between wake and anesthesia and correlation with PCIst.

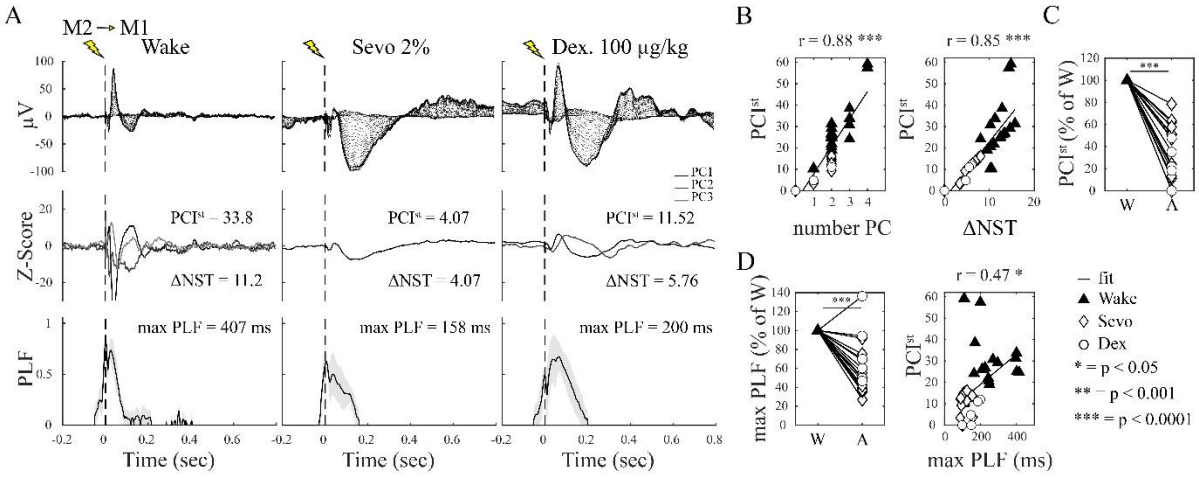

Figure 4. Changes in PCIst depending on the depth of stimulation. A, histology in a representative rat. **B,** schematic location of stimulating and recording electrodes in the 4 rats used for depth analysis. **C**, example of ERPs and PCIst values after stimulation in PtA at 4 different depths and recording in ipsilateral M2 in one rat (asterisk in panel B). **D**, example of ERPs and PCIst values after stimulation in PtA at 4 different depths and recording in contralateral PtA in one rat (asterisk in panel B). **E-F,** sleep/wake changes in PCIst for all 4 rats, shown separately depending on depth of stimulation. The different symbols refer to the areas indicated in panel B, with filled and open symbols indicating ipsilateral and contralateral stimulation, respectively.

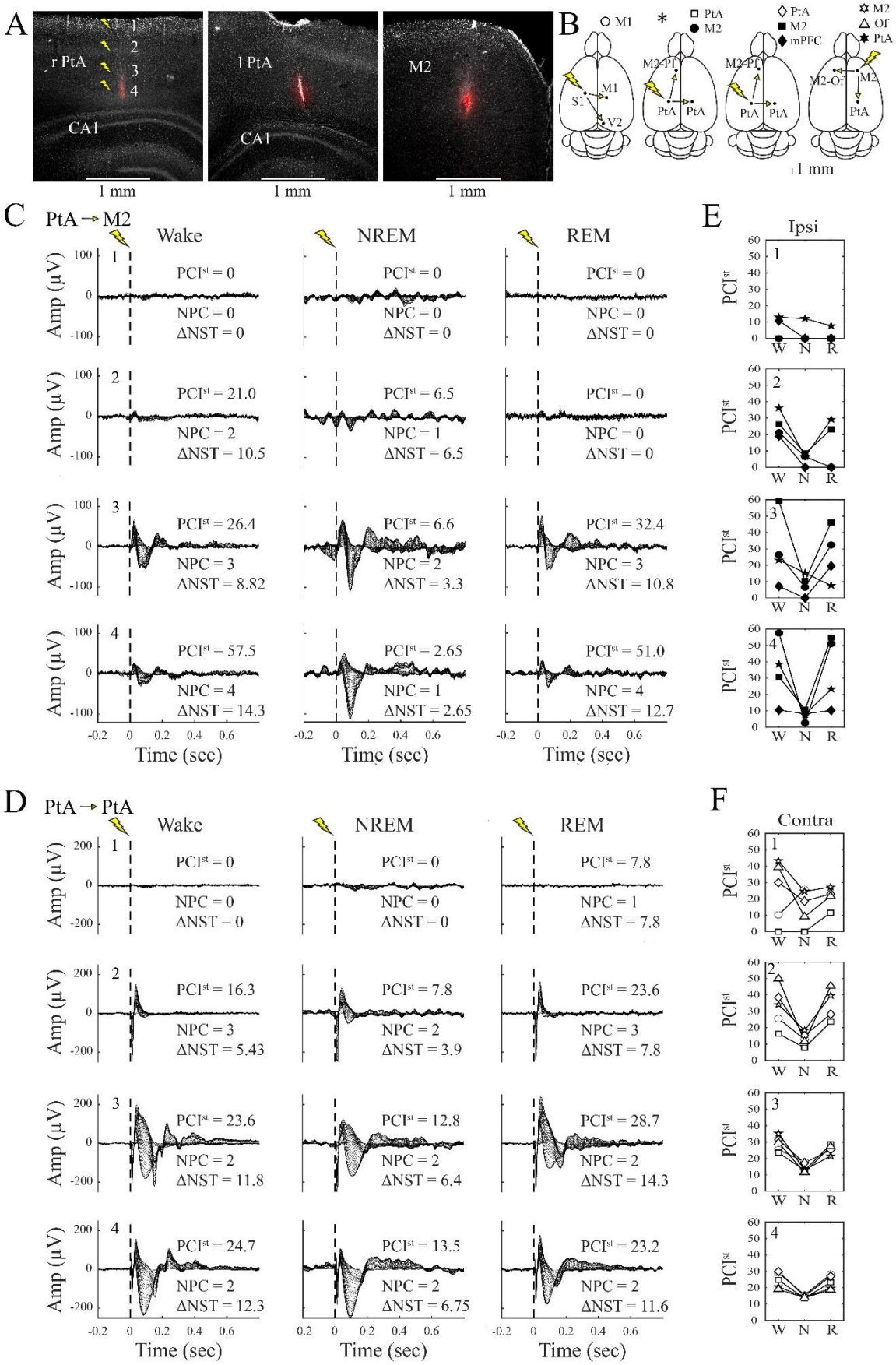
A
r PtA
l PtA
M2
CA1
CA1
1
2
3
4
1 mm
1 mm
1 mm
B
M1
PtA
M2
mPFC
Of
M2-PtA
M2-Of
S1
V2
1 mm
C
PtA → M2
Wake
NREM
REM
Amp (μV)
PCIst = 0
NPC = 0
ΔNST = 0
PCIst = 21.0
NPC = 2
ΔNST = 10.5
PCIst = 6.5
NPC = 1
ΔNST = 6.5
PCIst = 26.4
NPC = 3
ΔNST = 8.82
PCIst = 6.6
NPC = 2
ΔNST = 3.3
PCIst = 32.4
NPC = 3
ΔNST = 10.8
PCIst = 57.5
NPC = 4
ΔNST = 14.3
PCIst = 2.65
NPC = 1
ΔNST = 2.65
PCIst = 51.0
NPC = 4
ΔNST = 12.7
Time (sec)
D
PtA → PtA
PCIst = 7.8
NPC = 1
ΔNST = 7.8
PCIst = 16.3
NPC = 3
ΔNST = 5.43
PCIst = 23.6
NPC = 3
ΔNST = 7.8
PCIst = 23.6
NPC = 2
ΔNST = 11.8
PCIst = 12.8
NPC = 2
ΔNST = 6.4
PCIst = 28.7
NPC = 2
ΔNST = 14.3
PCIst = 24.7
NPC = 2
ΔNST = 12.3
PCIst = 13.5
NPC = 2
ΔNST = 6.75
PCIst = 23.2
NPC = 2
ΔNST = 11.6
E
Ipsi
F
Contra
PCIst
W N R

Figure 5. OFF periods triggered by electrical stimulation in rats. A, Nine examples of ERPs in 6 rats (top), corresponding changes in firing rate across all trials (middle) and mean changes in firing rate (normalized to the wake values, NFR). In each example, the first and second cortical area indicate the site of stimulation and recording, respectively, followed by a symbol that identifies the specific animal. OFFd, duration of the evoked OFF period. **B**, example of the comparison between spontaneous slow waves (n =1662, detected during recovery sleep) and evoked slow waves (n = 94) in one site (orbitofrontal cortex, Of), showing similar amplitude, laminar distribution (CSD, current source density) and unit activity (FR, firing rate). Here and in C, time zero (vertical dashed line) represents slow-wave zero crossing (spont) and electrical stimulation (evoked). The electrode location was estimated using histological reconstruction of the electrode track (left panels) and based on the peak in gamma (>120Hz) power, which is a reliable marker of layer 5 in rodent cortex [37,38]. **C**, example of single-unit peri-stimulus time histograms (PSTH) locked to the slow wave zero-crossing (n =1025, detected during recovery sleep) or the electrical stimulation in wake, NREM sleep and REM sleep (80 pulses per state) in a parietal probe (PtA), sorted by depth. Each row corresponds to the PSTH of a single unit. For each single unit, evoked rates were zscore-normalized based on the mean and standard deviation of instantaneous evoked rates across bins from -2sec to -10msec before the pulses. Region boundaries were obtained from histological reconstruction (left panel); Cx, cortex; Hipp, hippocampus; Th, thalamus; Hypot, hypothalamus.

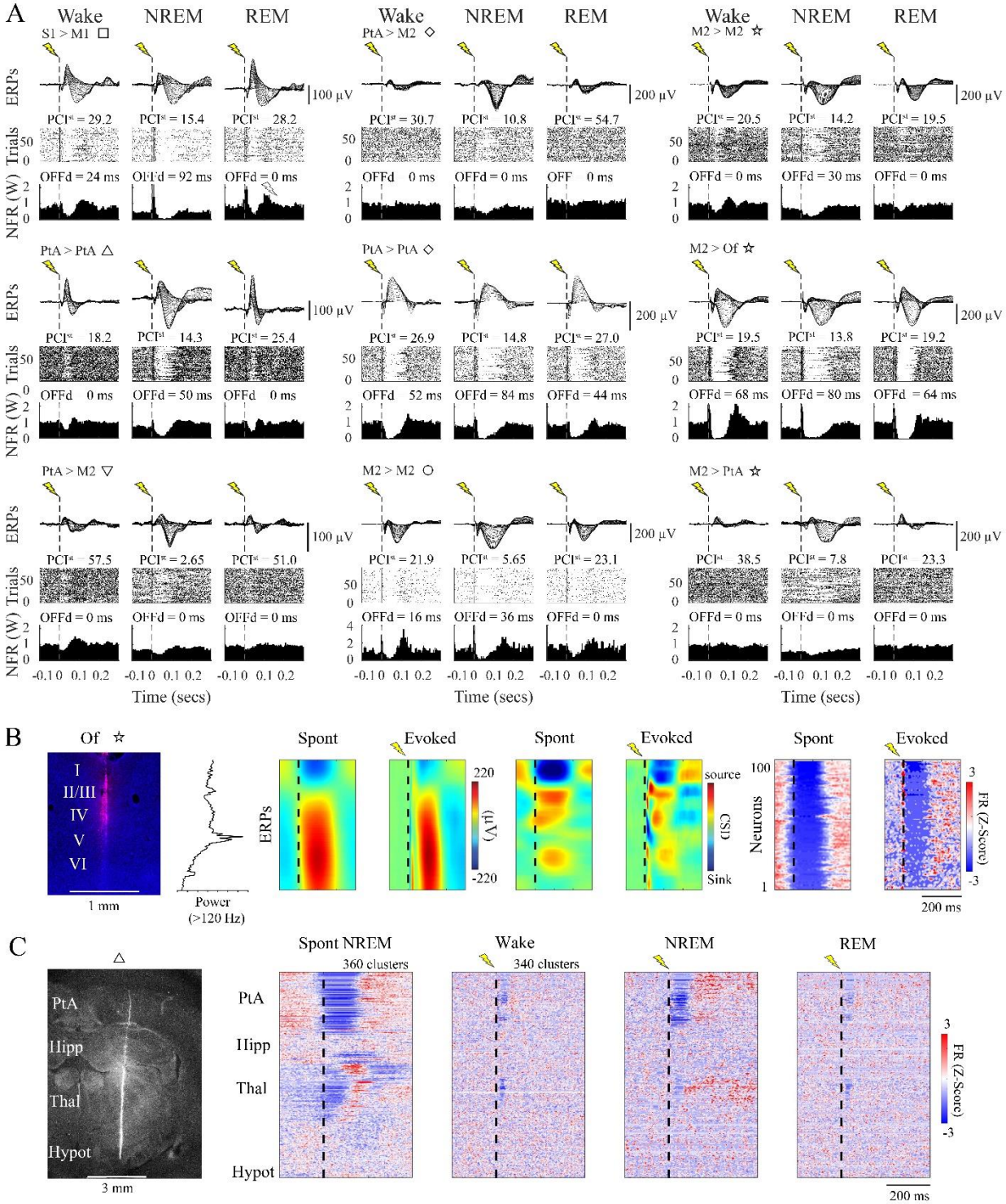
A
Wake
NREM
REM
S1 > M1 □
PtA > M2 ◇
M2 > M2 ☆
PtA > PtA △
PtA > PtA ◇
M2 > Of ☆
PtA > M2 ▽
M2 > M2 ○
M2 > PtA ☆
ERPs
Trials
NFR (W)
100 µV
200 µV
Time (secs)
B
Of ☆
I
II/III
IV
V
VI
1 mm
Power (>120 Hz)
Spont
Evoked
ERPs
220
-220
(µV)
source
CSD
Sink
Neurons
100
1
FR (Z-Score)
3
-3
200 ms
C
△
PtA
Hipp
Thal
Hypot
3 mm
Spont NREM
360 clusters
Wake
340 clusters
NREM
REM
FR (Z-Score)
200 ms

Figure 6. Sleep/wake changes in PCIst in mouse cortex. A, distribution of wake, NREM sleep and REM sleep during a continuous 24-hour recording in a representative mouse. The black line shows relative slow wave activity (SWA), which as in rats peaks at the beginning of the light period, Optogenetic stimuli were delivered during the light phase only. **B,** schematic of the mouse brain displaying the position of the electrodes and coronal sections showing the location of stimulating and recording sites in two mice with stimulation in frontal or posterior cortex. DAPI and GFAP (glial fibrillary acidic protein) staining were used to identify cortical layers and probes, respectively. **C,E,** examples of ERPs (top) and their principal components (PCs, bottom) for 3 mice. **D,** schematic location of stimulating and recording electrodes in each animal, with corresponding PCIst values in wake (W), NREM sleep (N) and REM sleep (R). Empty and filled symbols indicate more anterior and more posterior regions, respectively, where the recording electrode was located. Cases in which ERPs were absent in wake are not included (n = 5). S1, primary sensory; M2, secondary motor; mPFC, medial prefrontal; PtA, parietal association; V2, secondary visual. **F**, number of PCs and changes in the number of state transitions for all experiments, shown separately for anterior and posterior regions. **G**, group level sleep/wake changes in PCIst recorded in anterior and posterior regions.

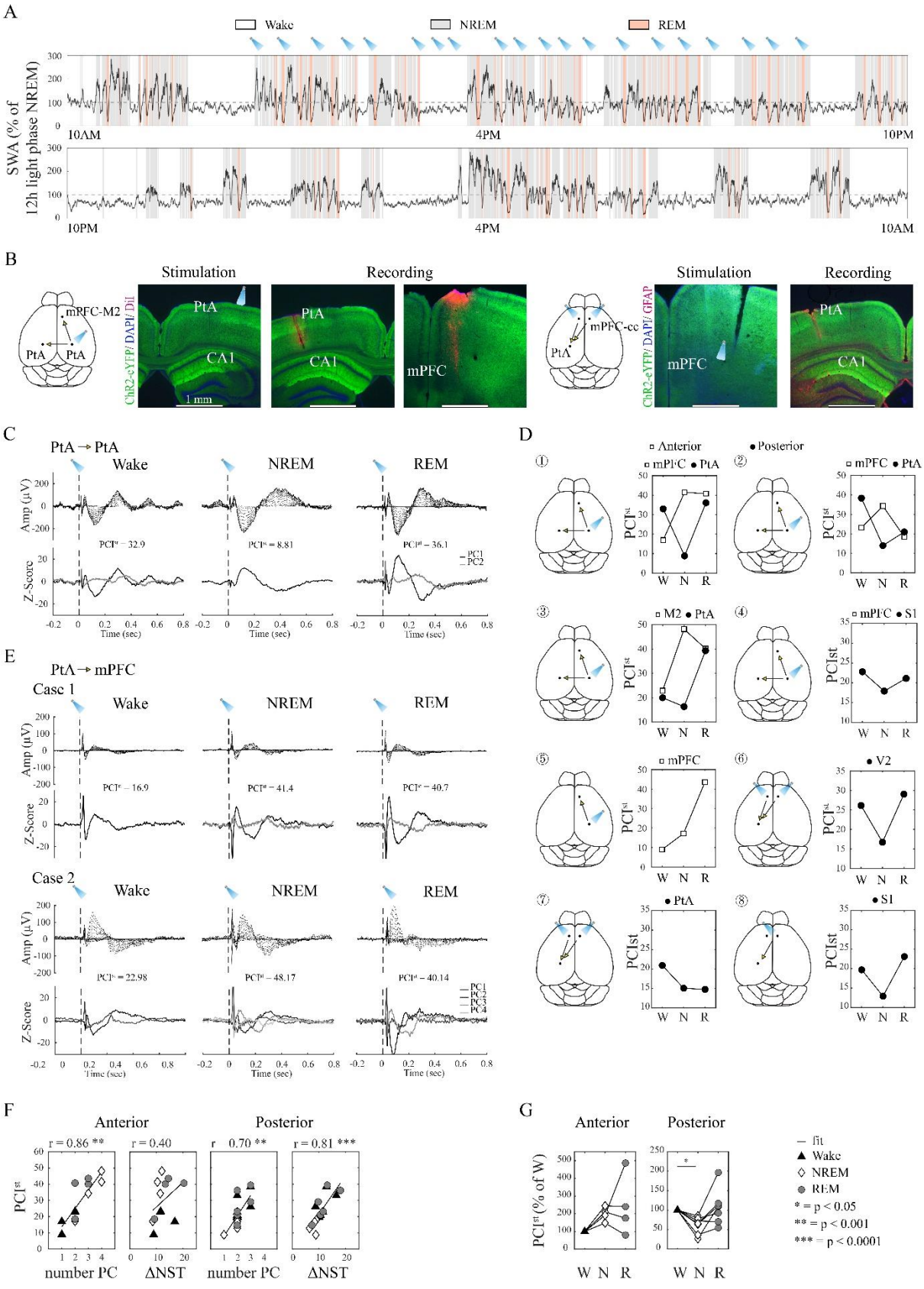
A
Wake
NREM
REM
SWA (% of 12h light phase NREM)
10AM
4PM
10PM
10PM
4PM
10AM
B
Stimulation
Recording
Stimulation
Recording
mPFC-M2
PtA
PtA
ChR2-eYFP/ DAPI/ DiI
CA1
1 mm
mPFC
mPFC-ec
GFAP
C
PtA → PtA
Wake
NREM
REM
Amp (μV)
Z-Score
Time (sec)
PC1
PC2
D
Anterior
Posterior
mPFC • PtA
M2 • PtA
mPFC • S1
mPFC
V2
PtA
S1
PCIst
W N R
E
PtA → mPFC
Case 1
Case 2
PC1
PC2
PC3
PC4
F
Anterior
Posterior
r = 0.86 **
r = 0.40
r 0.70 **
r = 0.81 ***
number PC
ΔNST
G
PCIst (% of W)
Fit
Wake
NREM
REM
* = p < 0.05
** = p < 0.001
*** = p < 0.0001

Figure 7. Anesthesia-induced changes in PCIst in mouse cortex. A,B example of ERPs and their principal components (PC) for two mice. **C**, schematic location of stimulating and recording electrodes in each animal, with corresponding PCIst values in wake (W) and anesthesia. Empty and filled symbols indicate more anterior and more posterior regions, respectively, where the recording electrode was located. Mice are arranged following the order in Figure 6 (anesthesia data are missing in 3 mice). Areas are labelled as in Figure 6. Cases in which ERPs were absent in wake (n = 3) are not included. **D,** group level changes in PCIst between wake and anesthesia.

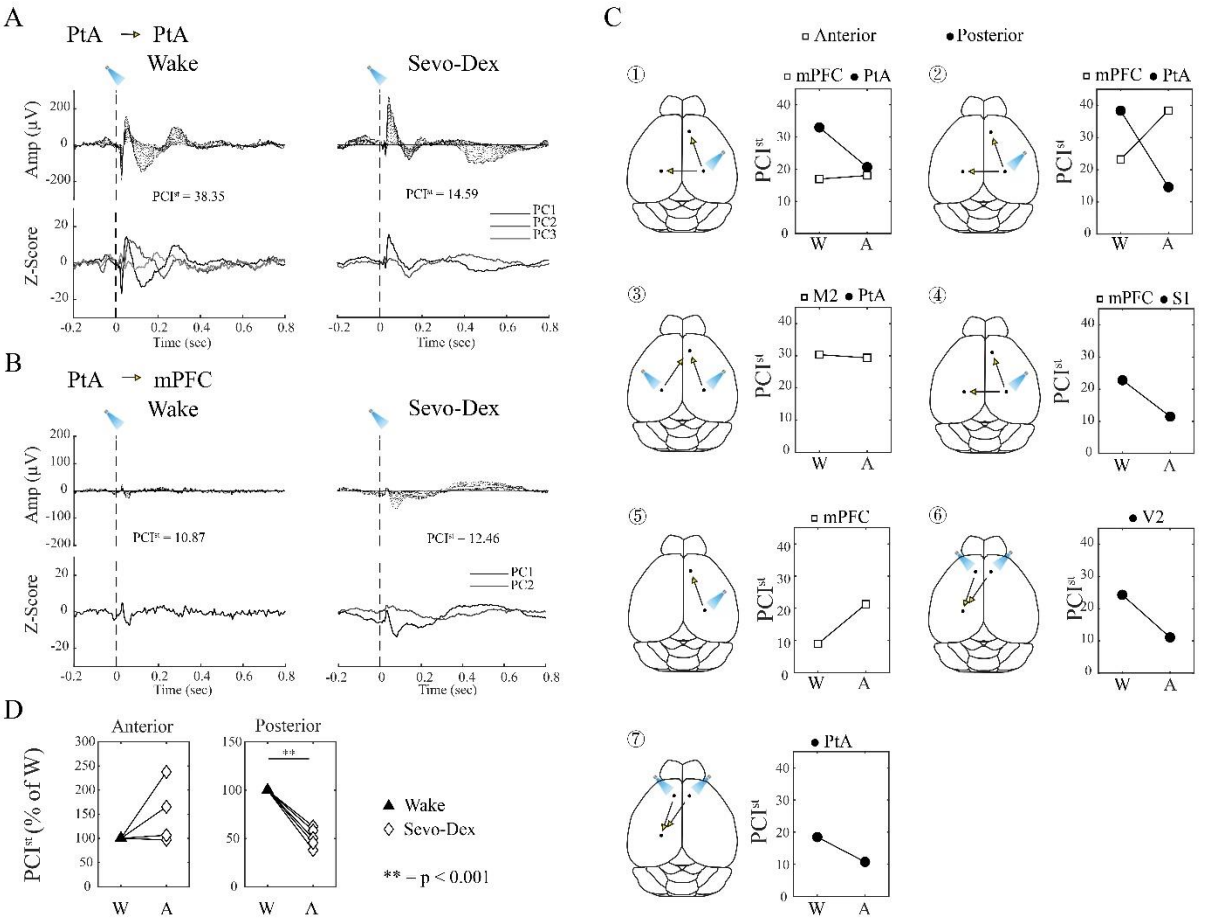

Figure 8. OFF periods triggered by optogenetic stimulation in mice. Four examples of ERPs (top), corresponding changes in firing rate across all trials (middle) and mean changes in firing rate (normalized to the wake values, NFR). In each example, the first and second cortical area indicate the site of stimulation and recording, respectively. OFFd, duration of the evoked OFF period.

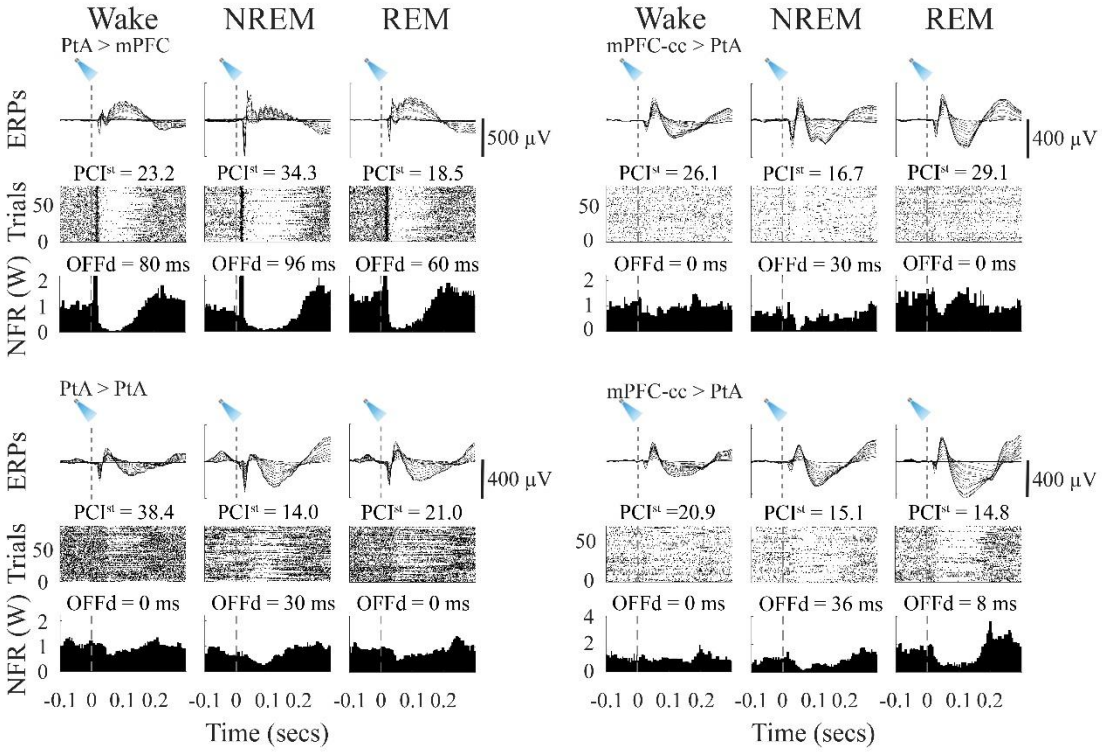

Figure 9. Effects of background activity. **A**, from left to right, coronal section from one representative rat showing the location of the Neuropixels probe spanning the dorsal hippocampus (CA1, DG); theta power (5-9 Hz) in the same rat, shown across all wake trials and as a function of recording depth; the peak of theta power is located in the stratum lacunosum moleculare; wake trials ranked according to max theta power. **B**, multi-unit activity peri-stimulus time histograms (PSTH) locked to electrical stimulation during wake in a parietal probe (PtA; normalized firing rate, FR). Trials were sorted by baseline theta power (last sec before the pulse, left) and by the duration of the evoked OFF periods (eOFF, right). **C**, correlation between normalized theta power and evoked OFF period duration (same example as in B). **D**, Group level changes (5 rats) in evoked OFF period duration for wake trials with the lowest 20% theta (LT) vs wake trials with the highest 20% theta (HT). **E**, Group level changes (5 rats) in PCI^{st} for LT and HT wake trials. **F-I**, same as in B-E, but for REM sleep trials. **J**, examples of PSTH locked to electrical stimulation during NREM sleep in a frontal probe (Of). Trials were sorted by the amount of time spent OFF during the last 500 ms before the pulse (bOFF; left) and by evoked OFF period duration (right). **K**, correlation between pre-pulse time spent OFF and evoked OFF period duration (same example as in J). **L,** Group level changes (6 rats) in evoked OFF period duration for NREM sleep trials with the lowest 20% total amount of time OFF (L bOFF) vs trials with the highest 20% (H bOFF; right). **M,** Group level changes (6 rats) in PCI^{st} for L bOFF and H bOFF trials. **N,O,** same as in L, M, for 3 mice.

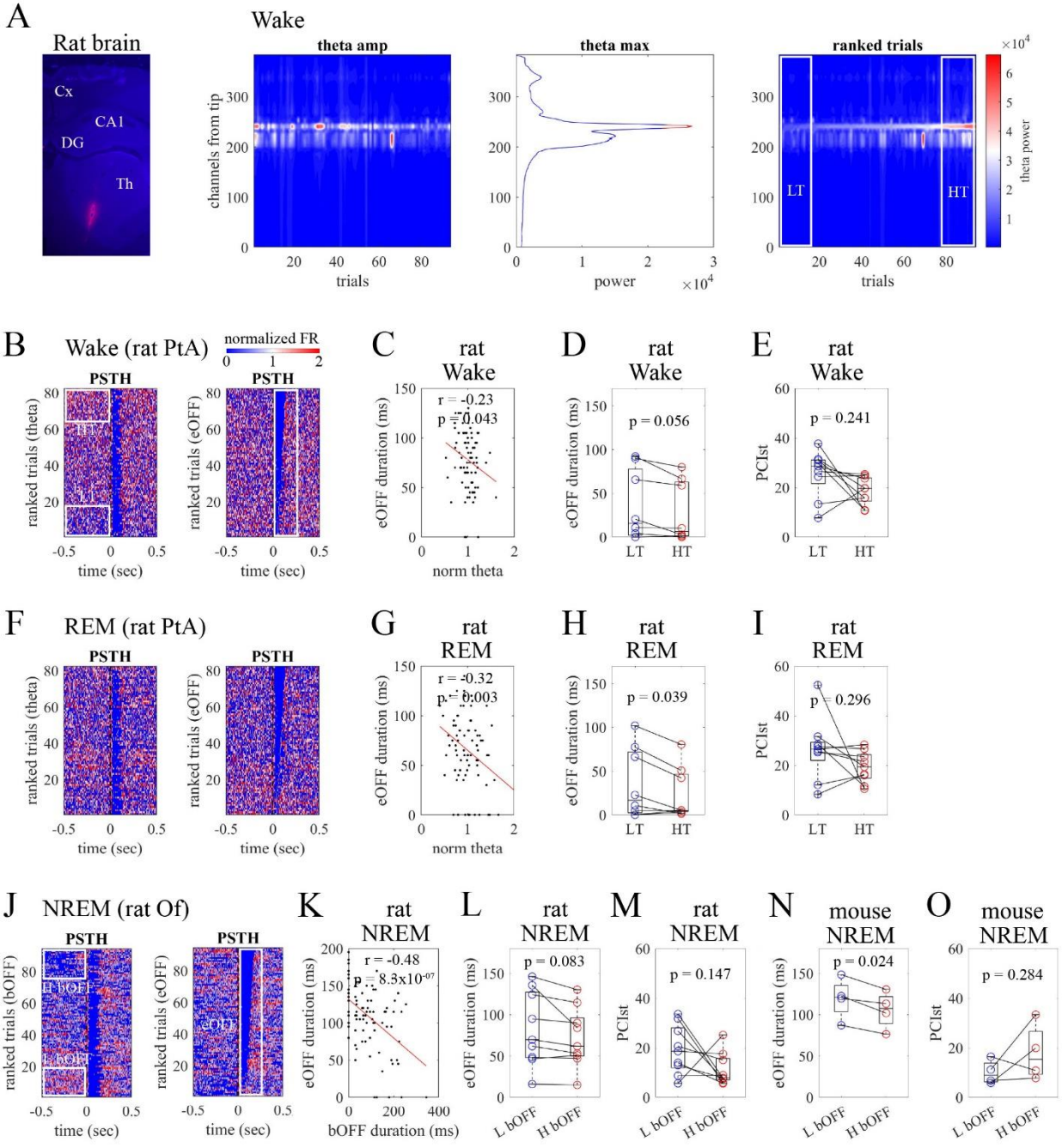
A
Rat brain
Cx
CA1
DG
Th
Wake
theta amp
channels from tip
trials
theta max
power
ranked trials
LT
HT
theta power
B
Wake (rat PtA)
normalized FR
PSTH
ranked trials (theta)
ranked trials (eOFF)
time (sec)
C
rat
Wake
r = -0.23
p = 0.043
eOFF duration (ms)
norm theta
D
rat
Wake
p = 0.056
E
rat
Wake
p = 0.241
PCIst
F
REM (rat PtA)
G
rat
REM
r = -0.32
p = 0.003
H
rat
REM
p = 0.039
I
rat
REM
p = 0.296
J
NREM (rat Of)
ranked trials (bOFF)
K
rat
NREM
r = -0.48
p = 8.3x10-07
bOFF duration (ms)
L
rat
NREM
p = 0.083
L bOFF
H bOFF
M
rat
NREM
p = 0.147
N
mouse
NREM
p = 0.024
O
mouse
NREM
p = 0.284

STAR METHODS

1. RESOURCE AVAILABILITY

- **Lead contact.** Additional information and requests for resources and reagents should be sent and will be fulfilled by the lead contact, Chiara Cirelli (ccirelli@wisc.edu).
- **Materials availability.** This study did not generate new unique reagents.
- **Data and code availability.** Data reported in this paper will be shared by the lead contact upon request. This paper does not report original code but the analysis scripts are available (https://github.com/cavelligonca/Cavelli-Mao-2022). Any additional information required to reanalyze the data reported in this paper is available from the lead contact upon request.

2. EXPERIMENTAL MODEL AND SUBJECT DETAILS

Experimental animals. Adult rats (Sprague Dawley, males, 300–340 g, 2-3 months old; RRID: RGD_734476) and adult mice (CaMKIIα::ChR2 mice, both sexes, 19-28 g, 2-3 months old) were maintained on a 12 h light/12 h dark cycle with food and water available ad libitum (21–26 °C, 30–40% relative humidity). CaMKIIα::ChR2 mice were obtained by crossing CaMKIIα-Cre mice (Jackson Laboratory; T29-1; RRID: IMSR_JAX:005359) with Cre-dependent ChR2(H134R)/EYFP expressing mice (Jackson Laboratory; Ai32; RRID: IMSR_JAX:024109). All animals were group housed until the time of surgery and randomly assigned to experimental

groups. All animals were healthy, drug naive, and were not used in previous procedures. All animal procedures and experimental protocols followed the National Institutes of Health Guide for the Care and Use of Laboratory Animals and were approved by the licensing committee. Animal facilities were reviewed and approved by the institutional animal care and use committee (IACUC) of the University of Wisconsin-Madison and were inspected and accredited by the association for assessment and accreditation of laboratory animal care (AAALAC).

3. METHOD DETAILS

Surgical procedures

Rats. Stereotactic implant of the recording and stimulation electrodes was performed under isoflurane anesthesia (3% induction, 1.5-2.5% maintenance). Using sterile techniques, a midline incision was made to expose the skull and after cleaning the surface with bonding agent (OptiBond™), several small burr holes were made in the skull using a dental drill. Two stainless steel screws (0.8 mm tip diameter) were implanted to serve as ground for the stimulation probe (over contralateral olfactory bulb) and ground and reference for the recording probes (over the cerebellum). A 16-channel probe (NeuroNexus Technologies; A1x16-3mm-100-703-CM16LP) was implanted perpendicular to the cortical surface to be used as stimulation electrode, together with 1 or 2 Neuropixels 1.0 recording electrodes [39]. The Neuropixels probes implanted in the frontal cortex (A/P +3.4, M/L +1.0 or A/P +4.2, M/L +2.0 angled towards the midline), reached secondary motor cortex (M2), prelimbic cortex (A32, PrL), or ventral/lateral orbital area (VO or LO). For simplicity, from here on we refer to VO and LO as orbitofrontal cortex (Of). In several animals, before insertion, the shank of the probes was coated with a red fluorescent cell-labeling

solution (CM-Dil, Thermo Fisher Scientific) for later electrode track localization in postmortem histology. After probe alignment, insertion was performed using a robotic micromanipulator (New Scale Technologies) at a speed of 5 µm/s. At the end of the insertion the holes were sealed with silicone elastomer (Kwik-Sil™) and electrodes and probes were fixed to the skull using dental cement (C&B Metabond®). The implant was protected using a 3D-printed headcap based on the OpenEphys shuttleDrive enclosure [40]. At the end of surgery the margins of the implant were cleaned and antibiotic ointment was applied.

Mice. Surgery was performed under isoflurane anesthesia (2.0% induction; 0.8-1.5% maintenance) following sterile techniques. CaMKIIα::ChR2 mice of both sexes were implanted with optic fibers (Doric Lenses; core diameter = 200µm; NA = 0.22; diffuser layer tip) for optogenetic stimulations in either posterior (n = 9; 3 females) or anterior (n = 3; 1 female) cortex. For mice with posterior stimulation, optic fibers were placed on the cortical surface over the posterior parietal association cortex (PtA) (A/P -2.00, M/L ±1.80). For mice with anterior stimulation, optic fibers were implanted deeply in the cortex (A/P +1.93, M/L ±1.65, or A/P +1.77, M/L -0.60, angled towards the midline), to target anterior cingulate cortex (i.e., A24, Cg) and infralimbic cortex (i.e. A25, IL). For simplicity, from here on we refer to this targeted region together with PrL as mPFC (medial prefrontal cortex) [41-43].

To perform electrophysiology recordings, all mice were also implanted with laminar silicon probes (NeuroNexus Technologies; A1x16-3mm-50-177-CM16LP, A1x16-5mm-50-177-CM16LP, or A4x4-3mm-50-125-177-CM16LP), EEG and electromyogram (EMG) electrodes. To facilitate histological localization, in some cases the silicon probe shanks were coated with CM-DiI immediately before implantation. A right frontal silicon probe was implanted deeply in the

cortex (A/P +1.93, M/L +0.40, or A/P +1.77, M/L +0.50, angled towards the midline), with electrodes targeting mPFC (Cg, IL or PrL). A left posterior parietal silicon probe was implanted in PtA (A/P -2.00, M/L -2.20), with electrodes targeting all layers. Reference screws were implanted over the cerebellum and olfactory bulb. EEG screw electrodes were implanted over left M2 (A/P +2.50, M/L -1.50) and right secondary somatosensory cortex (S2; A/P -1.30, M/L +4.0). EMG stainless steel wires were implanted bilaterally in the dorsal neck musculature and in the whisker musculature. The craniotomies and silicon probes were covered with surgical silicone adhesive (Kwik-Sil™), and all implants were fixed to the skull with dental cement (C&B-Metabond®, Fusio™ or Flow-It™ ALC™, Pentron).

Experimental procedures and design

***Rats*.** After surgery, all rats were kept in a temperature-controlled room (21-24 ° C) with a 12:12 light/dark cycle (light on at 9am) and with water and food available *ad libitum*. Rats were single housed in a transparent recording box (53 x 32 x 46 cm) containing bedding material and fully enclosed in a Faraday cage. After at least one week of recovery, the probes were connected to the recording system through a protection spring linked to a commutator, to allow free movements. After two days of adaptation, continuous recordings were performed for at least 48 hours to evaluate the sleep/wake pattern in baseline conditions, followed by 6 hours of sleep deprivation with novel objects (9am to 3pm) and subsequent sleep rebound (3pm to 9am the next day) to assess the homeostatic response to sleep loss (see OFF period analysis). Several days after sleep deprivation the stimulation sessions started and were conducted only during the light period, between 10am and 8pm, during wake, NREM sleep, REM sleep, as well as during anesthesia with sevoflurane (2%) or dexmedetomidine (0.1 mg/kg, IP). Most of the rats were exposed to both

anesthetics in a randomized order. Electrical stimulation of the cortical tissue was performed by delivering a vertical, 200-300 μm, bipolar, monophasic, current pulse of 0.5 ms of various intensities (30-100 μA across rats). The depth of stimulation varied across experiments, always with cathode ventral. In each animal, a single stimulation intensity was used, corresponding to the weakest stimulus capable of triggering a slow wave during NREM sleep [44]. Local field potentials (LFPs) and behavior were continuously monitored by the experimenter and stimuli were delivered only during consolidated episodes of wake and sleep, with the final goal of collecting 110 pulses for each behavioral state. In each session, stimuli were spaced apart at least 10 seconds, with often longer intervals to avoid sleep/wake state transitions. Shorter intervals (at least 4 secs) were sometimes used for REM sleep, whose bouts normally last approximately 100 secs and account for less than 10% of the total behavioral time [45]. In each rat stimulation sessions spanned 2 to 4 weeks, interleaved with resting periods of at least 48 hours.

Mice. After surgery, all mice were kept in a temperature-controlled room (24-26 ° C) with a 12:12 light/dark cycle (light on at 10am) and with water and food available *ad libitum*. Mice were individually housed in transparent plastic cages (Allentown Caging; 24.5 x 21.5 x 21cm). The implanted silicon probes, electrodes and optic fibers were connected to the recording/stimulation system around one week after surgery to allow for recovery. Baseline recordings were acquired after the mice were accustomed to the system, then the experiments started after the temporal organization of sleep and wakefulness had normalized. All stimulation sessions were conducted during the light period. The implanted optic fibers were connected to a blue laser station (473nm, OEM Laser Systems DPSSL Driver, 100mW), which is triggered by the TDT system, with the laser output power manually controlled by an analog control knob on

the driver. Based on the excitation threshold of specific opsins [46-48], and the intended activation radius in the target area, the laser power to start with was estimated based on an established online calculator (https://web.stanford.edu/group/dlab/cgi-bin/graph/chart.php), which is modeled based on direct measurements in mammalian brain tissue. Laser power ranged from 0.2 to 2.9 mW (across mice) at the tip of the optic fiber, and laser trains (8ms pulse width, 2000ms off between pulses, around 15 pulses per train) were delivered. Like in rats, the stimulation amplitude in each mouse was set as the weakest one capable of triggering a slow wave during NREM sleep. Behavior and electrophysiology data were continuously monitored by the experimenter, and stimuli were delivered during wake, NREM sleep, REM sleep, and under anesthesia with sevoflurane (1.0-2.0%) co-administered with dexmedetomidine (70-100 μg/kg, IP). The final goal was to collect around 80 pulses for each consolidated behavioral state.

Histology

Rats. At the end of the last recording session, under general anesthesia (isoflurane 2-3%), rats were intracardially perfused with PBS (phosphate buffer solution with heparin 5000 IU/l) and 4% paraformaldehyde (PFA) in PBS for tissue fixation. Brains were then extracted and processed for histology. After fixation, brains were cryoprotected by exposure to increasing concentration of sucrose in PBS solutions at 4°C. Brains were then quickly frozen and sliced in coronal sections (40-50 μm thick) with a cryostat (Thermo Fisher Scientific; CryoStar^{TM} NX50). Sections were dried overnight and mounted with medium containing DAPI (SouthernBiotech^{TM}; DAPI-Fluoromount-G). In some animals in which CM-DiI was not applied the sections were subjected to cresyl-violet (Nissl) staining. To verify the probe location sections were imaged with an upright epifluorescence microscope (Leica; DM2500).

Mice. To verify opsin expression, recording and cannula locations, mice were transcardially perfused under deep anesthesia (3.0% isoflurane, with a flush (~30 s) of saline followed by 4% paraformaldehyde (PFA) in phosphate buffer (PB). Brains were removed and postfixed for 24 h in the same fixative, then cut in 50um thick coronal sections on a cryostat (CryoStar^{TM} NX50 or Leica CM1900) after cryoprotection and flash-freezing. Sections were collected in PBS, mounted, air-dried, cover slipped (DAPI-Fluoromount-G, Vectashield, or Permount) and examined under a fluorescent or confocal microscope (Leica, Olympus). In some animals, to localize the silicon probes without fluorescent dye coating, glial fibrillary acidic protein (GFAP) staining was performed (rabbit-anti-GFAP primary antibody, DAKO Z0334, 1:1000 in blocking solution; Donkey-anti-Rabbit AF594 secondary antibody, 1:500 in blocking solution). In some cases Crystal Violet staining was performed to better visualize the location of the cannulas. To characterize the opsin expression of the CaMKIIα::ChR2 mice, in pilot experiments in 2 mice eYFP amplification staining was performed (rabbit anti-GFP primary antibody, Invitrogen, A11122, 1:1000 in blocking solution; goat anti-rabbit Alexa-488 conjugated secondary antibody, Invitrogen, A11008, 1:1000 in blocking solution).

Electrophysiological recordings and stimulation

Rats. Electrophysiological recordings were performed using available Neuropixels 1.0 acquisition hardware [49]. Neuropixels probes consist of a single shank (70 µm wide; 24 µm thick, 10 mm long) with 960 electrodes (2 columns; inter-electrode distance 20 µm), of which 384 can be recorded simultaneously (neuropixels.org). All experiments used the same electrode mapping, with a simple column expanding for 7.64 mm starting at the tip of the probe. Probes were connected to a head stage that transmit the data to a PXIe acquisition module mounted in a PXI

chassis (National Instruments; PXIe-1071 chassis). The SpikeGLX software was used to acquire and visualize the data (https://github.com/billkarsh/SpikeGLX). In each probe the signal was amplified (x 500), digitized (10 bits) and filtered in two bands, one for the LFPs (0.5-500 Hz) and one for action potentials (AP; 0.3-10 kHz). LFP and AP signals were digitized at 2.5 and 30 kHz respectively with some small variation applicable after in brain calibration. Electrical stimulation was performed using a battery-powered 32 channels microstimulator system (Tucker-Davis Technologies; IZ2-32) connected to the 16 channels probe throughout a passive head stage and controlled with an electrophysiological recording software (Tucker-Davis Technologies; Synapse). Stimulus parameters and applied currents were recorded simultaneously in all channels.

All sessions were recorded with video (White Matter LLC; e3Vision system), and all data streams (video, stimulation, electrophysiology, etc.) were synchronized off-line using digital barcodes as described by the DAQ Synchronization Project from the Optogenetics and Neural Engineering Core at the University of Colorado Denver (https://optogeneticsandneuralengineeringcore.gitlab.io/ONECoreSite/projects/DAQSyncronization/).

Mice. Electrophysiological recording and optogenetic stimulation were performed using RZ2 BioAmp processor and OpenEx software (Tucker-Davis Technologies). Silicon probes were connected through a head stage to an amplifier (Tucker-Davis Technologies; PZ5 NeuroDigitizer Amplifier) before reaching the RZ2 processor. EEGs and LFPs were filtered by 0.1-100Hz, and multi-unit activities (MUAs) were filtered by 0.3-5kHz. Sampling rate for storage was 256Hz for LFPs, EEGs and EMGs; 25kHz for MUAs. Spike data were collected discreetly from the same LFPs channels. Amplitude thresholds for online spike detection were set manually based on visual

control. Whenever the recorded voltage exceeded a predefined threshold, a segment of 46 samples (0.48 ms before, 1.36 ms after the threshold crossing) was extracted and stored for later use. All sessions were recorded with video.

Sleep scoring and data processing

Sleep scoring was performed manually using a fork (https://github.com/TomBugnon/visbrain) of Visbrain Sleep [50], which includes several enhancements to facilitate the scoring of non-human sleep. Analysis of electrophysiological data was performed in MATLAB R2019b and R2021b (MathWorks®). LFP data were visually inspected to remove artefacts. Isolated bad channels were replaced by the mean of the immediately surrounding good channels. All LFP channels were subjected to linear detrend and lowpass filtering (200 Hz), using a zero-phase distortion third order Butterworth filter. Single trials were extracted in a ±4 sec window using stimulation time as zero. All trials and channels were visually inspected (SpikeGLX). Trials were discarded if there were artifacts in the few seconds around the stimulus, or when the stimulus was delivered close to a sleep/wake transition.

PCIst

The spatiotemporal complexity of cortical event related potentials (ERPs) was quantified using a variant of the original perturbational complexity index or PCI [1,51], called the PCI state transition (PCIst) variant [6]. With this method the principal components accounting for at least 99% of the variance present in the ERP response are obtained through singular value decomposition and then selected based on their own baseline level (signal-to-noise ratio, SNR_{min}). The number of state transitions (NST) is then measured for each principal component during baseline (-800 to -100 msecs) and after the stimulus (10 to 800 msecs). NST is a measurement adapted from recurrent

quantification analysis over the ERP distance matrices [6]. PCI^{st} is the sum of the differences in NST between the baseline and the response for each principal component. Results did not significantly change depending on whether the post-stimulus time interval used for the analysis started 10 msec after the stimulus or at the peak or the end of the slow wave induced by the stimulation, nor did they change when the duration of the post-stimulus time interval increased from 10-800 msec to 10-1000 msec.

Phase Locking Factor (PLF)

The instantaneous PLF was calculated as in [9,52] to determine how the stimulation affected the phase of ongoing oscillations across trials. To focus on phase coupling that could only be explained by the stimulus, we assumed a Rayleigh distribution of the PLF values during baseline (-600 to -100 ms), and then performed a statistical comparison with the baseline for each electrode. PLF values below threshold ($\alpha < 0.05$) were set to zero. Initially, the spectral PLF contribution was calculated using a moving band pass filter window that ranged from 0 to 200 Hz (4 Hz width; 2 Hz superposition) and for each band the instantaneous PLF was calculated. In agreement with previous experiments in humans [9], this analysis revealed that the 8 to 40 Hz frequencies, encompassing the alpha and beta bands, but not the higher frequencies (40-200 Hz), were useful to distinguish between wake and NREM sleep, as well to distinguish between NREM sleep and REM sleep. Thus, all final PLF analyses used the 8 to 40 Hz frequency range.

Detection of spontaneous and evoked slow waves

Detection of individual slow waves was performed as previously described [44,53,54] on the spontaneous LFP signal during baseline sleep, recovery sleep after sleep deprivation (3PM to 5PM) and during the induction of slow waves by electrical stimulation. From the continuous

recording, all NREM windows were extracted based on standard criteria for scoring vigilance states: wake was characterized by a low-voltage, high-frequency LFP activity and phasic muscle activity; NREM sleep was characterized by the occurrence of high-amplitude slow waves, spindles, and low tonic muscle activity; in REM sleep, cortical LFPs resembled those seen in wake but muscle tone was absent, with the exception of occasional twitches. Waveforms were detected using a bipolar transcortical arrangement [44] between deep and superficial LFPs cortical channels (layers 5-6 vs layers 1-2). The signal was first filtered in the slow activity band (0.5-4 Hz; Chebyshev Type II filter) and all positive and negative peaks were detected. Slow waves were defined as positive deflections between two consecutive negative deflections below the zero-crossing with a duration of at least 100 ms, as in previous studies [53]. Only slow wave with an amplitude greater than the 75th percentile were used [17]. Slow wave polarity reversal in the dorsoventral axis, along with the presence of a peak in high gamma power in mid-layer 5, and histology were used to estimate the electrode location [17,37,38,55].

Spike analysis

Preprocessing. Recordings were preprocessed separately with the CatGT command-line tool (github.com/billkarsh/SpikeGLX), performing 300–9000Hz band-pass filtering, global demultiplexing common average referencing and automatic artifact detection and removal with default parameters.

Spike sorting. For each animal, probe and each stimulation depth, the preprocessed recordings containing the wake, NREM sleep and REM sleep pulses were then concatenated into a single recording on which spike sorting was performed using the Kilosort2.5 algorithm [11]. Recordings for the sevoflurane condition were sorted separately. In order to account for fast and

slow drift, the algorithm first performs a drift correction pre-processing step [56]: for each temporal batch, a fingerprint of the distribution of units along the probe is constructed from the histogram of spike amplitudes at each channel. This fingerprint is used to compute, for each temporal batch, the vertical offset of each channel relative to a template obtained from iterative averaging of the rigidly aligned fingerprints. The data used for sorting is then corrected using kriging interpolation. Since we did not observe significant drift on fast timescales, we used 8 sec batches (instead of the default 2 sec) to increase the reliability of the batches' fingerprint. Besides the batch size, we used default values for all but two kilosort parameters: the projection thresholds *Th* were set to [12 10] instead of [10 5] and *lambda* was set to 50 instead of 10, as we observed that these values reduced the number of putative false positive spike detections in our data.

Postprocessing, curation and unit selection. We used Jennifer Colonnell's fork of the Allen institute's *ecephys_spike_sorting* toolbox to postprocess kilosort's output (https://github.com/jenniferColonell/ecephys_spike_sorting). This allowed us to mark some of the clusters as noise based on their template's spatial and temporal spread and remove the spikes occasionally double-counted by Kilosort. We then removed the remaining noise clusters using *phy* (https://github.com/cortex-lab/phy). Finally, we excluded all clusters with firing rate below 0.5 Hz. Overall, the total number of clusters throughout the probe selected for further analyses ranged from 65 to 402. Sorting data was extracted using the *SpikeInterface* toolbox [57].

OFF period detection

Peri stimulus time histograms (PSTH). For the analysis of spikes locked to electrical or optogenetic stimulation, all time stamps corresponding to individual spike occurrences were concatenated across all recording channels showing single and/or multi-unit activity. 4 ms bin

firing rate from -1 to +1 seconds, relative to stimulation time, was isolated and normalized to the baseline firing rate, defined as 1 to 0.4 seconds before the stimulation during wake.

Peri slow wave time histograms (PSWTH). For the analysis of spikes locked to slow waves, all time stamps corresponding to individual spike occurrences were concatenated across all recording channels showing single and/or multi-unit activity. 4 ms bin firing rate from -1 to +1 seconds, relative to the slow-wave zero crossing, was isolated and normalized to the baseline firing rate, defined as 1 to 0.4 seconds before the slow wave zero crossing.

***OFF periods*.** Using both PSTH and PSWTH, the time when the firing rate drops below 25% of the baseline was defined as the onset of the OFF period, while the start of the ON period was defined as the time when the firing rate rose above 25% of the baseline. OFF duration is equal to ON start time minus OFF start time. Similar criteria were used at the single trial level to detect the evoked OFF periods and the amount of time OFF during the period before the stimulation. "Effectiveness" was defined as the percentage of trials with evoked OFF periods of at least 30 ms.

Current source density analysis (CSD)

For CSD analysis [55,58] the following formula was applied:

$$Im = (1/R) = (\Phi i + 10 - 2\,\Phi i + \Phi i\text{-}10) / (Z2),$$

where Φi is the field potential in mV at a given electrode i, R is in MΩ, Z is the distance between electrodes in mm, Im is CSD in μV/μm2. Im > 0 and Im < 0 indicate Source (outward current) and Sink (inward current), respectively.

4. QUANTIFICATION AND STATISTICAL ANALYSIS

The data were expressed as mean ± standard deviation. The significance of the differences among behavioral states was evaluated with repeated measures ANOVA, with the Greenhouse-Geisser correction, along with Tukey post hoc tests. For the comparison between waking and anesthesia a paired t-test was performed. A measure of effect size was reported for rmANOVA (η^2) and t-test (d). The criterion used to reject null hypotheses was $p < 0.05$. Details can be found in the results and figure legends.

KEY RESOURCES TABLE

REAGENT or RESOURCE	SOURCE	IDENTIFIER
Antibodies		
Rabbit Polyclonal Anti-Glial Fibrillary Acidic Protein	Agilent	Cat# Z0334; RRID: AB_10013382
Donkey Polyclonal Anti-Rabbit	Jackson ImmunoResearch	Cat# 711-585-152; RRID: AB_2340621
Experimental models: Organisms/strains		
Mouse: B6.Cg-Tg(Camk2a-cre)T29-1Stl/J	The Jackson Laboratory	RRID: IMSR_JAX:005359
Mouse: B6.Cg-Gt(ROSA)26Sor$^{tm32(CAG-COP4*H134R/EYFP)Hze}$/J	The Jackson Laboratory	RRID: IMSR_JAX:024109
Rat: Sprague Dawley Crl:CD(SD)	Charles River	RRID: RGD_734476
Software and algorithms		
MATLAB R2019b and R2021b	MathWorks	https://www.mathworks.com/products/matlab.html
SpikeGLX software	github	http://billkarsh.github.io/SpikeGLX/
Synapse software	TDT Tuker-Davis Technologies	https://www.tdt.com/component/synapse-software/
OpenEx software	TDT Tuker-Davis Technologies	https://www.tdt.com/component/openex-software-suite/
e3Vision software	White Matter	https://white-matter.com/products/e3vision/

DAQ Synchronization	Project from the Optogenetics and Neural Engineering Core at the University of Colorado Denver	https://optogeneticsandneuralengineeringcore.gitlab.io/ONECoreSite/projects/DAQSyncronization/
Visbrain Sleep	github	https://github.com/TomBugnon/visbrain
KiloSort 2.5	github	https://github.com/cortex-lab/KiloSort
ecephys_spike_sorting toolbox	github	https://github.com/jenniferColonell/ecephys_spike_sorting
Phy	github	https://github.com/cortex-lab/phy
Spike Interface	github	https://github.com/SpikeInterface/spikeinterface
mtspecgramc function	http://chronux.org/	http://chronux.org/chronuxFiles/Documentation/chronux/spectral_analysis/continuous/mtspecgramc.html
PCIst function	github	https://github.com/renzocom/PCIst
Cavelli-Mao-2022 code	github	https://github.com/cavelligonca/Cavelli-Mao-2022

References

1. Casali, A.G., Gosseries, O., Rosanova, M., Boly, M., Sarasso, S., Casali, K.R., Casarotto, S., Bruno, M.-A., Laureys, S., Tononi, G., and Massimini, M. (2013). A theoretically based index of consciousness independent of sensory processing and behavior. Sci Transl Med *5*, 198ra105-198ra105.
2. Tononi, G. (2004). An information integration theory of consciousness. BMC neuroscience *5*, 42. 1471-2202-5-42 [pii] 10.1186/1471-2202-5-42.
3. Tononi, G., Boly, M., Massimini, M., and Koch, C. (2016). Integrated information theory: from consciousness to its physical substrate. Nat Rev Neurosci *17*, 450-461. 10.1038/nrn.2016.44.
4. Tononi, G., Sporns, O., and Edelman, G.M. (1994). A measure for brain complexity: relating functional segregation and integration in the nervous system. Proceedings of the National Academy of Sciences of the United States of America *91*, 5033-5037.
5. Casarotto, S., Comanducci, A., Rosanova, M., Sarasso, S., Fecchio, M., Napolitani, M., Pigorini, A., A, G.C., Trimarchi, P.D., Boly, M., et al. (2016). Stratification of unresponsive patients by an independently validated index of brain complexity. Ann Neurol *80*, 718-729. 10.1002/ana.24779.
6. Comolatti, R., Pigorini, A., Casarotto, S., Fecchio, M., Faria, G., Sarasso, S., Rosanova, M., Gosseries, O., Boly, M., Bodart, O., et al. (2019). A fast and general method to empirically estimate the complexity of brain responses to transcranial and intracranial stimulations. Brain stimulation *12*, 1280-1289. 10.1016/j.brs.2019.05.013.
7. Sarasso, S., Casali, A., Casarotto, S., Rosanova, M., Sinigaglia, C., and M, M. (2021). Consciousness and complexity: a consilience of evidence Neuroscience of Consciousness, niab023.
8. Steriade, M., Nunez, A., and Amzica, F. (1993). A novel slow (< 1 Hz) oscillation of neocortical neurons in vivo: depolarizing and hyperpolarizing components. The Journal of neuroscience : the official journal of the Society for Neuroscience *13*, 3252-3265.
9. Pigorini, A., Sarasso, S., Proserpio, P., Szymanski, C., Arnulfo, G., Casarotto, S., Fecchio, M., Rosanova, M., Mariotti, M., Lo Russo, G., et al. (2015). Bistability breaks-off deterministic responses to intracortical stimulation during non-REM sleep. NeuroImage *112*, 105-113. 10.1016/j.neuroimage.2015.02.056.
10. Arena, A., Comolatti, R., Thon, S., Casali, A.G., and Storm, J.F. (2021). General Anesthesia Disrupts Complex Cortical Dynamics in Response to Intracranial Electrical Stimulation in Rats. eNeuro *8*. 10.1523/ENEURO.0343-20.2021.
11. Pachitariu, M., Steinmetz, N., Kadir, S., Carandini, M., and D, H.K. (2016). Kilosort: Realtime Spike-Sorting for Extracellular Electrophysiology with Hundreds of Channels. Preprint. Neuroscience. , https://doi.org/10.1101/061481.
12. Stark, E., Roux, L., Eichler, R., Senzai, Y., Royer, S., and Buzsaki, G. (2014). Pyramidal cell-interneuron interactions underlie hippocampal ripple oscillations. Neuron *83*, 467-480. 10.1016/j.neuron.2014.06.023.
13. Zhou, H., Neville, K.R., Goldstein, N., Kabu, S., Kausar, N., Ye, R., Nguyen, T.T., Gelwan, N., Hyman, B.T., and Gomperts, S.N. (2019). Cholinergic modulation of hippocampal calcium activity across the sleep-wake cycle. Elife *8*. 10.7554/eLife.39777.

14. Dong, Y., Li, J., Zhou, M., Du, Y., and Liu, D. (2022). Cortical regulation of two-stage rapid eye movement sleep. Nature neuroscience *25*, 1675-1682. 10.1038/s41593-022-01195-2.
15. Cavelli, M., Rojas-Libano, D., Schwarzkopf, N., Castro-Zaballa, S., Gonzalez, J., Mondino, A., Santana, N., Benedetto, L., Falconi, A., and Torterolo, P. (2018). Power and coherence of cortical high-frequency oscillations during wakefulness and sleep. The European journal of neuroscience *48*, 2728-2737. 10.1111/ejn.13718.
16. Siclari, F., Baird, B., Perogamvros, L., Bernardi, G., LaRocque, J.J., Riedner, B., Boly, M., Postle, B.R., and Tononi, G. (2017). The neural correlates of dreaming. Nature neuroscience *20*, 872-878. 10.1038/nn.4545.
17. Funk, C.M., Peelman, K., Bellesi, M., Marshall, W., Cirelli, C., and Tononi, G. (2017). Role of Somatostatin-Positive Cortical Interneurons in the Generation of Sleep Slow Waves. The Journal of neuroscience : the official journal of the Society for Neuroscience *37*, 9132-9148. 10.1523/JNEUROSCI.1303-17.2017.
18. Maier, A., Adams, G.K., Aura, C., and Leopold, D.A. (2010). Distinct superficial and deep laminar domains of activity in the visual cortex during rest and stimulation. Front Syst Neurosci *4*. 10.3389/fnsys.2010.00031.
19. Buffalo, E.A., Fries, P., Landman, R., Buschman, T.J., and Desimone, R. (2011). Laminar differences in gamma and alpha coherence in the ventral stream. Proceedings of the National Academy of Sciences of the United States of America *108*, 11262-11267. 1011284108 [pii]
10.1073/pnas.1011284108.
20. Bastos, A.M., Loonis, R., Kornblith, S., Lundqvist, M., and Miller, E.K. (2018). Laminar recordings in frontal cortex suggest distinct layers for maintenance and control of working memory. Proceedings of the National Academy of Sciences of the United States of America *115*, 1117-1122. 10.1073/pnas.1710323115.
21. Bollimunta, A., Chen, Y., Schroeder, C.E., and Ding, M. (2008). Neuronal mechanisms of cortical alpha oscillations in awake-behaving macaques. The Journal of neuroscience : the official journal of the Society for Neuroscience *28*, 9976-9988. 10.1523/JNEUROSCI.2699-08.2008.
22. Haegens, S., Barczak, A., Musacchia, G., Lipton, M.L., Mehta, A.D., Lakatos, P., and Schroeder, C.E. (2015). Laminar Profile and Physiology of the alpha Rhythm in Primary Visual, Auditory, and Somatosensory Regions of Neocortex. The Journal of neuroscience : the official journal of the Society for Neuroscience *35*, 14341-14352. 10.1523/JNEUROSCI.0600-15.2015.
23. Lakatos, P., Chen, C.M., O'Connell, M.N., Mills, A., and Schroeder, C.E. (2007). Neuronal oscillations and multisensory interaction in primary auditory cortex. Neuron *53*, 279-292. S0896-6273(06)00996-2 [pii]
10.1016/j.neuron.2006.12.011.
24. van Kerkoerle, T., Self, M.W., Dagnino, B., Gariel-Mathis, M.A., Poort, J., van der Togt, C., and Roelfsema, P.R. (2014). Alpha and gamma oscillations characterize feedback and feedforward processing in monkey visual cortex. Proceedings of the National Academy of Sciences of the United States of America *111*, 14332-14341. 10.1073/pnas.1402773111.

25. Sakata, S., and Harris, K.D. (2009). Laminar structure of spontaneous and sensory-evoked population activity in auditory cortex. Neuron *64*, 404-418. 10.1016/j.neuron.2009.09.020.
26. Harris, K.D., and Shepherd, G.M. (2015). The neocortical circuit: themes and variations. Nature neuroscience *18*, 170-181. 10.1038/nn.3917.
27. He, B.J., and Raichle, M.E. (2009). The fMRI signal, slow cortical potential and consciousness. Trends in cognitive sciences *13*, 302-309. S1364-6613(09)00116-8 [pii] 10.1016/j.tics.2009.04.004.
28. Pins, D., and Ffytche, D. (2003). The neural correlates of conscious vision. Cerebral cortex *13*, 461-474.
29. Dembski, C., Koch, C., and Pitts, M. (2021). Perceptual awareness negativity: a physiological correlate of sensory consciousness. Trends in cognitive sciences *25*, 660-670. 10.1016/j.tics.2021.05.009.
30. Suzuki, M., and Larkum, M.E. (2020). General Anesthesia Decouples Cortical Pyramidal Neurons. Cell *180*, 666-676 e613. 10.1016/j.cell.2020.01.024.
31. Urbain, N., Fourcaud-Trocme, N., Laheux, S., Salin, P.A., and Gentet, L.J. (2019). Brain-State-Dependent Modulation of Neuronal Firing and Membrane Potential Dynamics in the Somatosensory Thalamus during Natural Sleep. Cell Rep *26*, 1443-1457 e1445. 10.1016/j.celrep.2019.01.038.
32. Crunelli, V., and Hughes, S.W. (2010). The slow (<1 Hz) rhythm of non-REM sleep: a dialogue between three cardinal oscillators. Nature neuroscience *13*, 9-17. 10.1038/nn.2445.
33. Van De Werd, H.J., Rajkowska, G., Evers, P., and Uylings, H.B. (2010). Cytoarchitectonic and chemoarchitectonic characterization of the prefrontal cortical areas in the mouse. Brain structure & function *214*, 339-353. 10.1007/s00429-010-0247-z.
34. Boly, M., Massimini, M., Tsuchiya, N., Postle, B.R., Koch, C., and Tononi, G. (2017). Are the Neural Correlates of Consciousness in the Front or in the Back of the Cerebral Cortex? Clinical and Neuroimaging Evidence. The Journal of neuroscience : the official journal of the Society for Neuroscience *37*, 9603-9613. 10.1523/JNEUROSCI.3218-16.2017.
35. Fuller, P.M., Sherman, D., Pedersen, N.P., Saper, C.B., and Lu, J. (2011). Reassessment of the structural basis of the ascending arousal system. J Comp Neurol *519*, 933-956. 10.1002/cne.22559.
36. Gao, S., and Calderon, D.P. (2020). Robust alternative to the righting reflex to assess arousal in rodents. Sci Rep *10*, 20280. 10.1038/s41598-020-77162-3.
37. Valero, M., Viney, T.J., Machold, R., Mederos, S., Zutshi, I., Schuman, B., Senzai, Y., Rudy, B., and Buzsaki, G. (2021). Sleep down state-active ID2/Nkx2.1 interneurons in the neocortex. Nature neuroscience *24*, 401-411. 10.1038/s41593-021-00797-6.
38. Senzai, Y., Fernandez-Ruiz, A., and Buzsaki, G. (2019). Layer-Specific Physiological Features and Interlaminar Interactions in the Primary Visual Cortex of the Mouse. Neuron *101*, 500-513 e505. 10.1016/j.neuron.2018.12.009.
39. Jun, J.J., Steinmetz, N.A., Siegle, J.H., Denman, D.J., Bauza, M., Barbarits, B., Lee, A.K., Anastassiou, C.A., Andrei, A., Aydin, C., et al. (2017). Fully integrated silicon

probes for high-density recording of neural activity. Nature *551*, 232-236. 10.1038/nature24636.

40. Voigts, J., Newman, J.P., Wilson, M.A., and Harnett, M.T. (2020). An easy-to-assemble, robust, and lightweight drive implant for chronic tetrode recordings in freely moving animals. J Neural Eng *17*, 026044. 10.1088/1741-2552/ab77f9.
41. Carlen, M. (2017). What constitutes the prefrontal cortex? Science *358*, 478-482. 10.1126/science.aan8868.
42. Laubach, M., Amarante, L.M., Swanson, K., and White, S.R. (2018). What, If Anything, Is Rodent Prefrontal Cortex? eNeuro *5*. 10.1523/ENEURO.0315-18.2018.
43. Le Merre, P., Ahrlund-Richter, S., and Carlen, M. (2021). The mouse prefrontal cortex: Unity in diversity. Neuron *109*, 1925-1944. 10.1016/j.neuron.2021.03.035.
44. Vyazovskiy, V.V., Faraguna, U., Cirelli, C., and Tononi, G. (2009). Triggering slow waves during NREM sleep in the rat by intracortical electrical stimulation: effects of sleep/wake history and background activity. Journal of neurophysiology *101*, 1921-1931. 10.1152/jn.91157.2008.
45. Gonzalez, J., Prieto, J.P., Rodriguez, P., Cavelli, M., Benedetto, L., Mondino, A., Pazos, M., Seoane, G., Carrera, I., Scorza, C., and Torterolo, P. (2018). Ibogaine Acute Administration in Rats Promotes Wakefulness, Long-Lasting REM Sleep Suppression, and a Distinctive Motor Profile. Front Pharmacol *9*, 374. 10.3389/fphar.2018.00374.
46. Nagel, G., Szellas, T., Kateriya, S., Adeishvili, N., Hegemann, P., and Bamberg, E. (2005). Channelrhodopsins: directly light-gated cation channels. Biochem Soc Trans *33*, 863-866. 10.1042/BST0330863.
47. Madisen, L., Mao, T., Koch, H., Zhuo, J.M., Berenyi, A., Fujisawa, S., Hsu, Y.W., Garcia, A.J., 3rd, Gu, X., Zanella, S., et al. (2012). A toolbox of Cre-dependent optogenetic transgenic mice for light-induced activation and silencing. Nature neuroscience *15*, 793-802. nn.3078 [pii] 10.1038/nn.3078.
48. Sidor, M.M., Davidson, T.J., Tye, K.M., Warden, M.R., Diesseroth, K., and McClung, C.A. (2015). In vivo optogenetic stimulation of the rodent central nervous system. J Vis Exp, 51483. 10.3791/51483.
49. Putzeys, J., Raducanu, B.C., Carton, A., De Ceulaer, J., Karsh, B., Siegle, J.H., Van Helleputte, N., Harris, T.D., Dutta, B., Musa, S., and Mora Lopez, C. (2019). Neuropixels Data-Acquisition System: A Scalable Platform for Parallel Recording of 10 000+ Electrophysiological Signals. IEEE Trans Biomed Circuits Syst *13*, 1635-1644. 10.1109/TBCAS.2019.2943077.
50. Combrisson, E., Vallat, R., O'Reilly, C., Jas, M., Pascarella, A., Saive, A.L., Thiery, T., Meunier, D., Altukhov, D., Lajnef, T., et al. (2019). Visbrain: A Multi-Purpose GPU-Accelerated Open-Source Suite for Multimodal Brain Data Visualization. Front Neuroinform *13*, 14. 10.3389/fninf.2019.00014.
51. Sarasso, S., Boly, M., Napolitani, M., Gosseries, O., Charland-Verville, V., Casarotto, S., Rosanova, M., Casali, A.G., Brichant, J.-F., and Boveroux, P. (2015). Consciousness and Complexity during Unresponsiveness Induced by Propofol, Xenon, and Ketamine. Current Biology *25*, 3099-3105.

52. Palva, J.M., Palva, S., and Kaila, K. (2005). Phase synchrony among neuronal oscillations in the human cortex. The Journal of neuroscience : the official journal of the Society for Neuroscience *25*, 3962-3972. 10.1523/JNEUROSCI.4250-04.2005.
53. Vyazovskiy, V., Riedner, B.A., Cirelli, C., and Tononi, G. (2007). Sleep homeostasis and cortical synchronization: II. A local field potential study of sleep slow waves in the rat. Sleep *30*, 1631-1642.
54. Vyazovskiy, V.V., Olcese, U., Lazimy, Y.M., Faraguna, U., Esser, S.K., Williams, J.C., Cirelli, C., and Tononi, G. (2009). Cortical firing and sleep homeostasis. Neuron *63*, 865-878. 10.1016/j.neuron.2009.08.024.
55. Chauvette, S., Volgushev, M., and Timofeev, I. (2010). Origin of active states in local neocortical networks during slow sleep oscillation. Cerebral cortex *20*, 2660-2674. bhq009 [pii]
10.1093/cercor/bhq009.
56. Steinmetz, N.A., Aydin, C., Lebedeva, A., Okun, M., Pachitariu, M., Bauza, M., Beau, M., Bhagat, J., Bohm, C., Broux, M., et al. (2021). Neuropixels 2.0: A miniaturized high-density probe for stable, long-term brain recordings. Science *372*. 10.1126/science.abf4588.
57. Buccino, A.P., Hurwitz, C.L., Garcia, S., Magland, J., Siegle, J.H., Hurwitz, R., and Hennig, M.H. (2020). SpikeInterface, a unified framework for spike sorting. Elife *9*. 10.7554/eLife.61834.
58. Nicholson, C., and Freeman, J.A. (1975). Theory of current source-density analysis and determination of conductivity tensor for anuran cerebellum. Journal of neurophysiology *38*, 356-368. 10.1152/jn.1975.38.2.356.

Chapter III:

Behavioral and cortical arousal from sleep, muscimol-induced coma, and anesthesia by direct optogenetic stimulation of cortical neurons

Rong Mao, Matias Lorenzo Cavelli, Graham Findlay, Kort Driessen, Michael J Peterson, William Marshall, Giulio Tononi, Chiara Cirelli

Submitted to *iScience*

Summary

The cerebral cortex is widely considered part of the neural substrate of consciousness. However, while several studies have demonstrated that stimulation of subcortical nuclei can produce EEG activation and restore consciousness, so far no direct causal evidence has been available for the cortex itself. Here we tested in mice whether optogenetic activation of cortical neurons in posterior parietal cortex (PtA) or medial prefrontal cortex (mPFC) is sufficient for arousal from three behavioral states characterized by progressively deeper unresponsiveness: sleep, a coma-like state induced by muscimol injection in the midbrain, and deep sevoflurane-dexmedetomidine anesthesia. We find that cortical stimulation always awakens the mice from both NREM sleep and REM sleep, with PtA requiring weaker/shorter light pulses than mPFC. Moreover, in most cases light pulses produce both cortical activation (decrease in low frequencies) and behavioral arousal (recovery of the righting reflex) from brainstem coma, as well as cortical activation from anesthesia. These findings provide evidence that direct activation of cortical neurons is sufficient for behavioral and/or cortical arousal from sleep, brainstem coma, and anesthesia.

Introduction

There is a long tradition of trying to wake up subjects from sleep or anesthesia by stimulating different parts of the brain, starting from the identification of the brainstem activating system by Moruzzi and Magoun (Moruzzi and Magoun, 1949). In that seminal study, electrical stimulation of the reticular formation rapidly converted the synchronized, high voltage low frequency EEG pattern induced by chloralose anesthesia into an "activated" pattern with low voltage fast activity (Moruzzi and Magoun, 1949). EEG activation occurred also after direct stimulation of the intralaminar thalamus, but it was still achievable after this area was lesioned (Moruzzi and Magoun, 1949). Thus, this early result suggested that certain thalamic nuclei may be dispensable for the EEG activating response, even though many excitatory projections from the reticular activating system reach the cortex via the thalamus. Since then, the view of the activating system has evolved from a monolithic reticular core to an ensemble of distinct cell groups that promote arousal, including cholinergic, noradrenergic, dopaminergic, and glutamatergic neurons. These cell groups have diffuse projections to the cerebral cortex and thalamus and share the property of being, on average, more active during waking than during non-rapid eye movement (NREM) sleep, when the EEG is dominated by synchronous, high voltage slow waves (Brown et al., 2012; Scammell et al., 2017). They also have descending projections to the caudal brainstem and spinal cord, whose effects on muscle tone and behavioral arousal were not studied in early experiments (Moruzzi and Magoun, 1949). In recent studies, the selective optogenetic stimulation of some of these systems, including the noradrenergic neurons of the locus coeruleus and the dopaminergic neurons of the midbrain and dorsal raphe region, was sufficient to induce both EEG activation and behavioral arousal from sleep (Carter et al., 2010; Eban-Rothschild et al., 2016; Cho et al., 2017) or anesthesia

(Taylor et al., 2016). Other recent studies have clarified the role of individual thalamic nuclei using electrical stimulation in monkeys (Redinbaugh et al., 2020; Bastos et al., 2021), and optogenetic stimulation in mice (Herrera et al., 2016; Honjoh et al., 2018). Arousal from NREM sleep and/or anesthesia occurs after stimulating thalamic nuclei with broad cortical projections, including the mouse ventromedial nucleus (VM) that projects to layer 1 of large parts of neocortex (Honjoh et al., 2018), as well as the monkey centrolateral nucleus that projects to superficial and deep layers of frontal and parietal cortex (Redinbaugh et al., 2020). By contrast, stimulation does not lead to arousal when directed at thalamic nuclei with more restricted projections, such as the mouse ventral posteromedial nucleus that connects to primary somatosensory cortex (Honjoh et al., 2018), and the monkey dorsomedial nucleus that is mainly connected to prefrontal cortex (Redinbaugh et al., 2020). Together, these results show that arousal from NREM sleep and/or anesthesia can be triggered from several distinct brainstem or thalamic nuclei, but only when their stimulation leads to broad activation of the cerebral cortex.

Whether arousal from unresponsive states can be obtained through direct activation of cortical neurons has not been tested. This is relevant given that the cerebral cortex is widely considered a central part of the neural substrate of consciousness and in most, although not all cases, consciousness is associated with responsiveness (Sanders et al., 2012). In fact, much of the current debate is not focused on whether the cortex contributes directly to consciousness but, rather, on whether this role can be ascribed to frontal or posterior cortical areas, or both (Boly et al., 2017; Odegaard et al., 2017). The reticular activating system and its components, on the other hand, are now generally viewed as supporting consciousness indirectly (Schiff, 2010; Koch et al., 2016), despite the fact that, in humans, lesions of the dorsolateral pontine tegmentum or paramedian

midbrain usually result in immediate coma (Parvizi and Damasio, 2003; Posner and Plum, 2007). This is because patients with wide frontoparietal cortical network dysfunction typically remain unresponsive, in vegetative state, even when the function of the brainstem reticular formation is preserved (Laureys et al., 2004; Boly et al., 2008).

If the cortex is the core substrate of consciousness and the reticular activating system is only a "background condition" (Koch et al., 2016), it should be the case that the direct activation of cortical neurons is sufficient for arousal from unresponsive states, including from brainstem coma, when the function of the reticular activating system is impaired. Here we tested this hypothesis in mice by direct optogenetic stimulation of cortical neurons during sleep, after induction of a coma-like state of unresponsiveness induced by the injection of the $GABA_A$ receptor agonist muscimol in the midbrain reticular core, and during sevoflurane-dexmedetomidine (sevo-dex) anesthesia. Muscimol injections are likely to disfacilitate cortex and thalamus by removing the ascending arousal influence coming from the rostral reticular core, but without directly impairing activity in the caudal brainstem and spinal cord. By contrast, sevo-dex anesthesia broadly affects brainstem, thalamus and cortex both indirectly, mainly via disfacilitation caused by the block of noradrenaline release (dexmedetomidine), and directly, through $GABA_A$-mediated inhibition (sevoflurane). We find here that stimulation of either posterior parietal association cortex (PtA) or medial prefrontal cortex (mPFC) can quickly wake up mice from sleep and, when stronger and/or longer light pulses are used, can reverse the muscimol-induced, coma-like state, leading to both fronto-parietal EEG activation and recovery of the righting reflex (RORR). When the same mice are stimulated under deep sevo-dex anesthesia, EEG activation occurs in both cases

without RORR. Thus, cortical activation and full arousal from unresponsive states such as sleep and “brainstem coma” can be triggered by direct stimulation of cortical neurons.

Results

Experimental design. Adult CaMKIIα::ChR2 mice of both sexes (> P56, n = 12, 5 females) were implanted with optic fibers for optogenetic stimulation of PtA or mPFC, intracortical laminar probes and surface electrodes for electroencephalographic (EEG) recordings, and cannulas aimed at the midbrain for muscimol injection (Fig. 1). Baseline 24-hour recordings of sleep and waking started at least a week after surgery, followed by stimulation experiments in which light pulses of different intensity were first administered during sleep and, later, during muscimol-induced coma and sevo-dex anesthesia.

CaMKIIα::ChR2 mice were obtained by crossing CaMKIIα-Cre mice with the Cre-dependent Ai32 strain, which expresses an improved channelrhodopsin-2/EYFP (ChR2-EYFP) fusion protein following exposure to Cre recombinase. Because the CaMKIIα promoter is broadly expressed in cortical glutamatergic neurons across areas and layers, the stimulation was expected to broadly excite the target area in both mPFC and PtA. Consistent with this, CaMKIIα::ChR2 mice showed broad cortical expression of ChR2-EYFP (Fig. 2A). For optogenetic experiments mice were implanted either with a single paramedian optic fiber inserted deep in the cortex to target mPFC of both sides (Fig. 2B), or with two optic fibers over left and right PtA (Fig. 2C). A few mice had two fibers in left and right mPFC, or one fiber over left PtA (see below).

Cortical optogenetic stimulation during sleep. In each CaMKIIα::ChR2 mouse laser pulses were delivered during NREM sleep using square pulses or 4-8 Hz train pulses lasting 1-5 sec. In many cases, laser pulses were also delivered during rapid eye movement (REM) sleep. Stimulation experiments occurred over several days, and each day only a limited number of pulses was delivered, usually spaced minutes apart. During NREM sleep the arousal threshold varies depending on the amount of slow wave activity (SWA), which peaks at sleep onset and declines in the course of sleep (Neckelmann and Ursin, 1993). To control for the possible confound due to these homeostatic changes, stimulation experiments during sleep (and later during muscimol-induced coma or anesthesia) were performed approximately 5 to 8 hours after the beginning of the light phase, when most sleep pressure in mice has been released (Cavelli et al., 2023).

We applied cortical optogenetic stimulation during NREM sleep, when the EEG is dominated by slow waves that reflect the synchronous ON/OFF firing of cortical neurons (Steriade et al., 2001), and during REM sleep, when EEG pattern and cortical firing are similar to those of waking (Fig. 3A). Independent of the specific pattern or site of the stimulation (PtA or mPFC), mice always woke up from both NREM sleep and REM sleep (Fig. 3B). In every mouse, the awakening from REM sleep required significantly more laser power and/or longer stimulation compared to awakening from NREM sleep ($p = 0.00003$; Fig. 3C). Moreover, across mice and independent of the pattern of stimulation, PtA stimulation was significantly more effective than mPFC stimulation, i.e. with PtA stimulation weaker and/or shorter pulses were needed to induce arousal ($p = 0.0001$; Fig. 3C).

Induction of a coma-like state in the mouse. In rats, the bilateral microinjection of $GABA_A$ receptor agonists in a brainstem region called the mesopontine tegmental anesthesia area triggers

an immediate and reversible state of profound unresponsiveness similar to coma or anesthesia (Devor and Zalkind, 2001). Although the exact mechanism underlying this state is complex, a likely candidate is a broad decline in excitability of the forebrain caused by the inhibition of the ascending reticular arousal system (Lanir-Azaria et al., 2018). In a first series of experiments, we tested whether we could induce a similar unresponsive state in mice. A total of 28 animals, including 14 CaMKIIα::ChR2 mice used in optogenetic experiments, 11 CaMKIIα-Cre mice, and 3 C57BL/6J mice, received a bilateral injection of the $GABA_A$ receptor agonist muscimol in the mesencephalic reticular formation (Fig. 4A). All mice were briefly anesthetized with sevoflurane during the injections and the anesthesia was discontinued as soon as the procedure was completed. In a control experiment with saline injection, RORR occurred within 2 min from the time sevoflurane was discontinued, quickly followed by a normal cycling of sleep and wake episodes as during baseline. After muscimol injection, RORR also occurred within 1-2 min from the time the anesthetic was discontinued, but it was followed by an average period of around 40 minutes characterized first by hyperactivity with repetitive circling behavior, then by progressive ataxia followed by quiescence with the mouse lying on one side, and finally by loss of the righting reflex (LORR). In 5 mice in which no cortical optogenetic stimulation was performed after LORR, the period between LORR and spontaneous RORR was more than 2 hours (129 ± 12min; mean ± sem, 5 mice). During this period, the EEG pattern was dominated by large slow waves (Fig. 4B) and the mouse was breathing regularly, resting on the floor of the cage without any or with a few short spontaneous movements of the extremities.

To establish the “depth” of this muscimol-induced state, we designed a battery of 6 stimuli that were delivered mostly in a fixed order, from mild to strong, before LORR (during NREM

sleep), in the period between LORR and RORR (every 30-60 min), and after RORR. Based on the response to each stimulus we computed a cumulative score of responsiveness that could range from 0 (no response to any stimulus) to 12 (clear positive response to all stimuli). As shown for one mouse (Fig. 5A), when the stimuli were delivered during NREM sleep the total score was typically 12, that is, each stimulus triggered a positive response resulting in EEG activation and behavioral arousal. After muscimol-induced LORR instead, the same mouse showed little or no response to the stimuli and the score was significantly reduced relative to NREM sleep (paired t-test, $p = 2.9x10^{-13}$, 9 experiments in 6 mice). After spontaneous RORR (i.e. experiments in which optogenetic stimulation did not occur), the animal tried to stand on its paws and was drowsy, and the score remained below baseline levels for several hours, with a particularly reduced response to olfactory stimuli. By the next day, the responsiveness score, overall behavior and the sleep/wake pattern were back to normal. In experiments in which optogenetic stimulation occurred, the average score during the period between LORR and the first light pulse was 3.8 ± 1.5 (mean ± SD). In many cases, the same muscimol-induced state of unresponsiveness could be induced in the same animal 2-3 times, with experiments spaced approximately 1 week apart (9 mice). Based on this behavioral analysis we conclude that muscimol induces a state of long-lasting unresponsiveness that is deeper than NREM sleep. For simplicity, we call this state muscimol-induced "coma".

Cortical optogenetic stimulation during muscimol-induced coma. In 14 CaMKIIα::ChR2 mice the induction of a coma-like state was followed by cortical optogenetic stimulation in PtA or mPFC. Below, we describe these results separately for the two areas. Before the onset of the stimulation,

the depth of the muscimol-induced coma was comparable in the two groups of animals. Specifically, latency to LORR (mean ± SD in min, PtA = 46.3 ± 21.0; mPFC = 41.0 ± 12.6; p = 0.71) and behavioral score after LORR, immediately before the stimulation, did not differ between mPFC and PtA mice (total score, mean ± SD, PtA = 3.9 ± 1.7; mPFC = 4.0 ± 1.3; p = 0.86) (Fig. 5B). In all mice the response to the vestibular stimulus (righting reflex) was negative. In each mouse, we measured high gamma power (70-100 Hz) during the light pulses to assess the immediate effects of the stimulation, and SWA (0.5-4 Hz) after the stimulation to test whether EEG activation had occurred (Fig. 4C). The mouse behavior was scored before, during, and after the stimulation in 4 categories (no/little movements, some movements, attempt to RORR, RORR).

PtA stimulation. In two mice carrying a single optic fiber over the left PtA light pulses (1 sec) were delivered every 2-4 seconds for a total of 10-20 sec. Optogenetic stimulation triggered immediately several movements of legs and body followed by attempts to right up (aRORR) after 30 or 60 sec from the onset of the stimulation, and full RORR in one of the two mice after 77 sec (Fig. 6A). Changes in gamma and SWA power were almost identical in the two mice. During the stimulation period, gamma power in the left parietal LFP electrode, the closest to the stimulated site, increased when the light was on, with little change in the other electrodes (Fig. 6B). EEG activation was evident on the stimulated side, with a large decrease in SWA in the left parietal LFP electrode and a smaller decrease in the left frontal electrode, while there were no changes contralaterally (Fig. 6B).

In six mice carrying two optic fibers over left and right PtA, optogenetic stimulation led to aRORR within 5-25 secs from the onset of stimulation, followed by RORR (latency from stimulation onset 23-174 sec). Consistent with the findings with unilateral PtA stimulation at 0.5

Hz, gamma power increased during the stimulation only in the parietal electrodes, those close to the optic fibers (Fig. 6C). EEG activation (SWA decrease) was prominent post-stimulation in the parietal electrodes and also clearly present in the frontal electrodes (Fig. 6D). While the stimulation at 0.5 Hz was effective in most cases, it failed to awake two animals. In both mice, the stimulation was maintained for more than 1 minute, but it only triggered some movements that never evolved into aRORR or RORR. In these two cases the increase in gamma power was small in the parietal electrodes, and SWA did not change. However, aRORR/RORR could be triggered in both mice using pulses at 4 or 5 Hz rather than at 0.5 Hz. Overall, across all experiments with PtA stimulation (n = 10), aRORR/RORR occurred in 60% of the cases with pulses at 0.5 Hz and in 100% of the cases with pulses at 4-5 Hz.

mPFC stimulation. In the first two mice two optic fibers were implanted, one in the mPFC of each side, and in both animals optogenetic stimulation at 5 Hz quickly induced RORR from muscimol-induced coma, associated with a large increase in gamma power mainly in the frontal LFP electrode and clear signs of EEG activation (Fig. 7 A,B). However, the histology revealed that in both animals the tip of the fibers was too deep and reached the white matter. To avoid this problem, in the next 4 mice a single fiber was implanted in the left mPFC more rostrally and close to the midline, to allow the light pulses to also reach the contralateral side (Fig. 2 B). In all four mice histology confirmed the position of the optic fiber within the prefrontal grey matter. In two of these animals the stimulation at 0.5 Hz failed to induce signs of EEG activation and RORR (Fig. 7 C,D). Stimulation at 5 Hz instead induced aRORR/RORR in 80% of cases (4/5 experiments), confirming that stimulation at 5 Hz was more effective than at 0.5 Hz. The 5 Hz stimulation mainly increased gamma power locally, in the frontal LFP electrode. Signs of EEG activation (SWA

decrease) were present but less pronounced than after parietal stimulation (Fig. 7 E,F). In 2 of the 4 mice abnormal, hypersynchronous activity occurred for several seconds after the stimulation and then subsided (Fig. 7 E). Overall, across all experiments with mPFC stimulation (n = 7), aRORR/RORR and/or EEG activation never occurred with pulses at 0.5 Hz, while they did happen in 80% of the cases with pulses at 5 Hz.

Stimulation during anesthesia. Optogenetic stimulation was performed during deep sevo-dex anesthesia (1-2% sevo, 70-100ug/kg dex, n= 9 mice), while cortical activity was dominated by highly synchronous, large slow waves (Fig. 8A). The combination of sevo-dex was chosen to maintain a stable level of slow-wave anesthesia, long enough to allow for the optogenetic stimulation. Sevo has low blood solubility and fast pharmacodynamics and in our experience, when given alone, is either unable to generate a steady level of anesthesia (at low dose) or leads to burst-suppression (at high dose).

Mice were lying on their side, and the total score on the behavioral battery performance was the lowest possible (total score = 0) and identical for mice that received mPFC or PtA stimulation. Stimulation never resulted in aRORR or RORR even when light pulses delivered during sevo-dex anesthesia were stronger and/or longer than those applied during muscimol-induced coma. In the two mice carrying a single optic fiber, unilateral PtA stimulation resulted in clear EEG activation (SWA decrease) in both frontal and parietal cortex of the stimulated side (Fig. 8 B,C). Bilateral strong PtA stimulation resulted in a broad increase in gamma power and EEG activation in all channels (Fig. 8 D,E). In the 4 mice carrying one fiber targeting mPFC, strong stimulation resulted in a transient increase in gamma power in the electrodes close to the optic fiber but SWA showed small or no decrease in any of the channels (Fig. 8 F,G).

Comparison between PtA and mPFC stimulation. As mentioned above, parietal stimulation required weaker and/or shorter light pulses than prefrontal stimulation to awaken the mice from sleep (generalized linear mixed effects model, $p = 0.0003$; Fig. 3C). For the coma and anesthesia experiments, the observed data showed that the stimulation was more effective when directed at PtA than at mPFC, in terms of proportion of aRORR/RORR from coma (80% mPFC, 100% PtA at 5 Hz) and post-stimulation decrease in SWA at stimulation site (-0.109 ± 0.149 mPFC; -0.439 ± 0.321 PtA). Due to the small number of mice and the highly unbalanced nature of these data (different numbers of mice in each group, different stimulation patterns, etc.), we used a classification analysis rather than a linear mixed effects model to test for differences between parietal and prefrontal stimulation. Specifically, we trained a regularized logistic regression classifier with K-fold cross validation to ask whether changes in gamma power and SWA could be used to predict whether the stimulation during coma or anesthesia was in PtA or mPFC. We found that this was the case with a cross-validated accuracy of 81.33%. Two factors accounted for most of this effect: the post-stimulation decrease in SWA in the local LFP channel, and the increase in gamma power in the distal LFP electrode during the first second of stimulation. Note that the stimulated area was broader in the mice implanted with two fibers in PtA compared to those carrying one fiber in mPFC. However, the unilateral PtA stimulation ($n = 2$ mice) was more effective than the bilateral mPFC stimulation ($n = 4$ mice), both during coma, when EEG activation and behavioral arousal (aRORR or RORR) with 0.5 or 0.25 Hz pulses occurred in 100% of cases with PtA stimulation and 0% with mPFC stimulation, and during anesthesia, when EEG activation always occurred with PtA stimulation and was absent or minimal with mPFC stimulation.

Discussion

In this study we used optogenetic stimulation to assess the ability of cortical pyramidal neurons to trigger cortical activation and behavioral arousal from sleep, muscimol-induced coma, and sevo-dex anesthesia, three states of progressively deeper unresponsiveness as measured using a behavioral test battery.

Cortical optogenetic stimulation could always awaken the mice from NREM sleep. This was also the case for REM sleep, although arousal from this phase required stronger and/or longer light pulses compared to NREM sleep. A candidate mechanism that could partially account for these results is the level of activity of the noradrenergic system of the locus coeruleus (LC), because LC activity is important for arousability and the LC is actively inhibited during REM sleep. Specifically, optogenetic stimulation of the LC invariably awakens the mice with short latency from both NREM sleep and REM sleep (Carter et al., 2010). Relative to controls, mice unable to produce noradrenaline require more noise to wake up from recovery sleep following sleep deprivation (Hunsley and Palmiter, 2004) and in rats, optogenetic silencing of LC neurons reduces the likelihood of sound evoked awakenings (Hayat et al., 2020). LC noradrenergic neurons fire maximally during waking, much less so in NREM sleep and not at all during REM sleep (Aston-Jones and Bloom, 1981b; Takahashi et al., 2010; Hayat et al., 2020), when LC neurons are actively inhibited (Nitz and Siegel, 1997; Verret et al., 2006; Luppi et al., 2011). Recent studies in mice using genetically encoded noradrenaline sensors (Feng et al., 2019) also showed that during NREM sleep noradrenaline levels continue to fluctuate up and down every 30-50 seconds in both thalamus (Osorio-Forero et al., 2021) and prefrontal cortex (Kjaerby et al., 2022), while they steadily decline in these regions during REM sleep. Intriguingly, other optogenetic experiments

that targeted the thalamus found even more extreme differences in arousability between NREM sleep and REM sleep. Bilateral optogenetic excitation of the matrix cells of the ventromedial thalamic nucleus (VM), which sends diffuse glutamatergic projections to layer 1 of neocortex, could wake up the mouse from NREM sleep but not from REM sleep (Honjoh et al., 2018). A similar result was observed after bilateral optogenetic inhibition of the GABAergic cells of the reticular thalamic nucleus, which strongly inhibits the rest of the thalamus (Takata, 2020). Of note, when arousal threshold is measured using peripheral (acoustic) stimuli, arousal from deep NREM sleep (slow wave sleep) requires louder stimuli than from REM sleep, in both humans and rodents (Rechtschaffen et al., 1966; Zepelin et al., 1984; Neckelmann and Ursin, 1993), although when tonic REM sleep and phasic REM sleep are tested separately, the latter is as deep as slow wave sleep (Ermis et al., 2010). Also, the scent of a predator wakes up a mouse more rapidly from REM sleep than from NREM sleep (Tseng et al., 2022). In response to a mild sound, LC unit activity strongly increases during wake and not at all in REM sleep, while during NREM sleep the evoked firing response is small but still present (Aston-Jones and Bloom, 1981a). Thus, in physiological conditions additional mechanisms must exist to regulate arousability from NREM sleep. Among them, the ON/OFF bistable pattern of activity in the thalamocortical system, which is responsible for the occurrence of slow waves, is a primary candidate because it disrupts thalamocortical and corticocortical connectivity (Massimini et al., 2005). In line with this, arousal thresholds within NREM sleep are positively correlated with SWA (Neckelmann and Ursin, 1993).

The direct excitation of cortical cells could also revert the state of unresponsiveness caused by muscimol injection in the midbrain. Cortical activity switched back to a wake-like, tonic pattern of firing and mice could stand up and walk, even if the midbrain was directly inhibited. Patients

do not recover consciousness if frontoparietal cortex is broadly damaged, even when the brainstem is intact (Laureys et al., 2004; Boly et al., 2008). Our results therefore complement clinical findings and provide independent evidence for the key role of the cortex, but not the brainstem, in supporting consciousness. During muscimol-induced coma, behavioral arousal as measured by RORR could be triggered by stimulation of either posterior parietal cortex or medial prefrontal cortex. In all successful cases the stimulation quickly recruited both frontal and parietal regions. This is consistent with the results of thalamic electrical stimulation in anesthetized monkeys, in which behavioral arousal occurred after activation of the centrolateral nucleus, which projects to both frontal and parietal cortex, but not after stimulation of the dorsomedial nucleus, which is mainly connected to prefrontal cortex (Redinbaugh et al., 2020).

During sevo-dex anesthesia the direct optogenetic stimulation of cortical cells produced cortical activation but did not result in behavioral arousal (RORR). Dexmedetomidine is a highly selective α2-adrenergic receptor agonist that causes sedation and, at higher doses, LORR (Zhang et al., 2015). It acts through several pre- and postsynaptic mechanisms, including the widespread block of noradrenaline release and the direct local inhibition of LC neurons (Zhang et al., 2015). Sevoflurane broadly inhibits neuronal activity mainly by acting as a positive modulator of the $GABA_A$ receptor, although it also antagonizes excitatory NMDA receptors, promotes two-pore domain potassium conductances, and blocks glutamate release (Vinje et al., 2002; Iqbal et al., 2019). Together, these drugs have profound depressing effects on most of the brain—not only on the cerebral cortex, but also on thalamus, basal ganglia, and brainstem. Cortical activation in the absence of behavioral arousal is characteristic of REM sleep, a behavioral state of quiescence and reduced responsiveness almost always accompanied by dreaming. When humans dream, whether

during REM sleep or NREM sleep, cortical activation, indexed like here by decreased slow wave activity, is observed primarily in posterior cortex, whereas prefrontal cortex remains deactivated (Siclari et al., 2017; Bernardi et al., 2019). Preserved consciousness accompanied by unresponsiveness or minimal responsiveness is also observed in neurological conditions, especially when associated with massive lesions of prefrontal-basal ganglia-thalamic circuits and of the dopaminergic system ((Schiff et al., 2014; Casarotto et al., 2016; Boly et al., 2017); for a striking example of akinetic mutism, see (Comanducci et al., 2023)). Thus, the induction of cortical arousal without behavioral arousal in our deep sevo-dex anesthesia condition may be due to the inability of cortical stimulation to activate prefrontal-basal ganglia-thalamic circuits, which seems to be one of the mechanisms that distinguish disconnected from connected consciousness (Sanders et al., 2012; Comanducci et al., 2023).

The lack of RORR with bilateral cortical stimulation under sevo-dex anesthesia contrasts with the results of the bilateral optogenetic stimulation of VM (Honjoh et al., 2018). In that study we found that all 6 mice anesthetized with sevo-dex showed cortical EEG activation, 5 of them exhibited continuous limb movements, and 4 had full RORR within 1-4 minutes from the onset of VM stimulation (Honjoh et al., 2018). The lower doses of sevoflurane and dexmedetomidine in that study (sevo: 1-1.2%; dex: 50-70 ug/kg) are unlikely to account for the different outcome of the stimulation because both studies used the minimum dose required for a stable slow wave anesthesia (in different ambient temperatures and mouse strains). Instead, a key factor may be that while here we stimulated a single cortical area, VM stimulation can broadly activate many cortical regions, as well as basal ganglia and mesencephalic circuits that are important for behavioral arousal. Anatomically, VM neurons are multi-area matrix cells that project to layer 1 of most of

the neocortex and further innervate the central region of the caudate-putamen and midbrain tegmentum (Herkenham, 1979). Intriguingly, VM stimulation induces RORR from sevo-dex anesthesia but not from REM sleep (Honjoh et al., 2018). The only area spared by VM axons is the retrosplenial cortex (Herkenham, 1979), which is increasingly recognized as a main cortical hub for the generation and maintenance of REM sleep (Dong et al., 2022; Wang et al., 2022).

In contrast with our results, a recent study in rats anesthetized with sevoflurane (Pal et al., 2018) concluded that "consciousness" could be restored by pharmacological activation of prefrontal prelimbic cortex (our mouse mPFC) but not posterior and medial posterior cortex (our mouse PtA). This conclusion was based on the fact that, while the injection of carbachol or noradrenaline in any of these areas triggered EEG activation and increased respiratory rate, only the pharmacological activation of prefrontal prelimbic cortex resulted in RORR in 4 out of 11 rats (Pal et al., 2018). These results cannot be directly compared to ours due to differences in species (rats vs mice), anesthesia (sevo vs sevo-dex), method of cortical stimulation (pharmacological vs optogenetic), and length of the stimulation. The last factor is especially important, because the drugs were infused continuously for 12.5 minutes and aRORR/RORR were observed after several minutes, making it difficult to rule out subcortical effects due to the diffusion of the drug. Of note, optogenetic stimulation of the dopaminergic axons targeting mPFC does not induce arousal from NREM sleep, while stimulation of dopaminergic fibers targeting the nucleus accumbens and the dorsolateral striatum does (Eban-Rothschild et al., 2016). Independent of the possible role of subcortical areas, it was the presence or absence of RORR and wake-like motor behavior that prompted the authors to conclude that prefrontal, but not posterior, cortex plays a key role in restoring "signs of consciousness" (Pal et al., 2018). Equating consciousness with behavioral

arousal, however, ignores the substantial evidence that consciousness can be present in unresponsive states during which posterior cortical regions are activated, as is the case with REM sleep and widespread prefrontal lesions. Indeed, in the Pal et al. study, pharmacological activation of posterior and medial posterior cortex triggered EEG activation with increased theta to SWA ratio, increased respiratory rate, increased cortical levels of acetylcholine, and in some cases muscle twitches. In the absence of large movements and locomotion, this combination of features is typical of REM sleep. Unlike humans, mice do not report whether they had been dreaming after awakenings from REM sleep. However, the perturbational complexity index--the most sensitive and specific maker of consciousness, validated in humans across many conditions of consciousness and unconsciousness—is similarly high in wakefulness and REM sleep in both humans (Massimini et al., 2010; Casarotto et al., 2016) and rodents (Cavelli et al., 2023). This further emphasizes the importance of distinguishing between consciousness and responsiveness (Sanders et al., 2012; Koch et al., 2016; Comanducci et al., 2023).

The present results show that awakening from both NREM and REM sleep through optogenetic stimulation required significantly weaker and/or shorter light pulses in parietal cortex than in prefrontal cortex. We also observed that PtA stimulation resulted in a greater proportion of RORR from muscimol-induced coma than mPFC stimulation, as well as a larger post-stimulation decrease in SWA at stimulation site. Direct comparisons between PtA and mPFC experiments are difficult because we cannot prove that the strength of the optogenetic stimulation was perfectly matched in the two groups of mice. However, we found no difference in the ability of PtA and mPFC stimulations to trigger a local increase in gamma power in the electrode close to the optic fiber ($p = 0.719$). This suggests that it is not the strength of the local activation, but rather the

downstream consequences that account for the different efficacy of PtA and mPFC stimulations in the recovery of consciousness, consistent with the critical role of posterior cortex in supporting consciousness.

Because animals were exclusively implanted with cortical electrodes, we could not assess the effects of optogenetic cortical stimulation on subcortical structures. Due to the duration of the stimulation paradigm (several seconds), cortical stimulation could have indirectly activated both diencephalic and brainstem nuclei. Thus, it is possible that cortical and behavioral arousal may have been mediated by the direct activation of cortico-cortical networks, the recruitment of cortico-thalamo-cortical loops, or the secondary involvement of brainstem circuits. However, the cortical and behavioral arousal from the deep coma induced by muscimol injections in the brainstem suggests that cortical stimulation awakened the mice despite the pharmacological suppression of brainstem circuits that normally control arousal. Thus, cortico-thalamic networks may be sufficient to autonomously support a conscious state, while brainstem arousal systems provide facilitating background conditions that can be substituted for by direct cortical activation.

Figure 1. Experimental design and timeline. Mice (n = 12, 5 females) were implanted with two cannulas to deliver muscimol to the midbrain, 1-2 optic fibers above parietal association cortex (PtA, top row), 1 optic fiber close to the midline for bilateral optogenetic stimulation of medial prefrontal frontal (mPFC, bottom row; 4 mice) and laminar probes spanning frontal and parietal cortex (X). EEG electrodes (not shown) were also implanted. Two of the 8 mice with parietal stimulation had only one optic fiber (not shown). Optogenetic experiments occurred first during sleep and later after the induction of a coma-like state via muscimol injection in the midbrain or under sevo-dex anesthesia. Surgery and stimulation experiments were spaced at least one week apart.

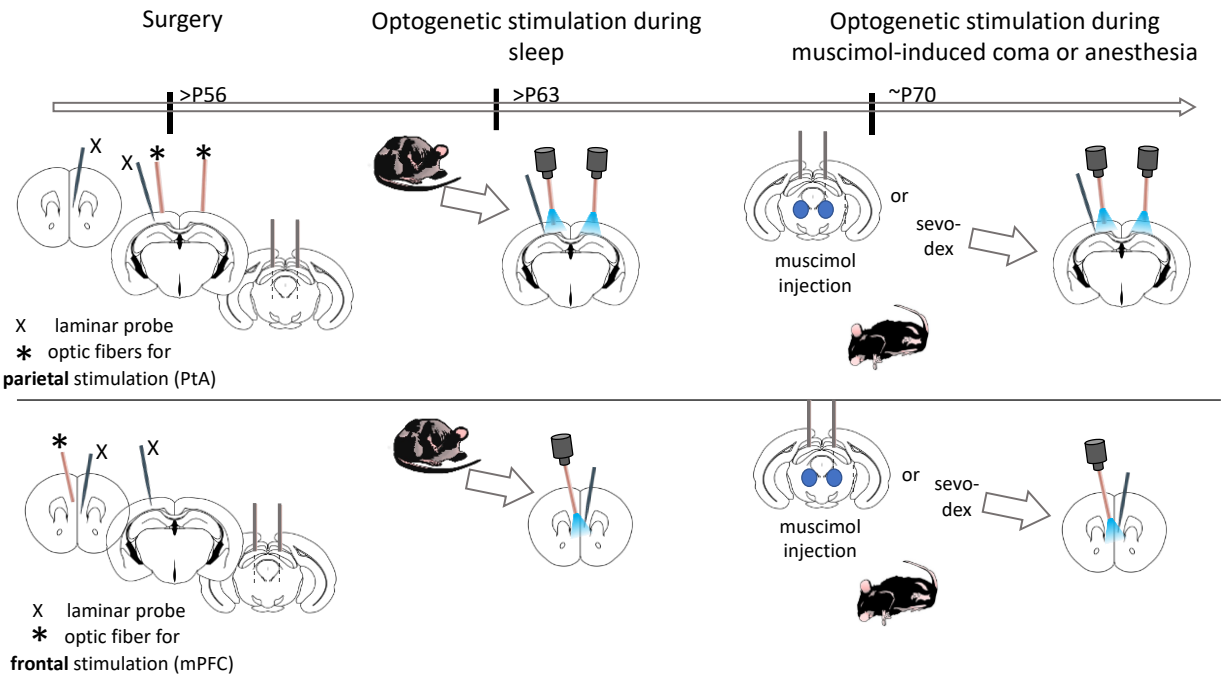

Figure 2. Immunohistochemical and histological analysis. A, representative coronal sections from one CaMKIIα::ChR2 mouse, confirming the broad cortical expression of ChR2-EYFP in frontal and parietal cortex. **B,** representative mouse with optogenetic stimulation in medial prefrontal cortex (mPFC). Left, dorsal schematic view of the mouse skull displaying the position of the optic fiber (red circle), laminar probes (X), and EEG screws (filled circles). Electrodes close to the optic fibers are in red. Middle and right, coronal sections showing the location of the tip of the optic fiber close to the midline in mPFC (*) and laminar probes in mPFC and posterior parietal cortex (PtA). The arrowheads indicate the tip of the laminar probes. DAPI and CM-DiI dye staining were used to identify cortical layers and probes, respectively. **C,** same as in B but for a representative mouse with optogenetic stimulation in PtA. In this case there were two optic fibers positioned above the cortical surface (one is shown, indicated by *). Coronal sections were stained with anti-GFAP (glial fibrillary acidic protein) antibody to identify the probes. Bars = 1 mm.

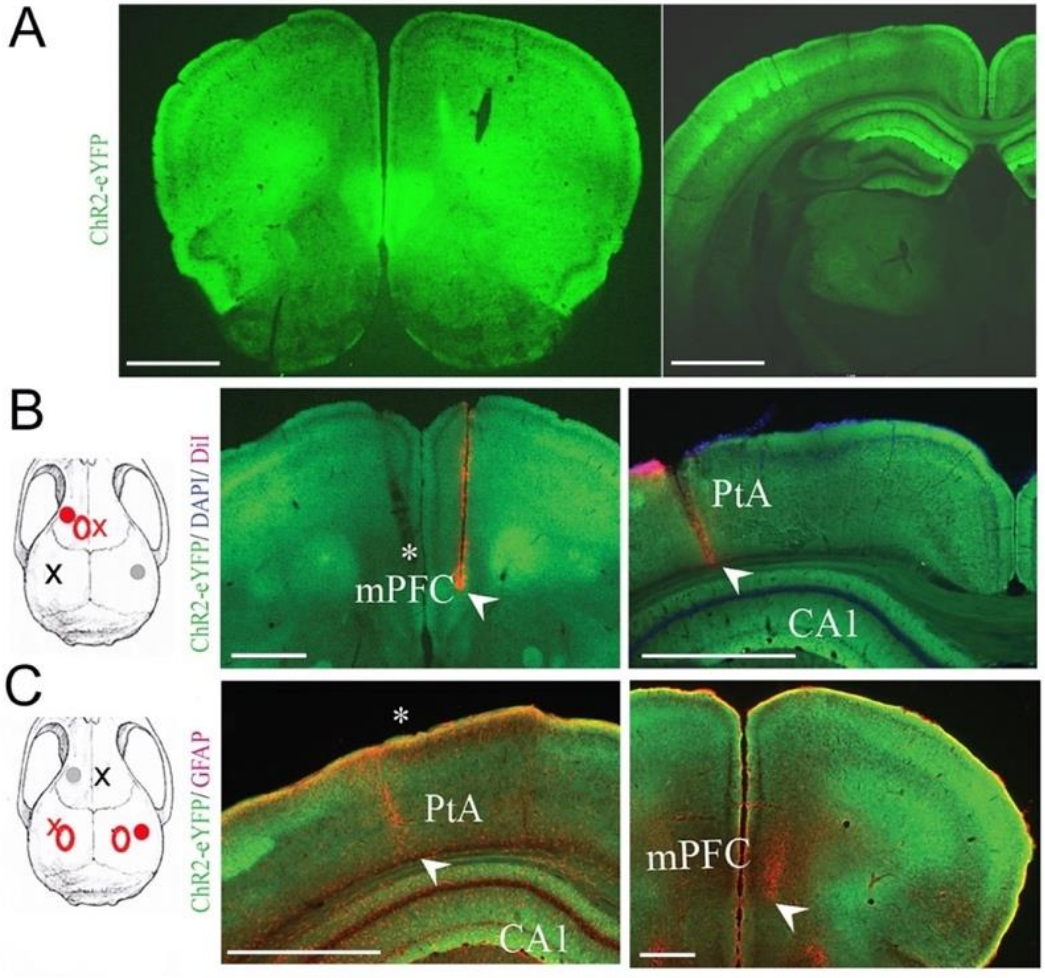
A
ChR2-eYFP
B
ChR2-eYFP/ DAPI/ DiI
mPFC
PtA
CA1
C
ChR2-eYFP/ GFAP
PtA
CA1
mPFC

Figure 3. Optogenetic stimulation in sleep. A, representative traces (~ 4 secs) of waking, NREM sleep, REM sleep in one representative mouse. For each behavioral state, the panel shows (from top to bottom) the electroencephalogram (EEG) from frontal and parietal cortex; local field potentials (LFPs) from frontal and parietal cortex recorded across layers with a laminar silicon probe (superficial on top) and thresholded spikes from the same LFP channels; electromyogram (EMG) from vibrissal (top) and neck musculature (bottom). LFPs and spikes from the same channel are color matched. **B,** example of the same optogenetic stimulation (5 Hz, 2.9 mW) leading to arousal from NREM sleep but not from REM sleep. Same mouse as in A. Stim. indicates when light pulses were given. **C,** Summary of the results of optogenetic stimulation during sleep. Each bar is a summary score representing the sum of the laser power and length of the stimulation needed to wake up a mouse from NREM sleep or REM sleep using optogenetic stimulation of posterior parietal association cortex (PtA, top) or medial prefrontal cortex (mPFC, bottom). Each column is the score of one mouse, showing the minimum stimulation parameters found to reliably awaken the mouse in each sleep state, based on 2-10 trials. Horizontal bars below the x axis link data from the same mouse.

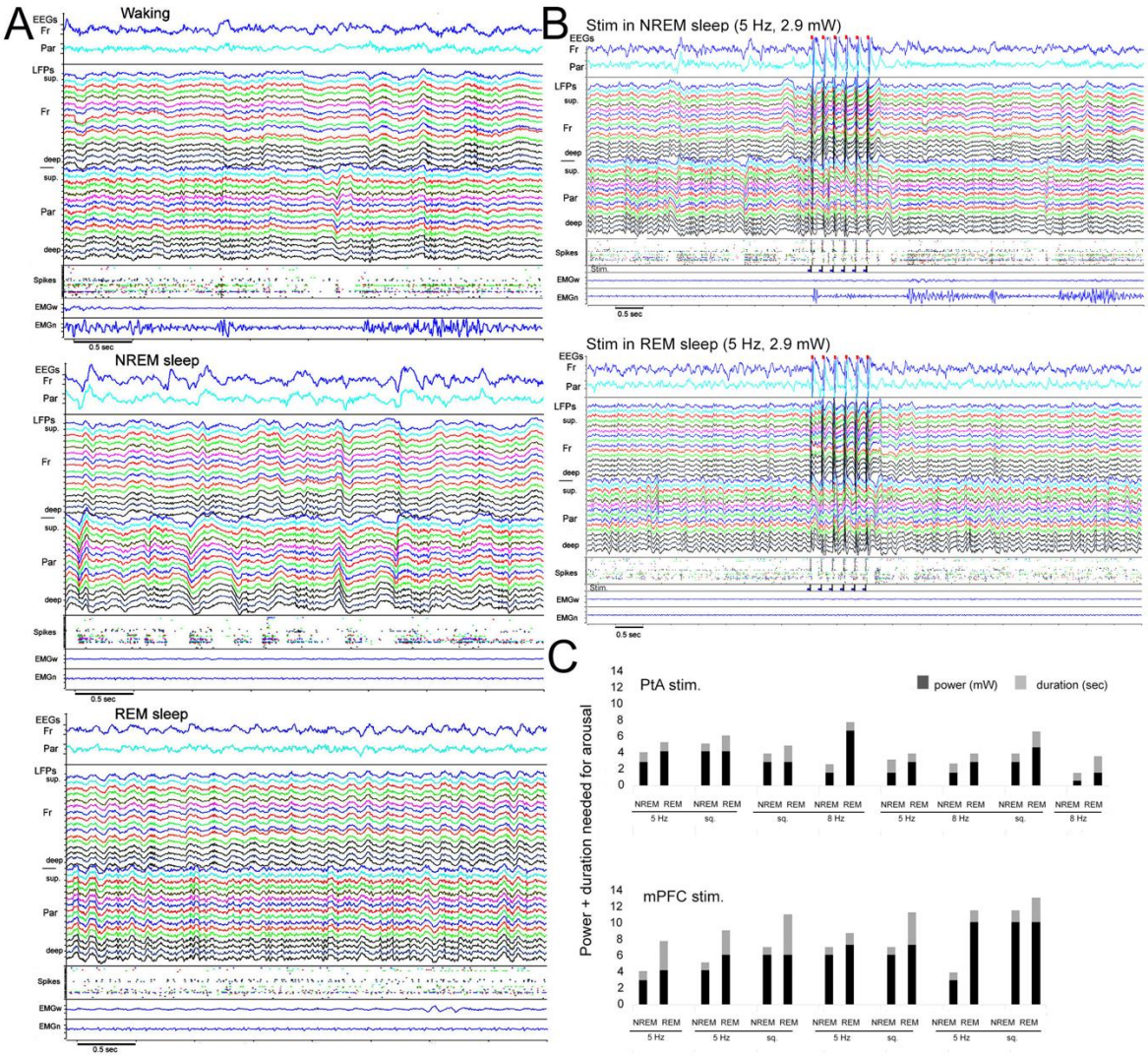
A
Waking
NREM sleep
REM sleep
EEGs
Fr
Par
LFPs
sup.
deep
Spikes
EMGw
EMGn
0.5 sec
B
Stim in NREM sleep (5 Hz, 2.9 mW)
Stim in REM sleep (5 Hz, 2.9 mW)
Stim.
C
PtA stim.
mPFC stim.
power (mW)
duration (sec)
Power + duration needed for arousal
NREM REM
5 Hz
sq.
8 Hz

Figure 4. Muscimol-induced coma. A, schematic view of muscimol injection site and coronal section of a representative mouse showing part of the cannula tracks in the midbrain; arrowheads indicate the tip of the cannulas. IP, interpeduncular nucleus; ml, medial lemniscus; MRF, mesencephalic reticular formation; PAG, periaqueductal gray; pn, pontine nuclei. **B**, representative traces (~ 4 secs) of cortical activity during muscimol-induced coma (after LORR). Same mouse as in Figure 3. The panel shows (from top to bottom) the electroencephalogram (EEG) from frontal and parietal cortex; local field potentials (LFPs) from frontal and parietal cortex recorded across layers with a laminar silicon probe (superficial on top) and thresholded spikes from the same LFP channels; electromyogram (EMG) from vibrissal (top) and neck musculature (bottom). LFPs and spikes from the same channel are color matched. **C**, example of the effect of PtA stimulation (8 pulses at 0.5 Hz, 2.9 mW) on EEG, LFP, and spike activity. Note the presence of slow waves in frontal and parietal LFPs, associated with bistable (on/off) firing (spikes) before stimulation, and EEG activation with tonic firing after the stimulation.

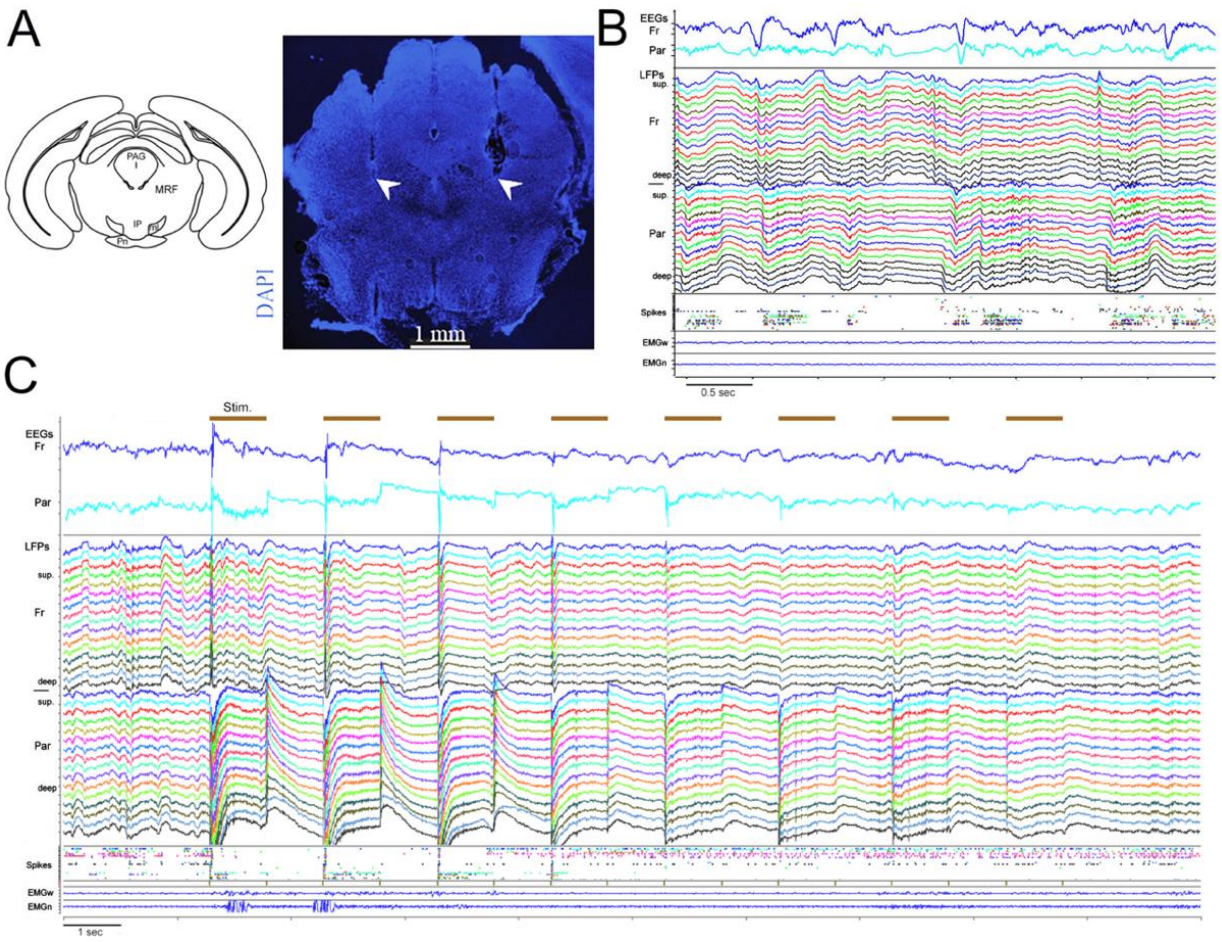
A
PAG
MRF
IP
Fr
DAPI
1 mm
B
EEGs
Fr
Par
LFPs
sup.
Fr
deep
sup.
Par
deep
Spikes
EMGw
EMGn
0.5 sec
C
Stim.
EEGs
Fr
Par
LFPs
sup.
Fr
deep
sup.
Par
deep
Spikes
EMGw
EMGn
1 sec

Figure 5. Behavioral characterization of muscimol-induced unresponsiveness. A, the behavioral test battery scores before, during and after the coma-like state in one mouse. LORR, loss of righting reflex. RORR, recovery of righting reflex. **B,** summary of the behavioral score results during coma immediately before stimulation across mice. Each column represents the sum score across all six behavioral tests for one coma experiment in one mouse. Mice are grouped based on the site of the optogenetic stimulation (PtA, left; mPFC, right). The result for each test is color-coded as shown in panel A. Horizontal bars below the x axis link results of two coma experiments in the same mouse; * marks the mice with unilateral PtA stimulation; # marks the mice with two-fiber mPFC-cc stimulation.

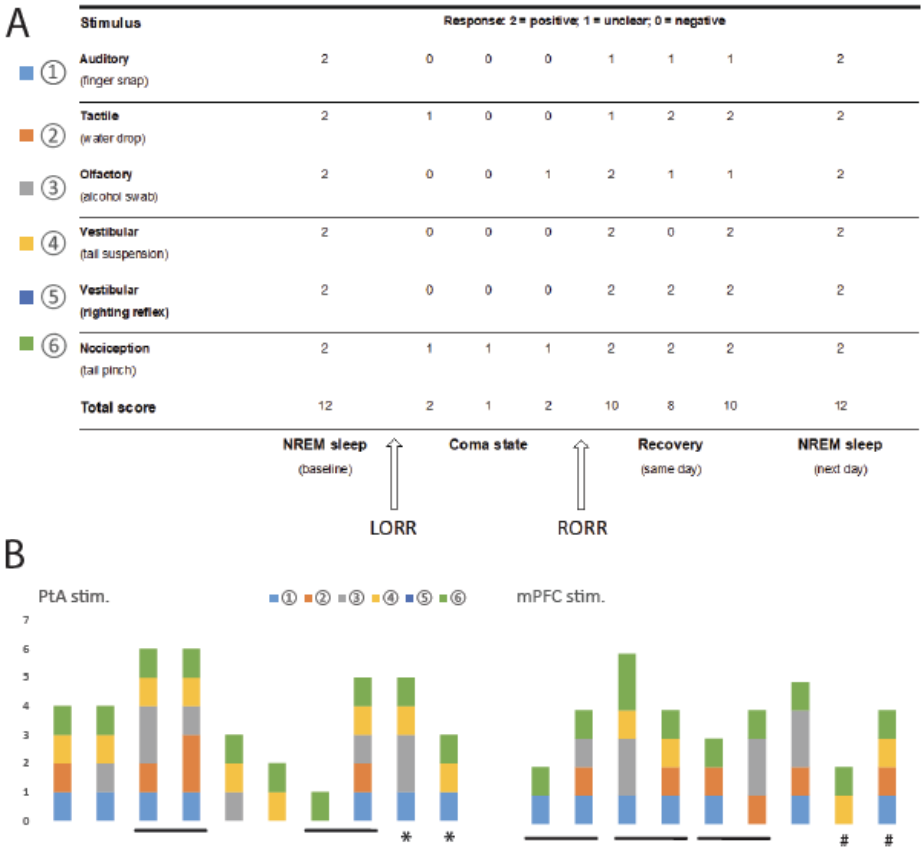

Figure 6. Optogenetic stimulation of PtA during muscimol-induced coma. A, mouse implanted with a single optic fiber (red circle) over left PtA just medial to the laminar probe (red X). Relative power spectrum for each of the 4 electrodes (3 EEGs indicated by circles, 1 deep LFP channel indicated by X) starting 20 sec before the stimulation (time 0), when the mouse was in a stable coma-like state. The power for each frequency bin (0.0078Hz) is normalized based on the last 50 to 1 sec before the first laser pulse. EMGs, electromyograms from vibrissal (top) and neck musculature (bottom). The duration of the stimulation is indicated by the blue horizontal bar on top, followed by a rectangle indicating the post-stimulation time window when SWA was measured. Behavior was scored using videorecording and is indicated by horizontal bars; grey bars indicate when no/few movements were present; yellow: more movements of limbs and body; orange: attempts to RORR (aRORR); red: RORR. **B**, summary of the changes in gamma power (during the stimulation) and SWA (first 20 sec post-stimulation). **C, D**, same as in A and B for a mouse implanted with two optic fibers (red circles) over left and right PtA. In this mouse the stimulation at 0.5 Hz triggered EEG activation and RORR.

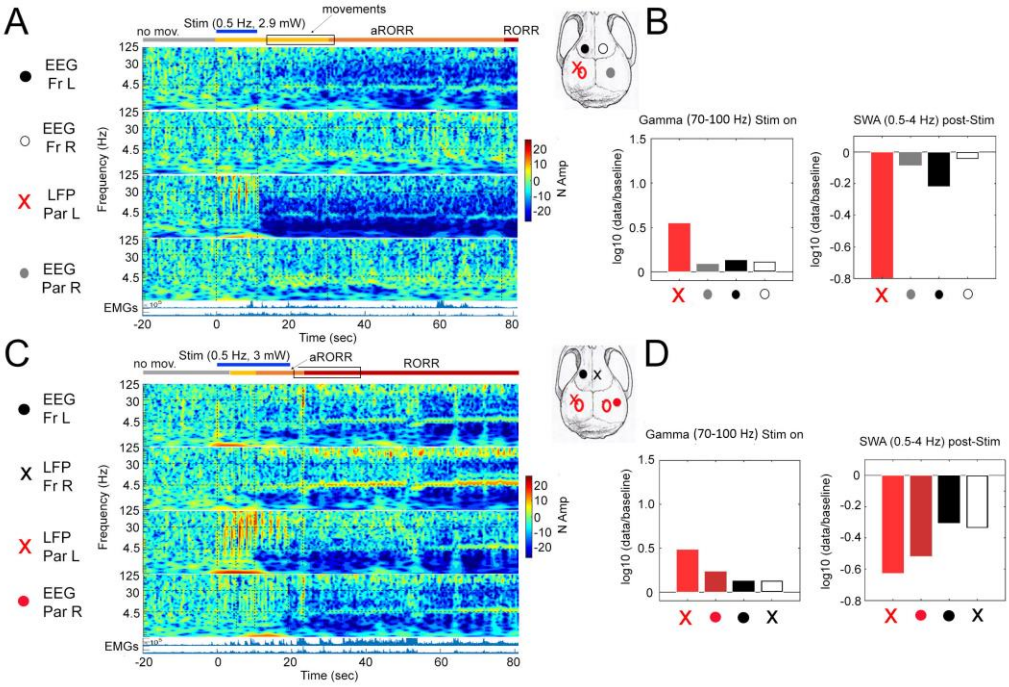
A
movements
no mov.
Stim (0.5 Hz, 2.9 mW)
aRORR
RORR
EEG Fr L
EEG Fr R
LFP Par L
EEG Par R
Frequency (Hz)
N Amp
EMGs
Time (sec)
B
Gamma (70-100 Hz) Stim on
SWA (0.5-4 Hz) post-Stim
log10 (data/baseline)
C
no mov.
Stim (0.5 Hz, 3 mW)
aRORR
RORR
EEG Fr L
LFP Fr R
LFP Par L
EEG Par R
Frequency (Hz)
N Amp
EMGs
Time (sec)
D
Gamma (70-100 Hz) Stim on
SWA (0.5-4 Hz) post-Stim
log10 (data/baseline)

Figure 7. Optogenetic stimulation of mPFC during muscimol-induced coma. A, mouse implanted with two optic fibers (red circles), in left and right mPFC. Relative power spectrum for each of the 4 electrodes (2 EEGs indicated by filled circles, 2 deep LFPs indicated by X). Time 0 indicates stimulation onset, which occurs when the mouse was in a stable coma-like state. The power for each frequency bin (0.0078Hz) is normalized based on the last 50 to 1 sec before the first laser pulse. EMGs, electromyograms from vibrissal (top) and neck musculature (bottom). The duration of the stimulation is indicated by the blue horizontal bar on top, followed by a rectangle indicating the post-stimulation time window when SWA was measured. Behavior was scored using videorecording and is indicated by horizontal bars; grey bars indicate when no/few movements were present; yellow: more movements of limbs and body; orange: attempts to RORR (aRORR); red: RORR. **B**, summary of the changes in gamma power (during the stimulation) and SWA (first 20 sec post-stimulation). In this mouse both optic fibers reached the white matter. **C, D**, same as in A and B for a mouse implanted with one optic fiber close to the midline (red circle). In this mouse the stimulation at 0.5 Hz triggered neither RORR nor EEG activation. **E, F**, same mouse as in C and D. The stimulation at 5 Hz triggered RORR and EEG activation, but hypersynchronous activity was obvious in all electrodes after the stimulation ended. SWA was measured at the end of this abnormal activity (~ 40 sec after the end of stimulation).

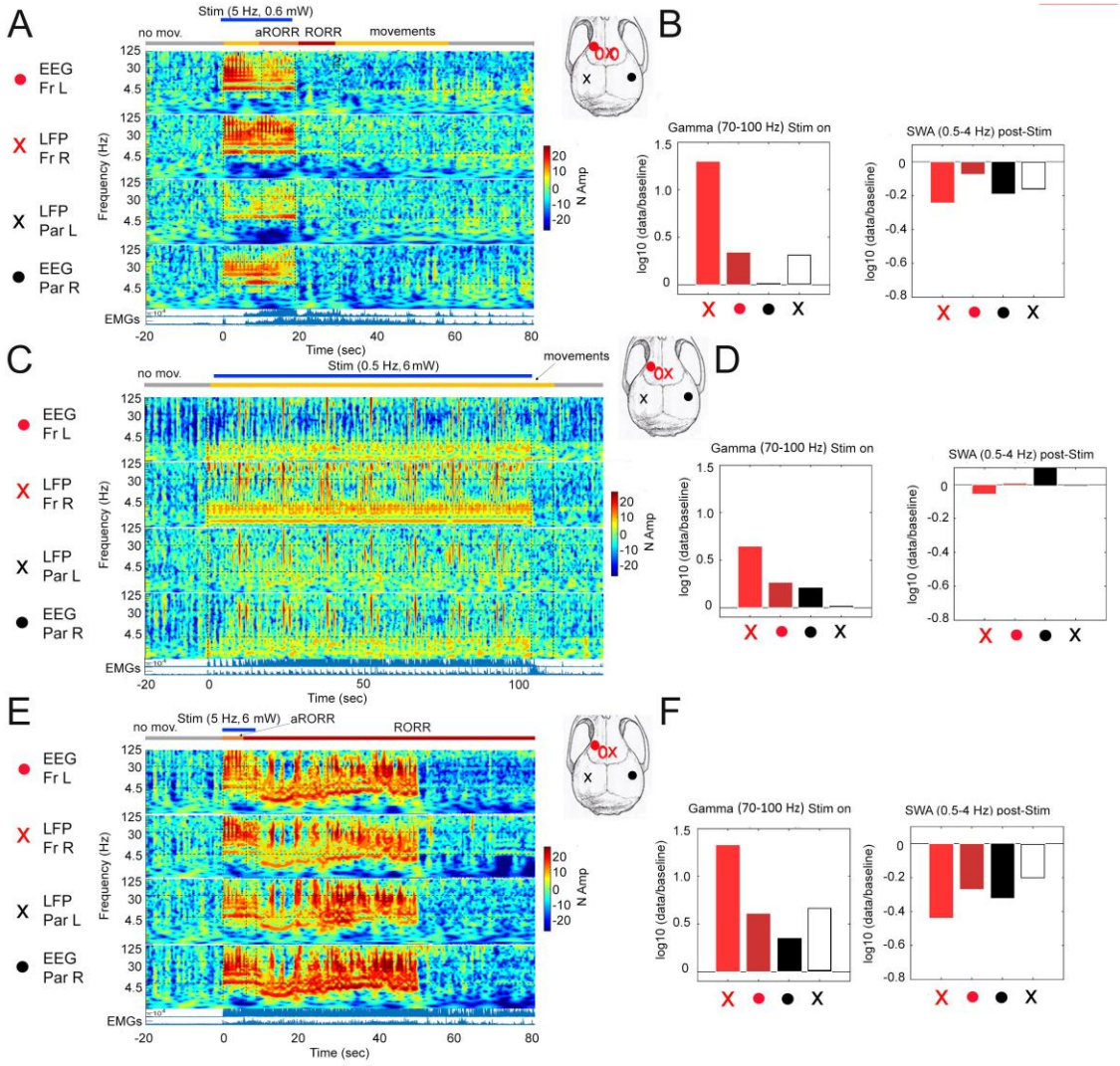
A
Stim (5 Hz, 0.6 mW)
no mov.
aRORR
RORR
movements
EEG Fr L
LFP Fr R
LFP Par L
EEG Par R
Frequency (Hz)
N Amp
EMGs
Time (sec)
B
Gamma (70-100 Hz) Stim on
SWA (0.5-4 Hz) post-Stim
log10 (data/baseline)
C
Stim (0.5 Hz, 6 mW)
D
E
Stim (5 Hz, 6 mW)
F

Figure 8. Optogenetic stimulation during sevo-dex anesthesia. **A**, representative traces of cortical activity during stable sevo-dex anesthesia (after LORR), one minute before stimulation (left) and just before and during stimulation (right). Blue arrow indicates the onset of the light pulses. Same mouse as in Figure 3. The panel shows (from top to bottom) the electroencephalogram (EEG) from frontal and parietal cortex; local field potentials (LFPs) from frontal and parietal cortex recorded across layers with a laminar silicon probe (superficial on top) and thresholded spikes from the same LFP channels; electromyogram (EMG) from vibrissal (top) and neck musculature (bottom). **B,** unilateral stimulation in PtA. Left, relative power spectrum for each of the 4 electrodes (3 EEGs indicated by circles, 1 deep LFP indicated by X). The electrode close to the optic fiber is shown in red. Time 0 indicates stimulation onset. The power for each frequency bin (0.0078Hz) is normalized based on the last 50 to 1 sec before the first laser pulse. EMGs, electromyograms from vibrissal (top) and neck musculature (bottom). The duration of the stimulation is indicated by the blue horizontal bar on top, followed by a rectangle indicating the post-stimulation time window when SWA was measured. Behavior was scored using videorecording and is indicated by horizontal bars (grey bars indicate when no/few movements were present). **C**, summary of the changes in gamma power (during the stimulation) and SWA (post-stimulation). **D, E,** as in B and C for as mouse with bilateral stimulation in PtA. Left, relative power spectrum for each of the 4 electrodes (2 EEGs indicated by filled circles, 2 deep LFPs indicated by X). Electrodes close to the optic fibers are shown in red. **F,G**, as in B and C for stimulation in mPFC.

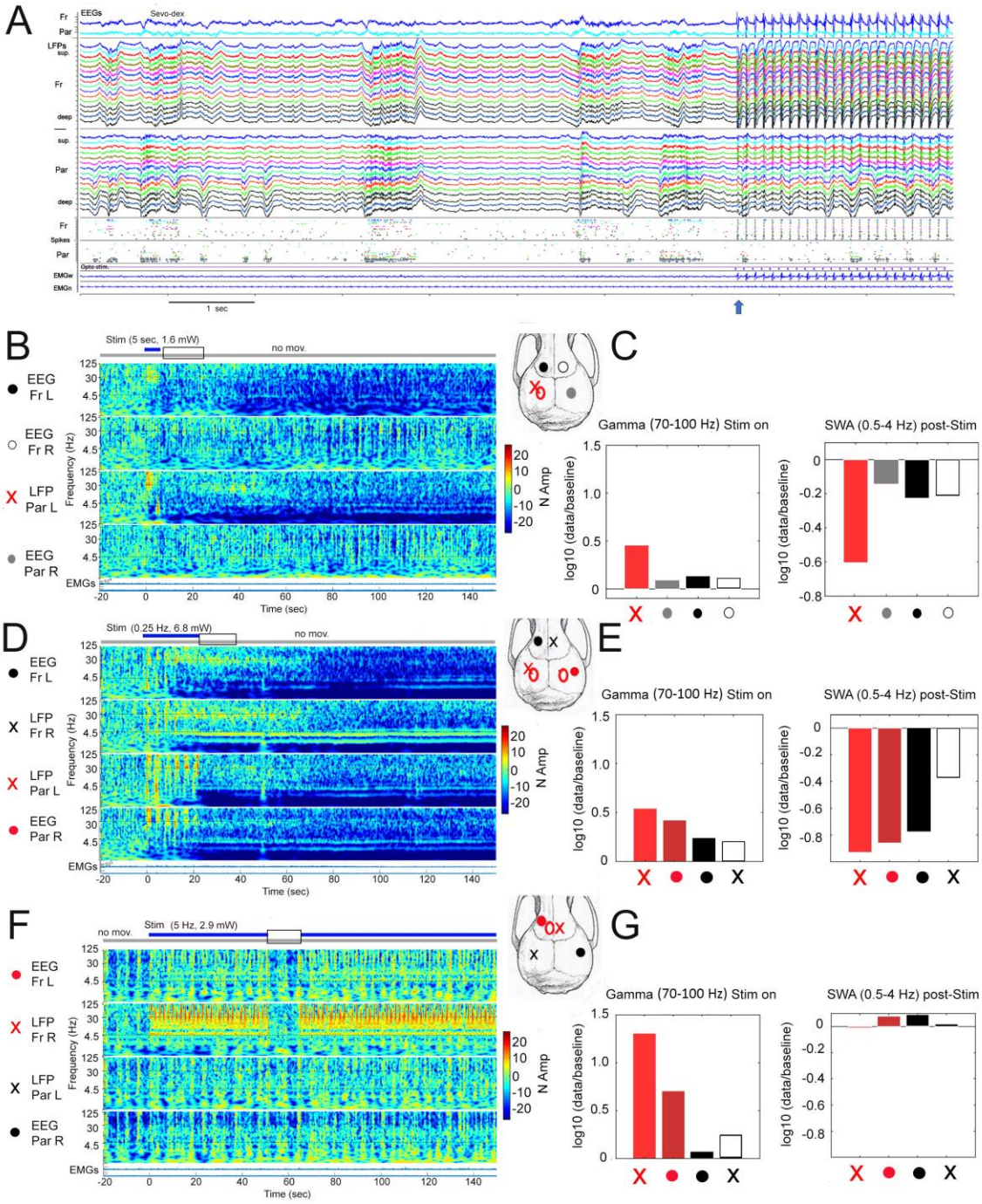
A
EEGs
Sevo-dex
Fr
Par
LFPs sup.
deep
Spikes
Opto stim.
EMGw
EMGn
1 sec
B
Stim (5 sec, 1.6 mW)
no mov.
EEG Fr L
EEG Fr R
LFP Par L
EEG Par R
EMGs
Frequency (Hz)
Time (sec)
N Amp
C
Gamma (70-100 Hz) Stim on
SWA (0.5-4 Hz) post-Stim
log10 (data/baseline)
D
Stim (0.25 Hz, 6.8 mW)
no mov.
EEG Fr L
LFP Fr R
LFP Par L
EEG Par R
E
F
Stim (5 Hz, 2.9 mW)
no mov.
G

Acknowledgements and Funding sources: We thank Matthew Banks for useful comments on the manuscript and Jonathan Lang for helping with the figures. Supported by U.S. Department of Defense grant W911NF1910280 (CC, GT), NIH grant 1R01GM116916 (GT), the Tiny Blue Dot Foundation (GT) and the Templeton World Charity Foundation (CC).

Author contributions: RM conducted the experiments, performed analysis, and wrote parts of the paper; MLC, GF, KD, WM performed analysis; MJP provided study reagents and contributed to the conceptualization of the work; GT and CC designed the experiments and wrote the paper.

Conflict of interest statement: Giulio Tononi is Chair of Board and has a financial interest in Intrinsic Powers Inc. Relevant patent: US 8,457,731 B2 (Method for assessing anesthetization; GT). All other authors declare no competing financial or non-financial interests.

STAR METHODS

5. RESOURCE AVAILABILITY

- **Lead contact.** Additional information and requests for resources and reagents should be sent and will be fulfilled by the lead contact, Chiara Cirelli (ccirelli@wisc.edu).
- **Materials availability.** This study did not generate new unique reagents.

- **Data and code availability.** Data reported in this paper will be shared by the lead contact upon request. This paper does not report original code but the analysis scripts are available (https://github.com/maomrong/mao-2023). Any additional information required to reanalyze the data reported in this paper is available from the lead contact upon request.

6. EXPERIMENTAL MODEL AND SUBJECT DETAILS

Experimental animals

Adult mice (CaMKIIα::ChR2 mice, both sexes, 19-28 g) were maintained on a 12 h light/12 h dark cycle with food and water available ad libitum (24–26 °C, 30–40% relative humidity). CaMKIIα::ChR2 mice were obtained by crossing CaMKIIα-Cre mice (Jackson Laboratory; T29-1; Stock No: 005359) with Cre-dependent ChR2(H134R)/EYFP expressing mice (Jackson Laboratory; Ai32; Stock No: 024109). For some pilot optogenetic experiments that require virus injection and optogenetic controls, CaMKIIα-Cre males were used instead. C57BL/6J males (Jackson Laboratory; B6; Stock No: 000664) were used for the initial characterization of the muscimol-induced coma-state. All animal procedures and experimental protocols followed the National Institutes of Health Guide for the Care and Use of Laboratory Animals and were approved by the licensing committee. Animal facilities were reviewed and approved by the institutional animal care and use committee (IACUC) of the University of Wisconsin-Madison and were inspected and accredited by the association for assessment and accreditation of laboratory animal care (AAALAC).

7. METHOD DETAILS

Surgical procedures

Surgery was performed under isoflurane anesthesia (2.0% induction; 0.8-1.5% maintenance) following aseptic techniques. For muscimol injection, all mice were implanted in the midbrain (A/P -3.75, M/L ±1.00, D/V -1.75) with bilateral guide cannulas (Plastics One). Dummy cannulas were inserted in the guide cannulas to prevent contamination and clogging. To perform electrophysiological recordings, all mice were also implanted with laminar silicon probes (NeuroNexus; A1x16; 50μm spacing), EEG screws, and electromyogram (EMG) wires. One silicon probe was implanted deeply in the right frontal cortex (A/P +1.93, M/L +0.40) to target Area (A)24a (i.e. anterior cingulate cortex, Cg2) and A25 (i.e. infralimbic cortex, IL). For simplicity, we refer to this entire targeted area as mPFC (medial prefrontal cortex) (Carlen, 2017; Laubach et al., 2018). Another silicon probe was implanted in the left posterior parietal cortex (PPtA; A/P -2.00, M/L -2.20) to target all layers. EEG screw electrodes were implanted over left secondary motor cortex (M2; A/P +2.50, M/L -1.50) and right secondary somatosensory cortex (S2; A/P -1.30, M/L +4.0). Reference screws were implanted over the cerebellum and olfactory bulb. EMG stainless steel wires were inserted bilaterally in the dorsal neck musculature and in the whisker musculature. Optic fibers (Doric Lenses; core diameter = 200μm; NA = 0.22; diffuser layer tip) were implanted for optogenetic stimulation. For frontal stimulation, one (n = 4 mice) or two (n = 2 mice) fibers were implanted in the right frontal cortex (A/P +1.77, M/L -0.60) to target mPFC. For parietal stimulation, one (n = 2 mice) or two (n = 6 mice) were placed on the cortical surface over PPtA (A/P -2.00, M/L ±1.80). The craniotomies and silicon probes were covered with surgical silicone adhesive (Kwik-Sil) and all implants were fixed to the skull with dental cement

(C&B-Metabond, Fusio or Flow-It). After surgery, mice were individually housed in transparent plastic cages (Allentown Caging; 24.5 x 21.5 x 21cm). At least one week was allowed for recovery from surgery, and experiments started only after the temporal organization of sleep and wakefulness had normalized.

Experimental procedures and design

Chronic sleep/wake recordings and sleep scoring. After recovering from surgery, mice were connected and accustomed to the recording system, and regularly monitored to ensure that the 24-hour patterns of sleep and waking were normal. Electrophysiological recording and optogenetic stimulation were performed using RZ2 BioAmp processor, OpenEx and Synapse software (Tucker-Davis Technologies). Silicon probes were connected through a head stage to an amplifier (Tucker-Davis Technologies; PZ5 NeuroDigitizer Amplifier) before reaching the RZ2 processor. EEGs and LFPs were filtered by 0.1-100Hz, and multi-unit activities (MUAs) were filtered by 0.3-5kHz. Sampling rate for storage was 256Hz for LFPs, EEGs and EMGs; 25kHz for MUAs. Spike data were collected discreetly from the same LFPs channels. Amplitude thresholds for online spike detection were set manually based on visual control. Whenever the recorded voltage exceeded a predefined threshold, a segment of 46 samples (0.48 ms before, 1.36 ms after the threshold crossing) was extracted and stored for later use. Sleep scoring was performed manually using SleepSign. Analysis of electrophysiological data was performed in MATLAB R2019b and R2021a (MathWorks®). LFP data were visually inspected to remove artefacts. Isolated bad channels were replaced by the mean of the immediately surrounding good channels.

All LFP channels were subjected to linear detrend and lowpass filtering (200 Hz), using a zero-phase distortion third order Butterworth filter.

Induction of a coma-like state. Continuous electrophysiological recordings started at light onset the day before the injection of muscimol and ended the day after the induction of the coma-like state. All sessions were recorded with video. In the afternoon of the experimental day, the first behavioral battery was performed during NREM sleep to obtain baseline levels of responsiveness for each individual mouse (see below). Mice were then briefly anesthetized with sevoflurane (5.0% induction; 3.0% maintenance) to facilitate muscimol injection. After the removal of the dummy cannulas, muscimol (Sigma-Aldrich; M1523; 1mg/mL in saline) was delivered through an internal cannula (Plastics One) whose tip extends beyond the implanted guide cannulas by 2 mm to reach the target area. With a microdialysis pump (Harvard Apparatus, CMA 400) a total of 0.5-0.75 μL of muscimol was injected at a rate of 1 μL/min into the left cannula. After a 30 s pause to limit backflow, the internal cannula was transferred to the right site, and the same procedure was repeated. Anesthesia was discontinued as soon as the procedure was completed. In control experiments (sham injection) the animal was injected with saline according to the same protocol described above for muscimol, then tested behaviorally and monitored until the emergence from anesthesia and recorded until the next day.

Behavioral test battery. Video and detailed behavioral notes for all mice were collected starting as soon as sevoflurane was discontinued after muscimol injection and lasted until RORR following the coma-like state. The behavioral battery was performed first during NREM sleep and/or wake before the injection (see above), then about 15 min after LORR, and then repeated approximately every 30 to 60 min for the duration of the coma-like state. At least one other

behavioral battery was performed shortly after RORR, and a final round was delivered the following day (see Figure 5A for one example in one mouse). To assess responsiveness, we used a customized scale developed in our laboratory. The battery included six sequential tests to assess the response to auditory, tactile, olfactory, vestibular and nociceptive stimuli. The result of each test was scored as 0 (no response), 1 (unclear response) or 2 (positive response) based on the mouse behavior within 5 sec from the onset of the stimulus. The six tests included 1) finger snap at a fixed distance from the mouse cage (0 = no response; 1 = small body tremor; 2 = clear body movement, usually a startle); 2) a drop of water was released about 5 cm above the neck of the mouse (0 = no response; 1 = small body tremor; 2 = full movement usually with grooming); 3) a freshly opened alcohol swab (BD Alcohol Swabs, 70% v/v Isopropyl Alcohol) was placed about 5 or 1cm in front of the mouse (0 = no response with either distance; 1 = withdrawal/head turning/grooming response only at 1cm distance; 2 = withdrawal/head turning/grooming response at 5 cm distance); 4) tail suspension: the mouse was gently picked up by the tail and suspended just above the ground (0 = no response; 1 = some/occasional kicks; 2 = strong body and legs' movements throughout the test/ wakes up from NREM sleep and moves away); 5) righting reflex: the mouse was gently flipped on its side by the tail (0 = laying on its side; 1 = flips back onto its feet after laying on its side; 2 = never really laying on its side/ wakes up from NREM sleep and moves away); 6) tail pinch (0 = no response; 1 = small movement; 2 = runs away/ wakes up from NREM sleep and moves away).

Optogenetic stimulation. Optic fibers were connected to a blue laser station (473nm, OEM Laser Systems DPSSL Driver, 100mW) controlled by the TDT system, with the laser output power manually regulated by an analog control knob on the driver. Based on the specific excitation

threshold of channelrhodopsin ChR2 (Nagel et al., 2005; Madisen et al., 2012; Sidor et al., 2015), and the intended activation radius in the target area, the corresponding laser power was estimated using an established online calculator (https://web.stanford.edu/group/dlab/cgi-bin/graph/chart.php). After the mice were accustomed to the system, and baseline recordings were acquired, brief laser pulses were delivered during NREM sleep to allow a within-mouse calibration of the effective laser power to deliver during the coma-like state. The minimal laser power that induced EEG activation and woke up the mouse from NREM sleep served as a reference for future experiments. To control for possible changes in sleep depth due to time of day, stimulation experiments during sleep, coma, or anesthesia were performed approximately 5 to 8 hours after the beginning of the light phase, when sleep pressure in mice is low (Cavelli et al., 2023). In a few cases the stimulation during sleep was delivered within the first hour of the light phase, and the results appeared to match those obtained when the laser pulses were given later during the day. Overall, across all stimulation experiments during sleep, anesthesia, and the coma-like state, the laser power ranged from 0.2 to 10 mW at fiber tip. Square pulse/s (lasting 1-5 sec) or trains (10ms pulse width; 4, 5, 8 or 10Hz) were delivered. Stimulation during the coma-like state was delivered approximately 30 min after LORR. In a control CaMKIIα-Cre mouse (no virus injection), laser stimulation during NREM sleep, REM sleep or sevo-dex anesthesia did not affect behavior or EEG cortical activity.

Anesthesia experiment. At least one week after the induction of the coma-like state another optogenetic stimulation experiment was performed after the mice were deeply anesthetized with sevo-dex (1-2% sevo, 70 or 100ug/kg dex). The dose of dex was 70ug/kg IP in males and 100ug/kg in females, because in our pilot experiments we noticed that female mice required higher doses of

dex. Sevo level was then adjusted to reach a state with slow waves in the EEG and stable LORR for at least 5min. The same pattern of stimulation used during the coma-like state, and the same or higher laser power, were used under anesthesia. Electrophysiological and video recordings were performed throughout the duration of the experiment.

Histology. Under deep isoflurane anesthesia (3.0%), mice were transcardially perfused with saline (for 30 secs) followed by 4% paraformaldehyde in phosphate buffer. Brains were removed and postfixed for 24 hours in the same fixative, then cut in 50um thick coronal sections on a cryostat (CryoStar^{TM} NX50 or Leica CM1900) after cryoprotection and flash-freezing. Sections were collected in PBS, mounted, air-dried, cover slipped (DAPI-Fluoromount-G, Vectashield, or Permount) and examined under a fluorescent or confocal microscope (Leica, Olympus). In some cases the silicon probe shanks were coated with CM-DiI dye (Thermo Fisher) immediately before implantation for better visualization of the probes' track. Glial fibrillary acidic protein (GFAP) staining was performed in some mice to localize the silicon probes without fluorescent dye coating (rabbit-anti-GFAP primary antibody, DAKO Z0334, 1:1000 in blocking solution; Donkey-anti-Rabbit AF594 secondary antibody, 1:500 in blocking solution). Crystal Violet staining was also performed in some animals to better visualize the location of the cannulas. EYFP amplification staining was performed in two CaMKIIα::ChR2 mice to confirm the broad cortical expression of the opsin (rabbit anti-GFP primary antibody, Invitrogen, A11122, 1:1000 in blocking solution; goat anti-rabbit Alexa-488 conjugated secondary antibody, Invitrogen, A11008, 1:1000 in blocking solution).

8. QUANTIFICATION AND STATISTICAL ANALYSIS

Statistical Analysis was performed using mixed effect models. The use of mixed effect models allows us to account for repeated measurements (the same mouse being used in multiple experiments). Linear mixed effect models were used to analyze continuous variables (e.g., SWA) (Laird and Ware, 1982), while generalized linear mixed effect models were used to analyze proportions (e.g., proportion of RORR) (Bolker et al., 2008). Due to the unbalanced nature of the experiment design, mixed effect models are preferred to traditional repeated measures ANOVA. Parameter estimation of LME and GLME models was performed using numerical maximum likelihood estimation, implemented in R by the lmer() and glmer() functions of the lme4 package (Bates et al., 2015). For the LME models, hypothesis testing is performed by fitting a reduced model with the factor of interest removed, and then comparing the fit of the two models using the asymptotic χ^2 test. For GLME models, hypothesis testing is performed using the asymptotic Wald test.

To compare behavioral score between NREM sleep and muscimol-induced coma, we fit a LME model for behavioral score with state (NREM vs. pre-stimulation coma) as a fixed effect and mouse as a random effect. We found a significant effect of state on the behavioral scores ($p = 2.9e\text{-}13$). To compare the mPFC and PtA groups before stimulation, we fit LME models with position (mPFC or PtA) as a fixed effect and mouse as a random effect. We found no significant effect of position when the response variable was the latency to LORR ($p = 0.6302$) or the behavioral score after LORR ($p = 0.8612$). For stimulation strength, we fit a LME model for strength (frequency + duration) with position (mPFC vs. PtA), state (REM vs. NREM), and frequency (0.5 Hz / 5 Hz / 8 Hz) as fixed effects, and mouse as a random effect. We found a significant effect of both position ($p = 0.0001$) and state ($p = 0.00003$). For gamma power at the

stimulation site during the stimulation, we fit an LME with position (mPFC vs. PtA), frequency (low vs. high), and condition (coma vs. anesthesia) as fixed effect, and mouse as a random effect. Before fitting the models, square root transformations were applied to the response variable to improve the validity of normality and constant variance assumptions. We found no significant effect of position on gamma power in the electrode closest to the optic fiber ($p = 0.348$).

Classification was performed using logistic regression, a generalized linear model that is often used for proportions or class probabilities. The inputs to the classifier were the gamma power and SWA from the LFP at the injection site, the mid and distal EEG, and the distal LFP. For two of the recordings, there was no distal LFP, so those data points were imputed using the k-nearest neighbours method (with $k = 3$). The model was fitted by maximum likelihood estimation with an $\ell 1$ penalty term using the glmnet() function in R (Friedman et al., 2010). The penalty term is used to prevent the model from overfitting to the data, and its strength is determined by a hyperparameter λ. The optimal value of λ was determined using 5-fold cross-validation to assess how well the model could classify independent test data. An optimal value of $\lambda = 0.068$ was identified with a corresponding cross-validated accuracy of 81.33%.

References

Aston-Jones G, Bloom FE (1981a) Norepinephrine-containing locus coeruleus neurons in behaving rats exhibit pronounced responses to non-noxious environmental stimuli. The Journal of neuroscience : the official journal of the Society for Neuroscience 1:887-900.

Aston-Jones G, Bloom FE (1981b) Activity of norepinephrine-containing locus coeruleus neurons in behaving rats anticipates fluctuations in the sleep-waking cycle. The Journal of neuroscience : the official journal of the Society for Neuroscience 1:876-886.

Bastos AM, Donoghue JA, Brincat SL, Mahnke M, Yanar J, Correa J, Waite AS, Lundqvist M, Roy J, Brown EN, Miller EK (2021) Neural effects of propofol-induced unconsciousness and its reversal using thalamic stimulation. Elife 10.

Bates D, Maechler M, Bolker B, Walker S (2015) Fitting Linear Mixed-Effects Models Using lme4. Journal of Statistical Software 67:1-48.

Bernardi G, Betta M, Ricciardi E, Pietrini P, Tononi G, Siclari F (2019) Regional Delta Waves In Human Rapid Eye Movement Sleep. The Journal of neuroscience : the official journal of the Society for Neuroscience 39:2686-2697.

Bolker BM, Brooks ME, Clark CJ, Geange SW, Poulsen JR, Stevens MHH, White J-SS (2008) Generalized linear mixed models: a practical guide for ecology and evolution. Trends in Ecology and Evolution 24:127-135.

Boly M, Massimini M, Tsuchiya N, Postle BR, Koch C, Tononi G (2017) Are the Neural Correlates of Consciousness in the Front or in the Back of the Cerebral Cortex? Clinical and Neuroimaging Evidence. The Journal of neuroscience : the official journal of the Society for Neuroscience 37:9603-9613.

Boly M, Phillips C, Tshibanda L, Vanhaudenhuyse A, Schabus M, Dang-Vu TT, Moonen G, Hustinx R, Maquet P, Laureys S (2008) Intrinsic brain activity in altered states of consciousness: how conscious is the default mode of brain function? Annals of the New York Academy of Sciences 1129:119-129.

Brown RE, Basheer R, McKenna JT, Strecker RE, McCarley RW (2012) Control of sleep and wakefulness. Physiol Rev 92:1087-1187.

Carlen M (2017) What constitutes the prefrontal cortex? Science 358:478-482.

Carter ME, Yizhar O, Chikahisa S, Nguyen H, Adamantidis A, Nishino S, Deisseroth K, de Lecea L (2010) Tuning arousal with optogenetic modulation of locus coeruleus neurons. Nature neuroscience 13:1526-1533.

Casarotto S, Comanducci A, Rosanova M, Sarasso S, Fecchio M, Napolitani M, Pigorini A, A GC, Trimarchi PD, Boly M, Gosseries O, Bodart O, Curto F, Landi C, Mariotti M, Devalle G, Laureys S, Tononi G, Massimini M (2016) Stratification of unresponsive patients by an independently validated index of brain complexity. Ann Neurol 80:718-729.

Cavelli ML, Mao R, Findlay G, Driessen K, Bugnon T, Tononi G, Cirelli C (2023) Sleep/wake changes in perturbational complexity in rats and mice. iScience 26:106186.

Cho JR, Treweek JB, Robinson JE, Xiao C, Bremner LR, Greenbaum A, Gradinaru V (2017) Dorsal Raphe Dopamine Neurons Modulate Arousal and Promote Wakefulness by Salient Stimuli. Neuron 94:1205-1219 e1208.

Comanducci A, Casarotto S, Rosanova M, Derchi CC, Vigano A, Pirastru A, Blasi V, Cazzoli M, Navarro J, Edlow BL, Baglio F, Massimini M (2023) Unconsciousness or unresponsiveness in akinetic mutism? Insights from a multimodal longitudinal exploration. The European journal of neuroscience.

Devor M, Zalkind V (2001) Reversible analgesia, atonia, and loss of consciousness on bilateral intracerebral microinjection of pentobarbital. Pain 94:101-112.

Dong Y, Li J, Zhou M, Du Y, Liu D (2022) Cortical regulation of two-stage rapid eye movement sleep. Nature neuroscience 25:1675-1682.

Eban-Rothschild A, Rothschild G, Giardino WJ, Jones JR, de Lecea L (2016) VTA dopaminergic neurons regulate ethologically relevant sleep-wake behaviors. Nature neuroscience 19:1356-+.

Ermis U, Krakow K, Voss U (2010) Arousal thresholds during human tonic and phasic REM sleep. J Sleep Res 19:400-406.

Feng J, Zhang C, Lischinsky JE, Jing M, Zhou J, Wang H, Zhang Y, Dong A, Wu Z, Wu H, Chen W, Zhang P, Zou J, Hires SA, Zhu JJ, Cui G, Lin D, Du J, Li Y (2019) A Genetically Encoded Fluorescent Sensor for Rapid and Specific In Vivo Detection of Norepinephrine. Neuron 102:745-761 e748.

Friedman J, Hastie T, Tibshirani R (2010) Regularization Paths for Generalized Linear Models via Coordinate Descent. J Stat Softw 33:1-22.

Hayat H, Regev N, Matosevich N, Sales A, Paredes-Rodriguez E, Krom AJ, Bergman L, Li Y, Lavigne M, Kremer EJ, Yizhar O, Pickering AE, Nir Y (2020) Locus coeruleus norepinephrine activity mediates sensory-evoked awakenings from sleep. Sci Adv 6:eaaz4232.

Herkenham M (1979) The afferent and efferent connections of the ventromedial thalamic nucleus in the rat. J Comp Neurol 183:487-517.

Herrera CG, Cadavieco MC, Jego S, Ponomarenko A, Korotkova T, Adamantidis A (2016) Hypothalamic feedforward inhibition of thalamocortical network controls arousal and consciousness. Nature neuroscience 19:290-298.

Honjoh S, Sasai S, Schiereck SS, Nagai H, Tononi G, Cirelli C (2018) Regulation of cortical activity and arousal by the matrix cells of the ventromedial thalamic nucleus. Nature communications 9:2100.

Hunsley MS, Palmiter RD (2004) Altered sleep latency and arousal regulation in mice lacking norepinephrine. Pharmacol Biochem Behav 78:765-773.

Iqbal F, Thompson AJ, Riaz S, Pehar M, Rice T, Syed NI (2019) Anesthetics: from modes of action to unconsciousness and neurotoxicity. Journal of neurophysiology 122:760-787.

Kjaerby C, Andersen M, Hauglund N, Untiet V, Dall C, Sigurdsson B, Ding F, Feng J, Li Y, Weikop P, Hirase H, Nedergaard M (2022) Memory-enhancing properties of sleep depend on the oscillatory amplitude of norepinephrine. Nature neuroscience 25:1059-1070.

Koch C, Massimini M, Boly M, Tononi G (2016) Neural correlates of consciousness: progress and problems. Nat Rev Neurosci 17:307-321.

Laird NM, Ware JH (1982) Random effects models for longitudinal data. Biometrics 38:963-974.

Lanir-Azaria S, Meiri G, Avigdor T, Minert A, Devor M (2018) Enhanced wakefulness following lesions of a mesopontine locus essential for the induction of general anesthesia. Behav Brain Res 341:198-211.

Laubach M, Amarante LM, Swanson K, White SR (2018) What, If Anything, Is Rodent Prefrontal Cortex? eNeuro 5.

Laureys S, Owen AM, Schiff ND (2004) Brain function in coma, vegetative state, and related disorders. Lancet Neurol 3:537-546.

Luppi PH, Clement O, Sapin E, Gervasoni D, Peyron C, Leger L, Salvert D, Fort P (2011) The neuronal network responsible for paradoxical sleep and its dysfunctions causing narcolepsy and rapid eye movement (REM) behavior disorder. Sleep Med Rev 15:153-163.

Madisen L et al. (2012) A toolbox of Cre-dependent optogenetic transgenic mice for light-induced activation and silencing. Nature neuroscience 15:793-802.

Massimini M, Ferrarelli F, Huber R, Esser SK, Singh H, Tononi G (2005) Breakdown of cortical effective connectivity during sleep. Science 309:2228-2232.

Massimini M, Ferrarelli F, Murphy M, Huber R, Riedner B, Casarotto S, Tononi G (2010) Cortical reactivity and effective connectivity during REM sleep in humans. Cognitive neuroscience 1:176-183.

Moruzzi G, Magoun HW (1949) Brain stem reticular formation and activation of the EEG. Electroencephalogr Clin Neurophysiol 1:455-473.

Nagel G, Szellas T, Kateriya S, Adeishvili N, Hegemann P, Bamberg E (2005) Channelrhodopsins: directly light-gated cation channels. Biochem Soc Trans 33:863-866.

Neckelmann D, Ursin R (1993) Sleep stages and EEG power spectrum in relation to acoustical stimulus arousal threshold in the rat. Sleep 16:467-477.

Nitz D, Siegel JM (1997) GABA release in the locus coeruleus as a function of sleep/wake state. Neuroscience 78:795-801.

Odegaard B, Knight RT, Lau H (2017) Should a Few Null Findings Falsify Prefrontal Theories of Conscious Perception? The Journal of neuroscience : the official journal of the Society for Neuroscience 37:9593-9602.

Osorio-Forero A, Cardis R, Vantomme G, Guillaume-Gentil A, Katsioudi G, Devenoges C, Fernandez LMJ, Luthi A (2021) Noradrenergic circuit control of non-REM sleep substates. Curr Biol 31:5009-5023 e5007.

Pal D, Dean JG, Liu T, Li D, Watson CJ, Hudetz AG, Mashour GA (2018) Differential Role of Prefrontal and Parietal Cortices in Controlling Level of Consciousness. Curr Biol 28:2145-2152 e2145.

Parvizi J, Damasio AR (2003) Neuroanatomical correlates of brainstem coma. Brain 126:1524-1536.

Posner JB, Plum F (2007) Plum and Posner's diagnosis of stupor and coma, 4th Edition. Oxford ; New York: Oxford University Press.

Rechtschaffen A, Hauri P, Zeitlin M (1966) Auditory awakening thresholds in REM and NREM sleep stages. Percept Mot Skills 22:927-942.

Redinbaugh MJ, Phillips JM, Kambi NA, Mohanta S, Andryk S, Dooley GL, Afrasiabi M, Raz A, Saalmann YB (2020) Thalamus Modulates Consciousness via Layer-Specific Control of Cortex. Neuron 106:66-75 e12.

Sanders RD, Tononi G, Laureys S, Sleigh J (2012) Unresponsiveness ≠ Unconsciousness. Anesthesiology 116:946-959.
Scammell TE, Arrigoni E, Lipton JO (2017) Neural Circuitry of Wakefulness and Sleep. Neuron 93:747-765.
Schiff ND (2010) Recovery of consciousness after brain injury: a mesocircuit hypothesis. Trends Neurosci 33:1-9.
Schiff ND, Nauvel T, Victor JD (2014) Large-scale brain dynamics in disorders of consciousness. Curr Opin Neurobiol 25:7-14.
Siclari F, Baird B, Perogamvros L, Bernardi G, LaRocque JJ, Riedner B, Boly M, Postle BR, Tononi G (2017) The neural correlates of dreaming. Nature neuroscience 20:872-878.
Sidor MM, Davidson TJ, Tye KM, Warden MR, Diesseroth K, McClung CA (2015) In vivo optogenetic stimulation of the rodent central nervous system. J Vis Exp:51483.
Steriade M, Timofeev I, Grenier F (2001) Natural waking and sleep states: a view from inside neocortical neurons. Journal of neurophysiology 85:1969-1985.
Takahashi K, Kayama Y, Lin JS, Sakai K (2010) Locus coeruleus neuronal activity during the sleep-waking cycle in mice. Neuroscience 169:1115-1126.
Takata N (2020) Thalamic reticular nucleus in the thalamocortical loop. Neurosci Res 156:32-40.
Taylor NE, Van Dort CJ, Kenny JD, Pei J, Guidera JA, Vlasov KY, Lee JT, Boyden ES, Brown EN, Solt K (2016) Optogenetic activation of dopamine neurons in the ventral tegmental area induces reanimation from general anesthesia. Proceedings of the National Academy of Sciences of the United States of America.
Tseng YT, Zhao B, Chen S, Ye J, Liu J, Liang L, Ding H, Schaefke B, Yang Q, Wang L, Wang F, Wang L (2022) The subthalamic corticotropin-releasing hormone neurons mediate adaptive REM-sleep responses to threat. Neuron.
Verret L, Fort P, Gervasoni D, Leger L, Luppi PH (2006) Localization of the neurons active during paradoxical (REM) sleep and projecting to the locus coeruleus noradrenergic neurons in the rat. J Comp Neurol 495:573-586.
Vinje ML, Moe MC, Valo ET, Berg-Johnsen J (2002) The effect of sevoflurane on glutamate release and uptake in rat cerebrocortical presynaptic terminals. Acta Anaesthesiol Scand 46:103-108.
Wang Z, Fei X, Liu X, Wang Y, Hu Y, Peng W, Wang YW, Zhang S, Xu M (2022) REM sleep is associated with distinct global cortical dynamics and controlled by occipital cortex. Nature communications 13:6896.
Zepelin H, McDonald CS, Zammit GK (1984) Effects of age on auditory awakening thresholds. J Gerontol 39:294-300.
Zhang Z, Ferretti V, Guntan I, Moro A, Steinberg EA, Ye Z, Zecharia AY, Yu X, Vyssotski AL, Brickley SG, Yustos R, Pillidge ZE, Harding EC, Wisden W, Franks NP (2015) Neuronal ensembles sufficient for recovery sleep and the sedative actions of alpha2 adrenergic agonists. Nature neuroscience 18:553-561.

Chapter IV:

Conclusion

The cerebral cortex and consciousness

Overall, the results of the experiments described in Chapter II and III reveal that 1) the PCI^{st} index obtained from cortical evoked responses can be used in mice and rats to assess the level of consciousness, and 2) the direct activation of the mouse cortical neurons is sufficient for behavioral arousal and/or cortical activation from sleep, brainstem coma, and anesthesia.

I show, in Chapter II, that in freely moving mice and rats PCI^{st} values are high during wakefulness and REM sleep and low during NREM sleep and under slow wave anesthesia with sevoflurane and/or dexmedetomidine, as it is the case in humans (Comolatti et al. 2019). In humans, wakefulness is associated with conscious awareness, and during REM sleep, dreaming is most often reported (Siclari et al. 2017). In contrast, consciousness is frequently diminished during NREM sleep and under slow wave anesthesia (Siclari et al. 2017; Casali et al. 2013). The discovery that PCI^{st} in rodents tracks the different levels of consciousness across behavioral states as was reported in humans, provides evidence in support of its underlying premise (Casali et al. 2013; Comolatti et al. 2019) that the cerebral cortex is a key part of the neural substrate of consciousness. By performing unit recordings in both rats and mice, I also uncovered that during NREM sleep and slow wave anesthesia, low PCI^{st} values are associated with a cortical OFF period of neuronal silence. This observation directly supports the hypothesis that the loss of consciousness in states of bistability is underlied by a breakdown of causal interactions within cortical networks (Massimini et al. 2005; Pigorini et al. 2015), and that the sustained causal interactions in the cortex are essential for consciousness.

In Chapter III, I show that direct stimulation of cortical neurons is capable of inducing behavioral arousal and/or cortical EEG activation from sleep, brainstem coma, and anesthesia.

Specifically, cortical optogenetic stimulation consistently awakens mice from both NREM sleep and REM sleep. In most cases the stimulation also leads to cortical activation, manifested as a decrease in low frequencies (SWA), during both brainstem coma and anesthesia, as well as full behavioral arousal, manifested as recovery of the righting reflex, from brainstem coma. Together with the previous clinical observations (Laureys, Owen, and Schiff 2004; Boly et al. 2008), these findings point to the crucial role of cerebral cortex in supporting consciousness.

The front, or the back of the cortex

The essential role of posterior cortical areas for consciousness is demonstrated by the results in rodents presented in Chapter II and III, while the contribution of anterior areas is possibly less significant.

As described in Chapter II, PCI^{st} shows consistent high values in wake and REM sleep and low values in NREM sleep and slow-wave anesthesia, regardless of the site of stimulation or recording, with the exception of recordings in the mouse prefrontal cortex, which displays inconsistent PCIst changes in relation to behavioral state. The optogenetic stimulation applied in mice excites local cortical pyramidal neurons, whereas the electrical stimulation used in rats activates a broader cortical network that includes passing fibers. Thus, a potential explanation for the results is that the stimulation in mice is less likely to trigger complex responses in a remote site, compared to the stimulation in rats. Nevertheless, in mice the responses are complex during wake and REM in PtA, but not mPFC. It is possible that the organization of prefrontal cortex is less conducive to sustaining the integrated and differentiated causal interactions required for

consciousness, as was also suggested by previous evidence (Brickner, 1952; Kampfl et al., 1998a; Laureys et al., 2004; Siclari et al., 2017).

Moreover, as shown in Chapter III, in three different conditions - sleep, brainstem coma and sevo-dex anesthesia - the activation of mouse posterior parietal cortex tends to produce more behavioral and/or cortical arousal compared to medial prefrontal cortex activation. In particular, the awakening from sleep requires significantly weaker/shorter light pulses when delivered in PtA compared to mPFC. Moreover, compared to mPFC stimulation, PtA stimulation resulted in a greater proportion of recovery of the righting reflex from muscimol-induced coma, as well as a larger post-stimulation decrease in SWA at stimulation site. Furthermore, a classification analysis shows that the effects of PtA and mPFC stimulations can be easily distinguished, indicating a fundamental difference between the parietal and frontal activation. In sum, these findings suggest that PtA may be more effective than mPFC in producing recovery of consciousness. However, there are major limitations in the study described in Chapter III that prevent any firm conclusion, including the relatively small number of mice, and, perhaps more crucially, the highly unbalanced design, with differences in the frequency (e.g. 0.5 Hz vs 5 Hz) and side (unilateral vs bilateral) of stimulation.

The superficial, or deep cortical layers

As shown in Chapter II, at the recording site both superficial and deep channels contribute to the high PCI^{st} values in wake and REM sleep and low PCI^{st} values in NREM sleep and anesthesia. This result indicates that both superficial and deep layers may be important for the presence and content of consciousness. However, there are other reports supporting the importance of only

superficial layers (He and Raichle, 2009) (Dembski, Koch, and Pitts 2021), deep layers (Suzuki and Larkum, 2020), or suggesting that it may be specific cell types that one should draw attention to (Hodge et al. 2019; Callaway et al. 2021; Yao et al. 2021).

While the recording site (superficial or deep layers) where PCI^{st} values are calculated does not seem to matter, the stimulation site makes a difference. Specifically, I found that stimulating the deep and middle cortical layers in either the anterior or posterior cortical areas in rats leads to consistent changes in PCI^{st} across sleep, wakefulness, and anesthesia. In contrast, stimulations in the superficial layers does not lead to the same reliable changes in PCI^{st}. A possible explanation is that deep and middle layer stimulations are more likely to recruit cortico-thalamic and other cortico-subcortical loops, and thus are in a better position to generate a complex evoked response that can be detected at a single distant recording site during wake.

References

Boly, M., C. Phillips, L. Tshibanda, A. Vanhaudenhuyse, M. Schabus, T.t. Dang-Vu, G. Moonen, R. Hustinx, P. Maquet, and S. Laureys. 2008. “Intrinsic Brain Activity in Altered States of Consciousness.” *Annals of the New York Academy of Sciences* 1129 (1): 119–29. https://doi.org/10.1196/annals.1417.015.

Callaway, Edward M., Hong-Wei Dong, Joseph R. Ecker, Michael J. Hawrylycz, Z. Josh Huang, Ed S. Lein, John Ngai, et al. 2021. “A Multimodal Cell Census and Atlas of the Mammalian Primary Motor Cortex.” *Nature* 598 (7879): 86–102. https://doi.org/10.1038/s41586-021-03950-0.

Casali, Adenauer G., Olivia Gosseries, Mario Rosanova, Mélanie Boly, Simone Sarasso, Karina R. Casali, Silvia Casarotto, et al. 2013. “A Theoretically Based Index of Consciousness Independent of Sensory Processing and Behavior.” *Science Translational Medicine* 5 (198): 198ra105-198ra105. https://doi.org/10.1126/scitranslmed.3006294.

Comolatti, Renzo, Andrea Pigorini, Silvia Casarotto, Matteo Fecchio, Guilherme Faria, Simone Sarasso, Mario Rosanova, et al. 2019. “A Fast and General Method to Empirically Estimate the Complexity of Brain Responses to Transcranial and Intracranial Stimulations.” *Brain Stimulation* 12 (5): 1280–89. https://doi.org/10.1016/j.brs.2019.05.013.

Dembski, Cole, Christof Koch, and Michael Pitts. 2021. “Perceptual Awareness Negativity: A Physiological Correlate of Sensory Consciousness.” *Trends in Cognitive Sciences*, June, S1364661321001467. https://doi.org/10.1016/j.tics.2021.05.009.

Hodge, Rebecca D., Trygve E. Bakken, Jeremy A. Miller, Kimberly A. Smith, Eliza R. Barkan, Lucas T. Graybuck, Jennie L. Close, et al. 2019. “Conserved Cell Types with Divergent Features in Human versus Mouse Cortex.” *Nature* 573 (7772): 61–68. https://doi.org/10.1038/s41586-019-1506-7.

Laureys, Steven, Adrian M Owen, and Nicholas D Schiff. 2004. “Brain Function in Coma, Vegetative State, and Related Disorders.” *The Lancet Neurology* 3 (9): 537–46. https://doi.org/10.1016/S1474-4422(04)00852-X.

Massimini, Marcello, Fabio Ferrarelli, Reto Huber, Steve K. Esser, Harpreet Singh, and Giulio Tononi. 2005. “Breakdown of Cortical Effective Connectivity During Sleep.” *Science* 309 (5744): 2228–32. https://doi.org/10.1126/science.1117256.

Pigorini, Andrea, Simone Sarasso, Paola Proserpio, Caroline Szymanski, Gabriele Arnulfo, Silvia Casarotto, Matteo Fecchio, et al. 2015. “Bistability Breaks-off Deterministic Responses to Intracortical Stimulation during Non-REM Sleep.” *NeuroImage* 112 (May): 105–13. https://doi.org/10.1016/j.neuroimage.2015.02.056.

Siclari, Francesca, Benjamin Baird, Lampros Perogamvros, Giulio Bernardi, Joshua J. LaRocque, Brady Riedner, Melanie Boly, Bradley R. Postle, and Giulio Tononi. 2017. “The Neural Correlates of Dreaming.” *Nature Neuroscience* 20 (6): 872–78. https://doi.org/10.1038/nn.4545.

Yao, Zizhen, Cindy T.J. van Velthoven, Thuc Nghi Nguyen, Jeff Goldy, Adriana E. Sedeno-Cortes, Fahimeh Baftizadeh, Darren Bertagnolli, et al. 2021. “A Taxonomy of Transcriptomic Cell Types across the Isocortex and Hippocampal Formation.” *Cell* 184 (12): 3222-3241.e26. https://doi.org/10.1016/j.cell.2021.04.021.